

**SR 97 –
Alternative models project**

**Discrete fracture network modelling
for performance assessment of Aberg**

Bill Dershowitz, Thorsten Eiben
Golder Associates Inc., Seattle

Sven Follin, Johan Andersson
Golder Grundteknik KB, Stockholm

August 1999

Svensk Kärnbränslehantering AB

Swedish Nuclear Fuel
and Waste Management Co
Box 5864
SE-102 40 Stockholm Sweden
Tel 08-459 84 00
+46 8 459 84 00
Fax 08-661 57 19
+46 8 661 57 19



SR 97 -
Alternative models project
Discrete fracture network modelling
for performance assessment of Aberg

Bill Dershowitz, Thorsten Eiben
Golder Associates Inc., Seattle

Sven Follin, Johan Andersson
Golder Grundteknik KB, Stockholm

August 1999

Keywords: Performance Assessment, Radionuclide Transport, Pathways Analysis, Fracture Flow, Near-Field, Far-Field, FARF31, COMP23, FracMan, PA Works.

This report concerns a study which was conducted for SKB. The conclusions and viewpoints presented in the report are those of the author(s) and do not necessarily coincide with those of the client.

ABSTRACT

As part of studies into the siting of a deep repository for nuclear waste, Swedish Nuclear Fuel and Waste Management Company (SKB) has commissioned the Alternative Models Project (AMP). The AMP is a comparison of three alternative modeling approaches for geosphere performance assessment for a single hypothetical site. The hypothetical site, arbitrarily named Aberg is based on parameters from the Äspö Hard Rock Laboratory in southern Sweden. The Aberg model domain, boundary conditions and canister locations are defined as a common reference case to facilitate comparisons between approaches.

This report presents the results of a discrete fracture pathways analysis of the Aberg site, within the context of the SR 97 performance assessment exercise. The Aberg discrete fracture network (DFN) site model is based on consensus Aberg parameters related to the Äspö HRL site. Discrete fracture pathways are identified from canister locations in a prototype repository design to the surface of the island or to the sea bottom. The discrete fracture pathways analysis presented in this report is used to provide the following parameters for SKB's performance assessment transport codes **FARF31** and **COMP23**:

- **F-factor**: Flow wetted surface normalized with regards to flow rate (yields an appreciation of the contact area available for diffusion and sorption processes) [TL^{-1}].
- **Travel Time**: Advective transport time from a canister location to the environmental discharge [T].
- **Canister Flux**: Darcy flux (flow rate per unit area) past a representative canister location [LT^{-1}].

In addition to the above, the discrete fracture pathways analysis in this report also provides information about:

- additional pathway parameters such as pathway length, pathway width, transport aperture, reactive surface area and transmissivity,
- percentage of canister locations with pathways to the surface discharge,
- spatial pattern of pathways and pathway discharges,
- visualization of pathways, and
- statistical analysis of variability between canister locations, and between stochastic realizations.

SAMMANFATTNING

Som en del av platsvalsprocessen för ett djupförvar för radioaktivt avfall har Svensk Kärnbränslehantering AB (SKB) beställt ett projekt med jämförelse av alternativa modeller (AMP – Alternative Models Project). AMP är en jämförelse av tre alternativa modellprinciper för säkerhetsanalys av berggrunden, alla för samma hypotetiska modellområde. Det hypotetiska modellområdet, kallat Aberg, antar värden på indata från Äspö Hard Rock Laboratory i södra Sverige. Modellerna är begränsade till ett givet område, givna randvillkor och givna kapselpositioner för att möjliggöra jämförelsen.

Föreliggande rapport presenteras resultat från en analys av diskreta flödesvägar mellan föreslagna kapselpositioner och förekommande utströmningsområden inom modellområdet. Resultaten presenteras i enlighet med den redovisningsmall som gäller för SR 97 och utgörs av värden på olika parametrar relaterade till SKB:s beräkningskedja för analys av berggrundens säkerhetsfunktion i händelse av kapselläckage. De datorprogram som åsyftas är **FARF31** and **COMP23** och de aktuella parametrarna som behandlas i denna rapport är:

- **F-faktorn:** Flödesnormaliserad våt sprickyta tillgänglig för diffusions- och sorptionsprocesser [TL^{-1}].
- **Transporttiden:** Advektiv transporttid från en kapselposition till utströmningsområdet [T].
- **Kapselflödeshastigheten:** Darcy-hastigheten (volymflöde per tidsenhet och areaenhet) hos vatten i de flödesvägar som passerar förbi en kapselposition [LT^{-1}].

Diskret flödesvägsanalys används i denna rapport för att ta fram effektivrörden på olika typer av säkerhetsrelaterade flödesvägsparametrar. Utöver de tre som angivits ovan kan nämnas längd, bredd, tjocklek och transmissivitet. Diskret flödesvägsanalys möjliggör:

- visualisering av flödesvägar, -mönster och utströmningsområden,
- statistisk analys av variabiliteten mellan olika kapselpositioner och mellan olika realiseringar av en stokastisk modell, samt
- beräkning av andelen kapselpositioner som är isolerade från, alternativt har kontakt med, utströmningsområdet.

TABLE OF CONTENTS

ABSTRACT

SAMMANFATTNING

TABLE OF CONTENTS

EXCECTUTIVE SUMMARY

1	INTRODUCTION	1
	1.1 THE ALTERNATIVE MODELS PROJECT	1
	1.2 METHODOLOGY	2
	1.3 SCOPE OF WORK	4
2	MODELING APPROACH	5
	2.1 THE PA MODEL CHAIN	5
	2.2 FRACTURE HYDROGEOLOGY	5
	2.2.1 ASSUMPTIONS AND LIMITATIONS	7
	2.2.2 GOVERNING EQUATIONS	8
	2.3 PATHWAYS ANALYSIS	10
	2.4 PATHWAY SEARCH	15
	2.5 EFFECTIVE PATHWAYS	16
	2.6 SR 97 PARAMETERS	17
	2.6.1 FARF31	17
	2.6.2 COMP23	18
	2.6.3 OTHER PARAMETERS	18
3	GENERAL PREMISES	21
	3.1 SITE DESCRIPTION	21
	3.2 HYDROGEOLOGY	22
	3.3 BOUNDARY CONDITIONS	22

4	ABERG DFN SITE MODEL	27
	4.1 ROCK MASS PARAMETERS	30
	4.2 FRACTURE ZONE PARAMETERS	33
	4.3 REFERENCE REPOSITORY LAYOUT	40
	4.4 BOUNDARY CONDITIONS	41
5	PATHWAYS ANALYSIS	43
	5.1 SIMULATION RESULTS	44
	5.2 PATHWAY SEARCH	45
	5.3 PATHWAY STATISTICS	49
	5.3.1 SECTOR 3	49
	5.3.2 SECTOR 4	52
	5.3.3 SECTOR 6	55
	5.3.4 SAMPLE HISTOGRAMS	58
	5.4 CONSISTENCY OF BOUNDARY FLUXES	71
	5.5 SUPPLEMENTARY PERFORMANCE PLOTS	73
6	CONCLUSIONS	79
7	ACKNOWLEDGEMENTS	81
8	REFERENCES	83
	APPENDICES	85
	<i>APPENDIX A: GOVERNING FLOW EQUATIONS</i>	
	<i>APPENDIX B: PIPE APPROXIMATION FOR FRACTURE NETWORK TOPOLOGY</i>	
	<i>APPENDIX C: EFFECTIVE PATHWAY PROPERTIES</i>	
	<i>APPENDIX D: GRAPHICAL DISPLAY OF PATHWAY DISCHARGE POINTS</i>	

EXECUTIVE SUMMARY

The Alternative Models Project (AMP) is part of the SKB SR 97 study, and consists of a comparison of three alternative modeling approaches to bedrock PA at the Aberg site. This study presents an application of the discrete fracture pathways approach. The majority of the model parameters and boundary conditions are explicitly specified by SKB in the project requirements memo by Ström and Selroos (1997).

The boundary conditions for this model are constant head boundaries, derived from a single stochastic realization of a regional-scale continuum model by Svensson (1997). The overall flow pattern is that of recharge on the inland areas discharging to the coastal waters. The transfer of regional heads via constant head boundaries is assumed to preserve this pattern in the site-scale model provided that the model domain is treated as a porous medium.

This project uses ten (10) realizations to evaluate three performance measures (F-factor, travel time and canister flux) for the proposed repository layout, which consists of three repository sectors labeled 3, 4 and 6. The advantage of the DFN approach is its ability to identify the variability due to different canister locations providing the source terms. As a consequence to this, the DFN analysis indicates a high variability of the mean, median, variance and range of (\log_{10}) F-factor, travel time and canister flux between realizations. The pooled results (all realizations and all canisters combined) suggest the following \log_{10} -statistics for the median of the three performance measures:

Parameter (M=median)	Repository Sector		
	#3	#4	#6
M- \log_{10} (F-factor), F in y/m	5.88	6.54	5.72
M- \log_{10} (travel time), t in y	1.20	1.77	0.93
M- \log_{10} (canister flux), q in m/y	-2.43	-2.64	-2.48

1 INTRODUCTION

1.1 THE ALTERNATIVE MODELS PROJECT

Swedish Nuclear Fuel and Waste Management Company (SKB) is responsible for the safe handling and disposal of nuclear wastes in Sweden. This responsibility includes conducting studies into the siting of a deep repository for high-level nuclear waste. The Safety Report for 1997 (SR 97) will present a performance assessment (PA) of the overall long-term safety of a deep repository at three hypothetical sites in Sweden. This will include hydrogeologic modeling to examine the possible transport of radionuclides from the emplaced waste packages through the host rock to the accessible environment. One important subtask of SR 97 is the Alternative Models Project (AMP), which is a comparison of three alternative modeling approaches to bedrock PA.

The overall goal of the AMP is to illustrate the consequences of the three primary alternative modeling approaches to PA used by SKB. These are the stochastic continuum (SC), discrete fracture network (DFN), and channel network (CN) approaches to groundwater flow and transport modeling. The AMP applies these different conceptual models to the safety assessment of a single hypothetical site for a deep bedrock repository for high-level wastes. The stated objectives of the AMP are:

- to illustrate rock barrier performance using three alternative conceptual models for groundwater flow and mass transport in fractured rocks, and
- to show the robustness of each assessment model in terms of relevant far field performance measures.

The emphasis of the AMP is that the results of the three approaches should be as comparable as possible. To help achieve this goal, Ström and Selroos (1997) have described the specific project requirements of the AMP. The hypothetical site, arbitrarily named Aberg, adopts input parameters from the Äspö Hard Rock Laboratory in southern Sweden, a site previously investigated by SKB. Rhén et al. (1997) and Walker et al. (1997) document the data. The models are restricted to treat an explicit domain, boundary conditions and canister locations. The size of the domain and its boundary conditions are based on the regional groundwater model of Svensson (1997). The canisters locations are based on a study by Munier et al. (1997).

This report presents an application of the discrete fracture pathways approach to the Aberg site within the context of the SR 97 Alternative Models Project.

1.2 METHODOLOGY

Figure 1-1 illustrates the approach taken by the current project. The project starts with a consensus regarding the Aberg hydrogeological model and repository layout. The hydrogeological model was defined by hydraulic boundary conditions on the edges of a 2 000 x 2 000 x 1 000 m³ rock block. The repository is defined by canister locations, without any consideration for emplacement or access drifts. This model is supplemented using discrete fracture statistical descriptions based on previous SKB reports (Uchida et al., 1994; Follin and Hermanson, 1996; Dershowitz et al., 1996). These discrete fracture networks are then converted to approximately equivalent pipe networks, where the pipe networks are defined to have equivalent connectivity, flow rate, and transport properties as the plate fractures which they are representing. Flow simulations are carried out in the pipe network to determine the head field within the model. Finally, down-gradient pathways are identified from a representative percentage of the repository canisters to discharge boundaries, and the properties of these pathways are calculated.

The project used the following software:

- **Microstation:** Generation of deterministic fractures representing planar fracture zones
- **FracMan/FracWorks:** Discrete fracture generation for stochastic fractures
- **FracMan/GenPipes:** Converts fracture (2-D) networks to pipe (1-D) networks
- **FracMan/EdPipe:** Assigns boundary conditions to pipe network
- **FracMan/MAFIC:** Solves head fields within pipe networks consistent with prescribed head boundary conditions
- **FracMan/PAWorks:** Identifies and characterizes pathways through pipe networks, using graph theory algorithms

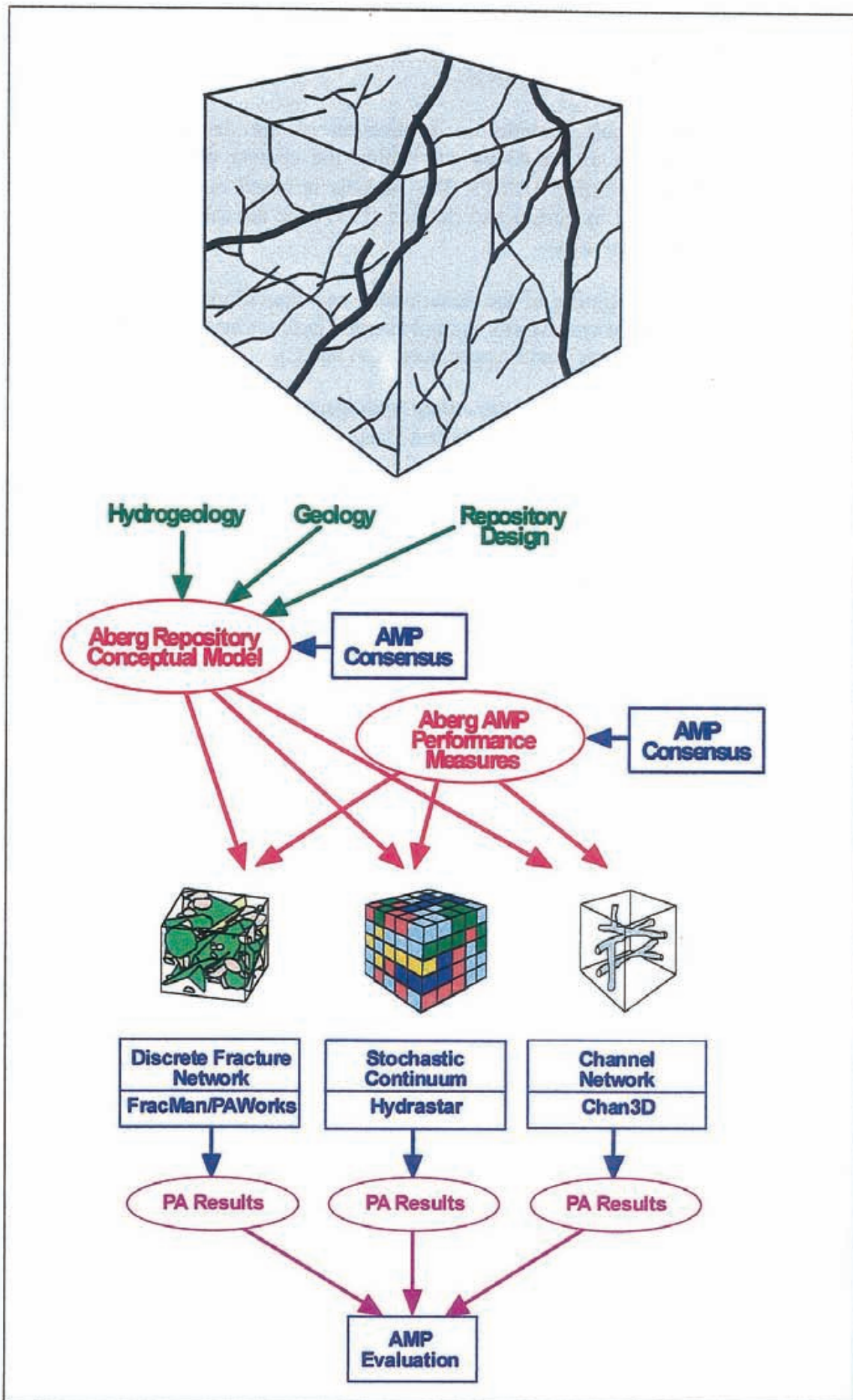


Figure 1-1 The Alternative Models Project approach.

1.3 SCOPE OF WORK

This report presents an application of the discrete fracture pathways approach to the Aberg site within the context of the SR 97 Alternative Models Project (AMP). The analysis is based on consensus assumptions provided by Ström and Selroos (1997) for the sake of AMP. The present report provides:

- description of the assumptions and limitations of the discrete fracture pathways analysis as implemented in FracMan/PAWorks for this project (Chapter 2 and Appendices A, B and C),
- parameters for the Aberg hydrogeological model and repository layout as implemented (Chapters 3 and 4), and
- pathways analysis results in formats for input to FARF31 (Norman and Kjellbert, 1990) and COMP23 (Romero et al., 1995) codes, and additional analyses of pathway connectivity to canisters (Chapter 5 and Appendix D).

Chapters 6 and 7 provide conclusions and acknowledgments.

2. MODELING APPROACH

2.1 THE PA MODEL CHAIN

COMP23 (Romero et al., 1995) and **FARF31** (Norman and Kjellbert, 1990) are SKB's performance assessment transport codes in the geosphere portion of the performance assessment model chain developed by SKB for use as a computational tool in the 1995 SKB safety analysis project (SR 95). Figure 2-1 illustrates the PA model chain, whose end product is the calculation of the probable doses to the biosphere.

COMP23 is the near-field model, which uses the canister fluxes to determine the release rate for radionuclides from the emplaced canisters and into the groundwater flow system.

FARF31 uses both the release rates from the canisters and the travel paths through the groundwater flow system to determine the far-field travel time and probable radionuclide flux to the biosphere (SKB, 1996).

The hydrogeologic model in SR 95 was **HYDRASTAR** (Norman, 1992), which was used to determine the Darcy groundwater flux at the canisters (canister flux) and the advective travel paths through the geosphere.

The AMP deals with hydrogeologic portion of the model chain only and this report presents an application of **FracMan/PAWorks** as an alternative to using **HYDRASTAR** or **CHAN3D** (cf. Figure 1-1).

2.2 FRACTURE HYDROGEOLOGY

Discrete fracture hydrogeology is based on two fundamental empirical observations:

1. Flow and transport in geological materials is controlled by structural features.
2. The hydraulic conductivity of geological materials tends to follow a log normal or similarly skewed distribution.

As a result of the first observation, it is desirable to have a hydrogeological model which can model structural features to as fine a level of detail as possible. As a consequence of the second, it is possible to consider only a small portion of geological features.

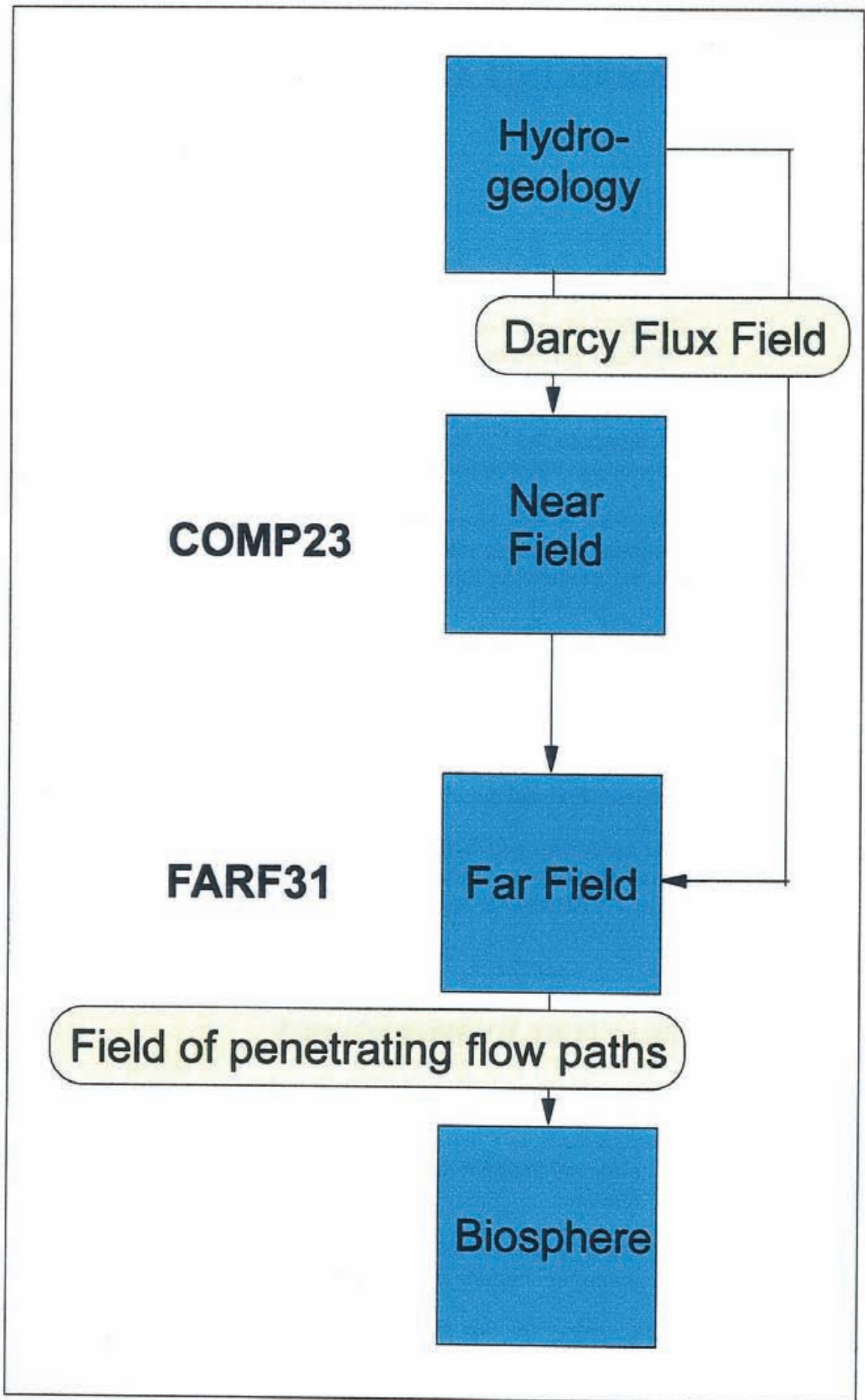


Figure 2-1 SKB SR 95 PA model chain. In the AMP the hydrogeologic information is generated with alternative conceptual models for groundwater flow and mass transport.

As a result of the second observation, it can be assumed that the vast majority of the geological material will not contribute significantly to the effective hydraulic properties, and can therefore be ignored. This leads to the use of a discrete fracture network (DFN) approach which concentrates on an accurate representation of conductive structures and flow barriers, sacrificing accuracy in the representation of smaller scale or less transmissive features.

The conceptual model used in the DFN approach assumes that discrete fractures provide the primary hydraulic flow paths and connections, and that accurate representation of flow path geometry is a key to successful hydrogeologic analysis. Discrete fractures may be fractures, faults, karsts, or paleochannels, depending on the scale and geology. Discrete fractures may be either one, two, or three dimensional features, but are generally modeled as polygons. Discrete fractures are generated in realistic three dimensional networks based on structural geology and statistical information, and can be conditioned to local measurements. Interaction between discrete fractures and the rock matrix is represented using 1-D approximate dual-porosity approaches, true dual-permeability approaches, or is ignored altogether.

2.2.1 Assumptions and Limitations

The key assumption and limitations of the DFN approach as applied in this project are shown in Figure 2-2 and may be summarized as follows:

Assumption 1: The rock matrix permeability can be represented by a proportional increase in the transmissivity for a subset of all discrete features, without a significant loss in effective permeability or connectivity.

Assumption 2: A range of scales of discrete features can be used to represent flow and transport behavior at any scale.

Assumption 3: Discrete feature geometric and hydraulic properties can be derived from structural information and hydraulic tests.

Assumption 4: Discrete features can be represented by a combination of simple one, two, and three dimensional structures such as plates, pipes, and prisms.

Assumption 5: Flow and transport in discrete features can be described by the same laws as used for continuum approaches (i.e., the Navier-Stokes and Darcy equations for flow, and the advection-dispersion equation for transport).

Assumption 6: Meaningful boundary conditions can be defined and assigned to discrete features at the edge of the model.

Assumption 7: Discrete features which have not been intersected or measured can be described statistically based on those features which have been intersected and characterized.

Assumption 8: Practical problems can be described by a limited number of stochastic realizations of the fracture pattern.

Limitation 1: The number of discrete features which can be modeled is limited by available computational power. The number of discrete features necessary for hydrogeological modeling at a given scale may be greater than that which can be modeled.

Limitation 2: Data may be insufficient to provide appropriate statistics for stochastically generated features.

Limitation 3: Hydraulically significant features may have different properties from the geologically identified features used to generate statistics.

Limitation 4: More complex geological structures may be difficult to represent by simple geometric features.

Limitation 5: Matrix permeability may play an important role in connectivity.

2.2.2 Governing Equations

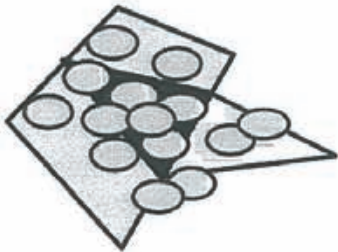
The governing equations assumed for flow in fracture planes are described in detail in the MAFIC User's Manual (Miller et al., 1994). PAWorks uses 1-D finite elements in order to describe the pipe network. The equations for 1-D pipe flow used in this project are provided in Appendix A.



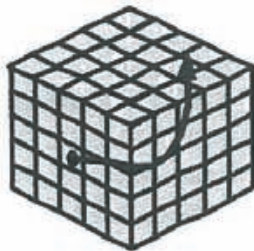
(a) Flow occurs primarily through fracture planes, not rock matrix



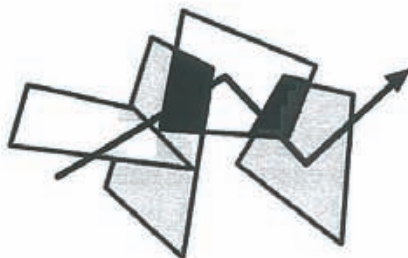
(b) Flow occurs on a defined portion of fracture surface, proportional to the areas between traces



(c) At larger scales, smaller or less transmissive fracture can be ignored or combined to effective properties of larger fractures



(d) Boundary Conditions can be defined as a head or flux at model edges



(e) Pathways and effective pathways can be identified by graphical searches

Figure 2-2 Assumption and limitations of the DFN approach in this project.

2.3 PATHWAYS ANALYSIS

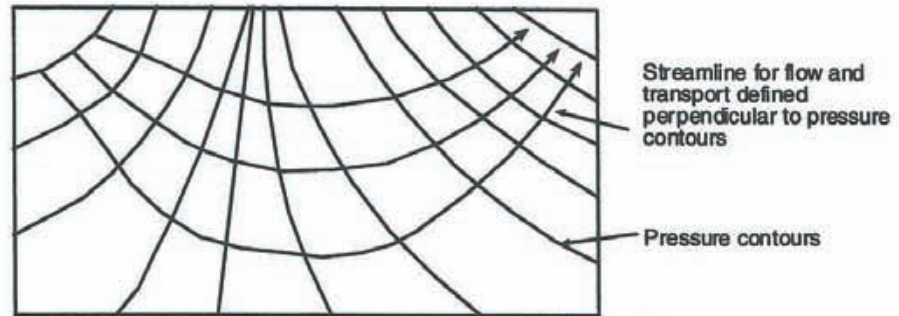
Performance assessment transport codes such as FARF31 (Norman and Kjellbert, 1990) and RIP (Miller et al., 1996) assume that groundwater transport in sparsely fractured crystalline rock can be simplified to a series of simple pipe pathways between the repository and the environmental “compliance boundary”. These boundaries, at which doses to humans are calculated, may be the ground surface, specific geological features, or arbitrary surfaces, depending on the specific application.

In general, these simple pipe transport pathways are derived from continuum streamlines. By definition, streamlines assume steady-state and a single fluid of constant density. However, the continuum streamline is not appropriate for fractured rocks such as those which are expected at many repository sites. Therefore, a more sophisticated method for deriving transport path geometries and properties is required.

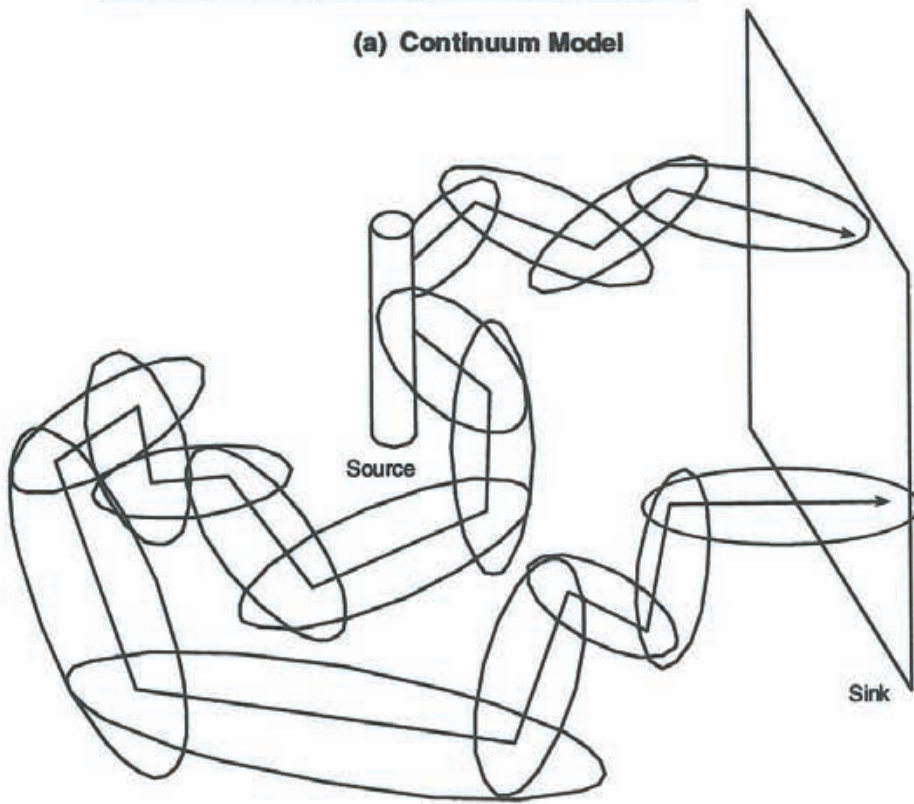
Continuum codes assume that solute transport can be described by a smooth, continuous field of streamlines, representing flow pathways. The number of pathways can be defined arbitrarily, dependent only on the contouring interval used for the pressure iso-contours perpendicular to the streamlines (Figure 2-3a). In fractured rock, the situation is quite different. The geometry of transport pathways is controlled by the geometry of discrete fractures, and cannot be defined based on pressure iso-contours (Figure 2-3b). FracMan/FracWorks generates realistic, three-dimensional fracture geometries, and is therefore an ideal method for deriving the pathways to be used in performance assessment calculations.

The approach used for the derivation of performance assessment pathways with PAWorks is illustrated in Figure 2-4. First, FracMan/FracWorks is used to generate stochastic fracture geometries based on the reference site data. The geometry of the pathways to be considered then need to be defined in terms of sources and sinks. The sources and sinks may be defined as boreholes, planar surfaces or fractures (Figure 2-5). Boundary conditions are then assigned and a finite element method is used to calculate heads within the fracture network. In the current study, the pathway source is defined by the canister emplacement holes, and the sink is defined by the top surface of the model (Figure 2-6). PAWorks then follows the gradient within the fracture network from the source locations to the sink locations. PAWorks uses a graph theory search to identify and characterize pathways between the sources and sinks. Note that the pathway algorithm is following the local gradients within the fracture network, which may be different in direction and magnitude from the applied regional gradient.

Flow and transport through fracture networks is constrained to occur through 3-D networks of interconnected 2-D fractures (planes). However, PAWorks use 1-D pipes (lines) to represent transport. Appendix B describes the simplifications of the topology of the fracture network as applied in this project.



(a) Continuum Model



(b) Pathways Controlled by Fracture Geometry

Figure 2-3 Pathways using continuum and discrete approaches.

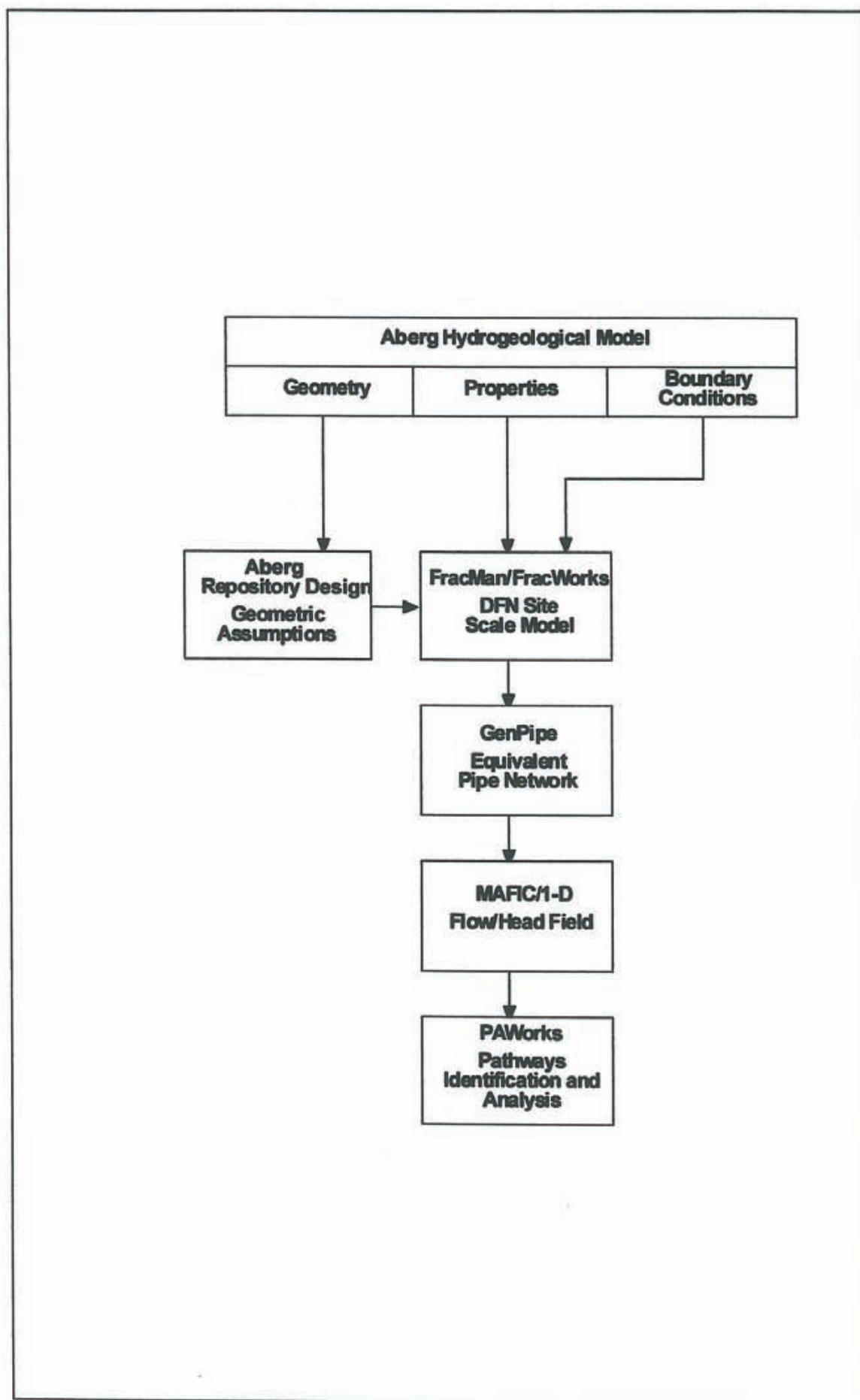


Figure 2-4 Discrete fracture pathways analysis flow chart.

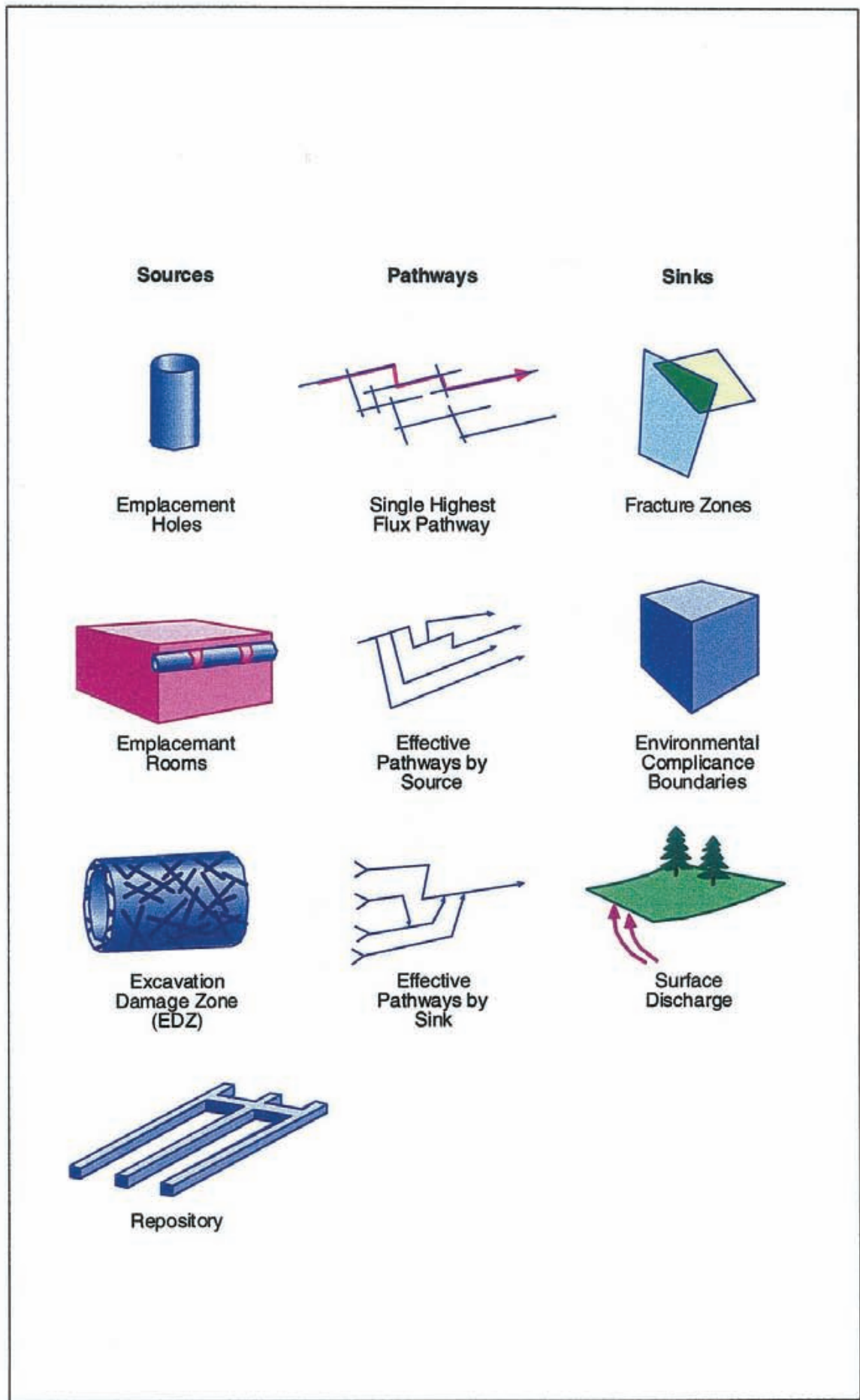


Figure 2-5 Pathways analysis schematic.

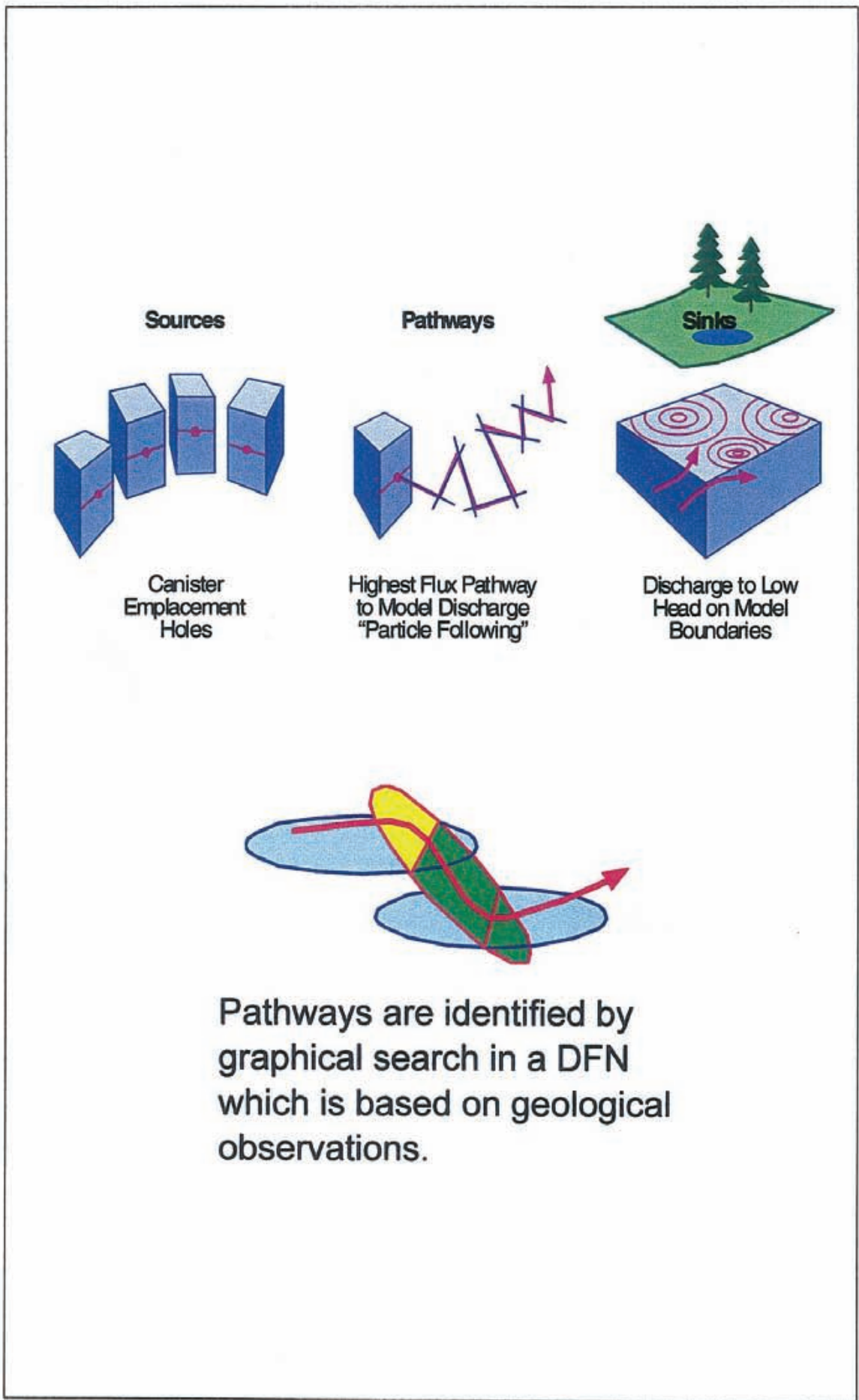


Figure 2-6 Pathways for AMP.

2.4 PATHWAY SEARCH

The pathway search algorithm is designed to identify the preferential pathways between specified sources and sinks. Preferential pathways are identified based on a combination of the geometry of the pipe network and a user assigned criteria.

Pathways are identified using a weighted, directed “priority first” graph algorithm. This search algorithm is based on Segdewick (1988). The priority first search uses the weights on each pipe to determine the pathway which optimizes the pathway criteria, and then looks for the pipe which is the second closest to matching that criteria. The search algorithm identifies a set of non-reentrant paths, including the “highest priority” path, based on the criteria established by the user. The algorithm does not identify all combinations of possible paths. The weighted, priority order search is summarized as follows:

1. All pipes directly connected to the source are identified, and the pipe with the highest value of the user specified “priority” ranking is selected and marked. In the current study, the source is defined by the canister hole fractures, and the priority ranking is based on flow rate.
2. All of the unmarked pipes directly connected to the marked pipe are identified.
3. The process is repeated until either a dead end or the sink is reached. When the sink is reached, all of the pipes which makeup the pathway are marked “visited”.
4. As the pathway is identified, the pathway properties are calculated using the equations below.

PAWorks also offers the option to search different branches. The same starting point is used but at the first possible location a different branch than that for the previous pathway is chosen. This branch is followed using the same approach until the sink is reached. Branches are selected in order of the strength of the branch as a percentage of the flow rate entering the intersection. The process is repeated until the specified maximum number of branches or maximum number of pathways is reached.

A preliminary study showed that by using the branch option with the Aberg fracture model a high number of very similar pathways was generated. This is due to the good connectivity within the repository scale fracture population and the less connected surrounding fracture and fracture zone network. Therefore this option was not used in the current study. Only the main branch with the highest flow rate was analyzed. The current analysis defines path priority by flow rate, which provides results similar to those obtained by particle tracking. Alternatively, the path priority could be based on transmissivity, resistance, or travel time.

2.5 EFFECTIVE PATHWAYS

The pathway search algorithm identifies the individual pathways from sources to sinks. These pathways consist of multiple elements (pipes). In the current study, an effective pathway is defined as a single homogeneous pipe connecting source to sink. Because no different branches for the same starting pipe were computed there is no need to average properties over different branches of a pathway. Hence, the effective properties of a pathway are only calculated from the series of pipes making up that pathway. This is considerably simpler than the approach used in the previous study (Dershowitz et al., 1997), where effective pathways were defined by a series circuit of fine segments.

One goal of PAWorks is to estimate the conductance, transmissivity, conductivity, and geometric properties of a representative pipe connecting source to sink. PAWorks can calculate these properties using two models:

1. The individual and representative pathways are rectangular pipe channels (idealized to be between two parallel surfaces) of specific length, width, and aperture, or
2. The individual and representative pathways are cylindrical tubes of specific length and radius.

These models represent extremes of possible fracture flow behavior; it is likely that flow will neither be perfectly even as between two parallel surfaces nor completely channelized into a single cylindrical tube.

In this study, effective pathway properties are calculated and reported based on the rectangular pipe model (Figure 2-7). The calculations used in this project are shown in Appendix C.

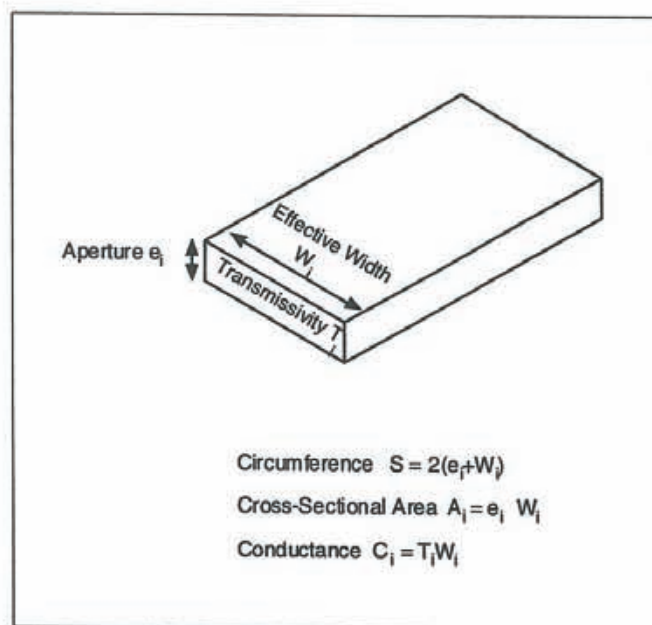


Figure 2-7 Rectangular Pipe geometry schematic.

2.6 SR 97 PARAMETERS

The FracMan/PAWorks approach provides complete information about the pathways from the canister hole to the accessible environment, including the geometry of the pathway, the variation in velocity and geochemistry, and the location of discharge. However, for the purposes of the present project, the AMP determined that only a few parameters directly related to the codes FARF31 and COMP23 need be calculated.

2.6.1 FARF31

The parameters specified by the AMP for FARF31 are:

- **F-Factor:** The normalized area along the pathway that is available for diffusion and sorption processes [TL^{-1}].
- **Travel Time:** The advective residence time from a canister location to the environmental discharge [T].

F-Factor

The F-Factor F_{pipe} is calculated for each pipe as:

$$F_{\text{pipe}} = 2 W_{\text{pipe}} L_{\text{pipe}} / Q_{\text{pipe}} \quad (2-1)$$

where W_{pipe} is the pipe width [L], L_{pipe} is the pipe length [L], and Q_{pipe} is the pipe flow rate [L^3T^{-1}].

The effective F-Factor F_{path} for the pathway is calculated as the sum of the F-Factors F_{pipe} for all of the pipes which make up the pathway:

$$F_{\text{path}} = \sum F_{\text{pipe}} \quad (2-2)$$

Travel Time

The travel time t_{pipe} for each pipe in each pathway is calculated as:

$$t_{\text{pipe}} = L_{\text{pipe}} a_{\text{pipe}} W_{\text{pipe}} / Q_{\text{pipe}} \quad (2-3)$$

where L_{pipe} is the pipe length [L], a_{pipe} is the pipe aperture [L], W_{pipe} is the pipe width [L], and Q_{pipe} is the pipe flow rate [L^3T^{-1}].

The travel time t_{path} for a pathway is calculated as the sum of the travel times for the pipes which make up the pathway:

$$t_{\text{path}} = \sum t_{\text{pipe}} \quad (2-4)$$

2.6.2 COMP23

The only parameter required by **COMP23** from this study is:

- **Canister Flux:** The Darcy flux (flow rate per unit area) past a representative canister location [LT^{-1}].

The value provided for this parameter depends on whether the canister is assumed to effect the flow field or not. In a previous study (Dershowitz et al., 1996), flow was assumed to be routed around the canisters such that the flow is concentrated in the canister perimeter (Figure 2-8a). This was modeled by reducing the transmissivity of fractures within the canister emplacement holes to zero, while representing the canister emplacement holes by features with a transmissivity of $10^{-8} \text{ m}^2/\text{s}$ (Figure 2-8b).

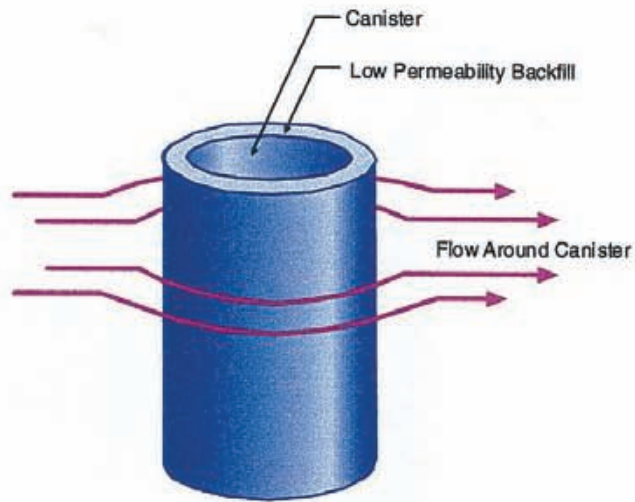
In the present exercise, the canister holes are assumed to have no net effect on the flow system - neither enhancing the flow along the holes, nor reducing the net flow. This is modeled by representing the canister holes by fractures with a transmissivity of $10^{-20} \text{ m}^2/\text{s}$, but not removing the connections through the canister holes. Clearly, this is not meant to imply that the fractures extending through the canister holes continue to exist even after the holes are constructed. However, if the canister holes do not influence the flow field, the flow through the canister holes would be rerouted into the portions of the fractures around the canister holes such that the net flow rate would be unchanged (Figure 2-8c).

The input to **COMP23** is calculated as follows. For each canister hole, PAWorks identifies pipes bringing flow rate to the canister hole, through the canister hole, and away from the canister hole (Figure 2-9). PAWorks calculates the sum of the flow rates away from the canister hole, as an approximation to the flow rate past the canister hole. The flow rate can be due to one or more pathways.

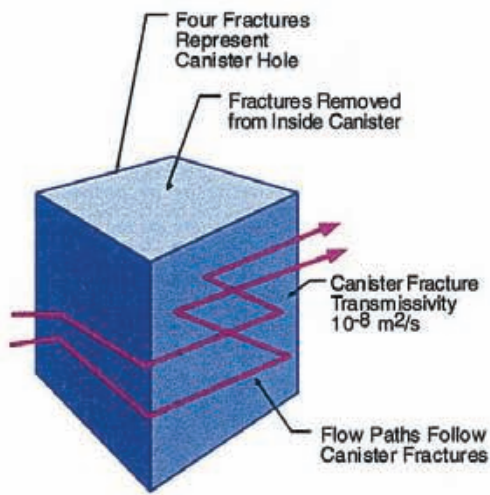
Canister flow statistics are reported as flow rate divided by the cross sectional area of the canister holes, which is 13.71 m^2 (1.75m OD by 7.833 m length). This is done due to the input requirements of **COMP23**.

2.6.3 Other Parameters

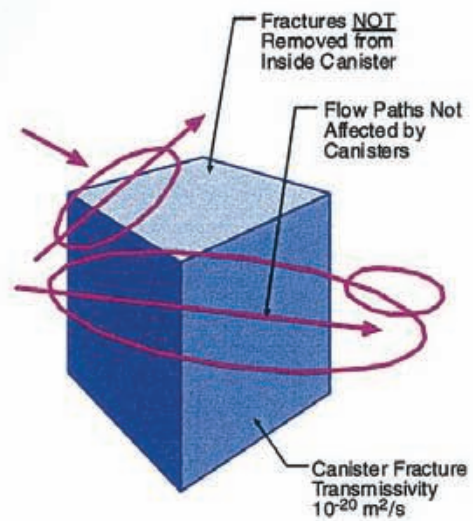
It should be noted that the discrete fracture pathways approach can provide a variety of useful information in addition to the **FARF31** and **COMP23** parameters above. For instance, for each pathway PAWorks can report pathway length, pathway width, pathway aperture, reactive surface area and transmissivity. Due to the large amount of statistics concerning the parameters for **FARF31** and **COMP23** specified by Ström and Selroos (1997) the amount of additional information presented in this report is limited (see Section 5.5).



(a) Canister Hole In-Situ

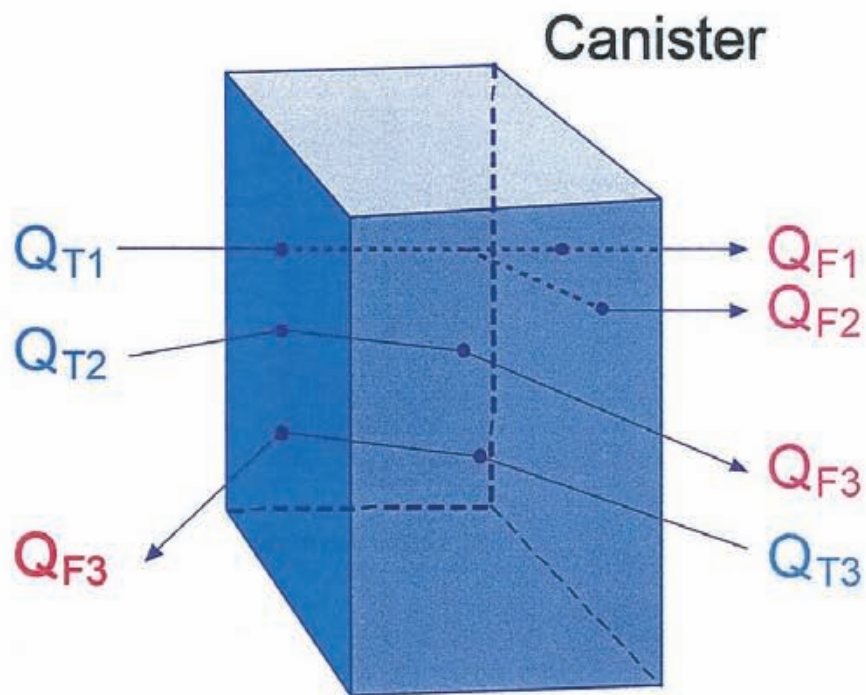


(b) Modeling Approach from Dershowitz et al (1996)



(c) Current Modeling Approach

Figure 2-8 Canister representation.



$$q_{\text{COMP23}} = (\text{Sum of all } Q_{Fi}) / A$$

Q_T = Flow rate into canister

Q_F = Flow rate from canister

A = Surface area of canister

Figure 2-9 COMP23 flux post canister.

3. GENERAL PREMISES

The memo by Ström and Selroos (1997) explicitly specifies the extent and boundary conditions for the model domain, the geologic structures, the waste canister locations and the transmissivities to be used for this application of FracMan.

3.1 SITE DESCRIPTION

Aberg takes its data from the Äspö site, which is located in southern Sweden, in the northern part of Småland (Figure 3-1). It is just off the Swedish coast in the Baltic Sea, near Oskarshamn nuclear power plant. The Äspö site is also the location of the Äspö Hard Rock Laboratory (HRL), an underground research facility owned and operated by SKB. From a hydrogeologic perspective, the region is notable for the low topographic relief, intrusion of saltwater from the Baltic Sea and the fracturing associated with the Äspö shear zone.

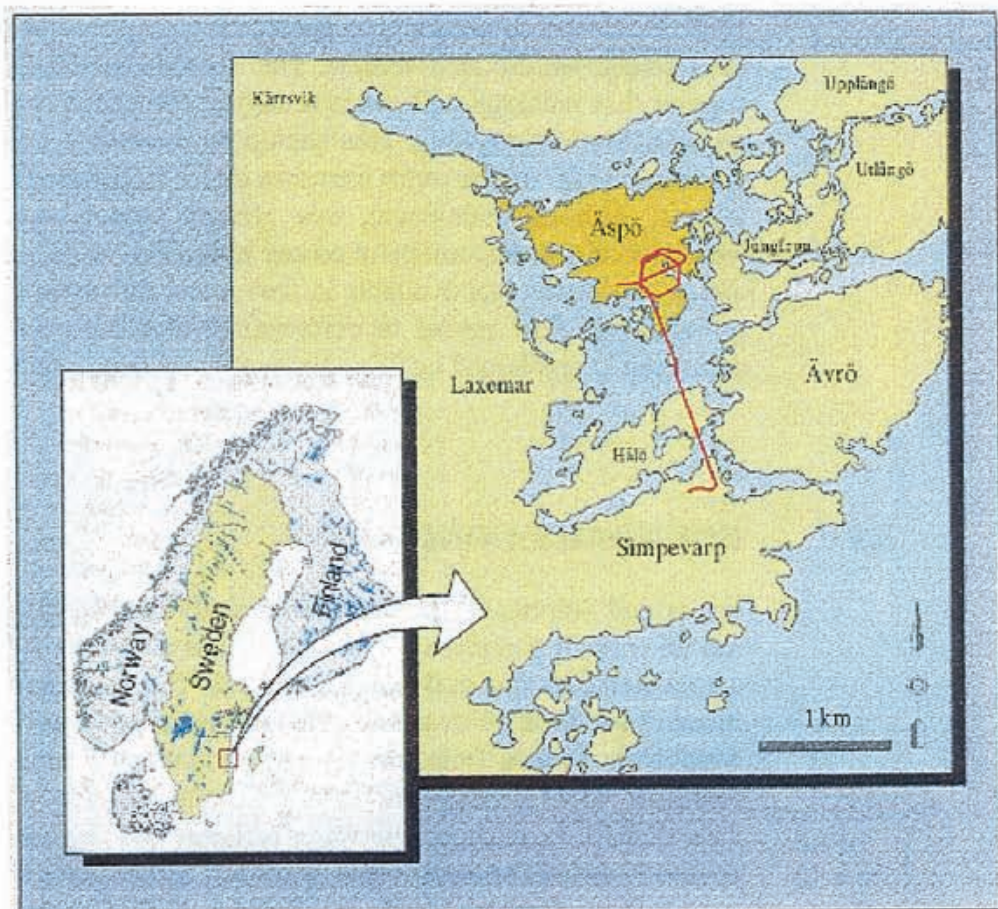


Figure 3-1 Location of Äspö and the Hard Rock Laboratory.

3.2 HYDROGEOLOGY

The geology and hydrogeology of the Äspö site has been studied in detail and are summarized in a series of reports (Wikberg et al., 1991; Rhén et al., 1997). A summary of site conditions emphasizing continuum modeling is presented by Walker et al. (1997).

Äspö regional geology is typical of coastal Scandinavia, with crystalline bedrock dominated by the heterogeneous Småland granite suite. The Äspö shear zone, running SW-NE through Äspö Island divides the bedrock into two parts. The region continues to experience isostatic rebound as a consequence of the last period of continental glaciation. This glaciation also deposited boulder till throughout the region. Peat lands are found in some depressions, as are fluvial sand and gravel. The soil cover is thin with numerous bedrock outcrops. Regional lineaments have been mapped and examined by various air photo, aerogeophysical, outcrop, seismic and borehole studies, revealing a number of major discontinuities that have been interpreted as steeply dipping fracture zones. The salinity profile of the groundwater system is typical of islands and coastal areas: fresh groundwater near the surface rests on saline water that has intruded from the sea.

The hydrology of the area around and on Äspö was compiled during 1986-1987. Precipitation generally exceeds evapotranspiration resulting in a small net recharge on the land surface. The classical model of topographic drive suggest that recharge will occur in higher elevations and flow to discharge areas in lower elevations. This should be combined conceptually with the classical model of sea water intrusion under freshwater in coastal areas and islands. Although simplistic, this general model is consistent with the locations of streams, mires, observed hydraulic heads, salinity distributions and geochemical data available in the region. Svensson (1995, 1997) used a groundwater flow model to demonstrate that the overall flow pattern at depth can be explained by this combination of conceptual models.

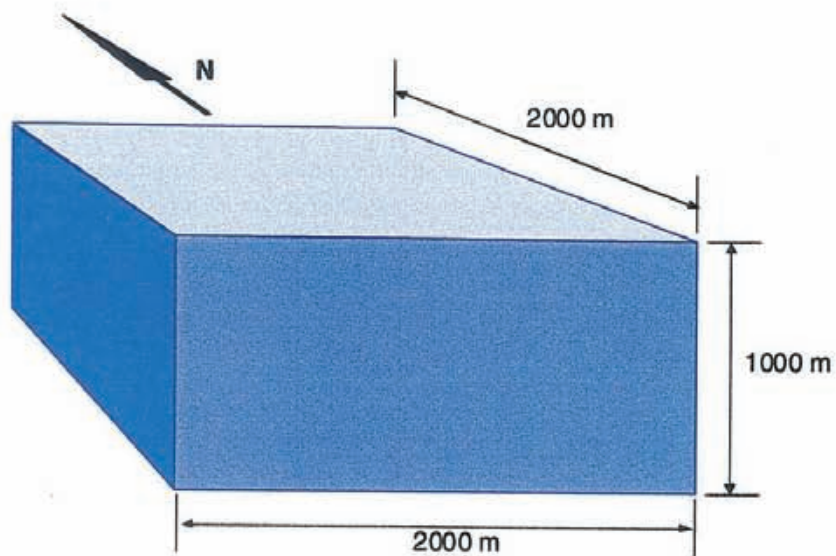
3.3 BOUNDARY CONDITIONS

Ström and Selroos (1997) specified that all three models in the AMP study use an explicit site-scale domain defined as a volume 2000 m by 2000 m of areal extent, 1000 m in depth (Figure 3-2). The upper surface of the model is given at sea level (0 masl). All of the AMP models are to rely on boundary conditions derived from the regional groundwater flow modeling study of Svensson (1997). Svensson used a finite difference continuum model, PHOENICS, to study ground water recharge and regional flow patterns. The results included the steady-state heads and fluxes along the limits of the site-scale model domain. Ström and Selroos (1997) specified that these head values should be used as constant head (Dirichlet) boundary conditions by all three of the AMP studies.

Figure 3-3 shows the fresh-water head contours at the Äspö Datum Level (0 masl) as used in this project. The contours are based on an interpolation of the results presented by Svensson (1997). The plus and minus signs denote local discharge (+) and recharge (-) areas.

Figure 3-4 shows the integrated flow rates for each of the six external boundaries using the results presented by Svensson (1997). The values of the flow arrows indicate that recharge to the model domain occurs predominantly across the western boundary, whereas discharge from the model domain occurs predominantly across the top boundary. Hence, the overall flow pattern is that of recharge on the inland areas discharging to the coastal waters.

Coordinate		
	Äspö	FracMan
East =	+1000	Y = -1000
North =	+8000	X = -1000
Up =	0	Z = 500



Coordinate		
	Äspö	FracMan
East =	+3000	Y = 1000
North =	+6000	X = 1000
Up =	-1000	Z = -500

Figure 3-2 Aberg model region.

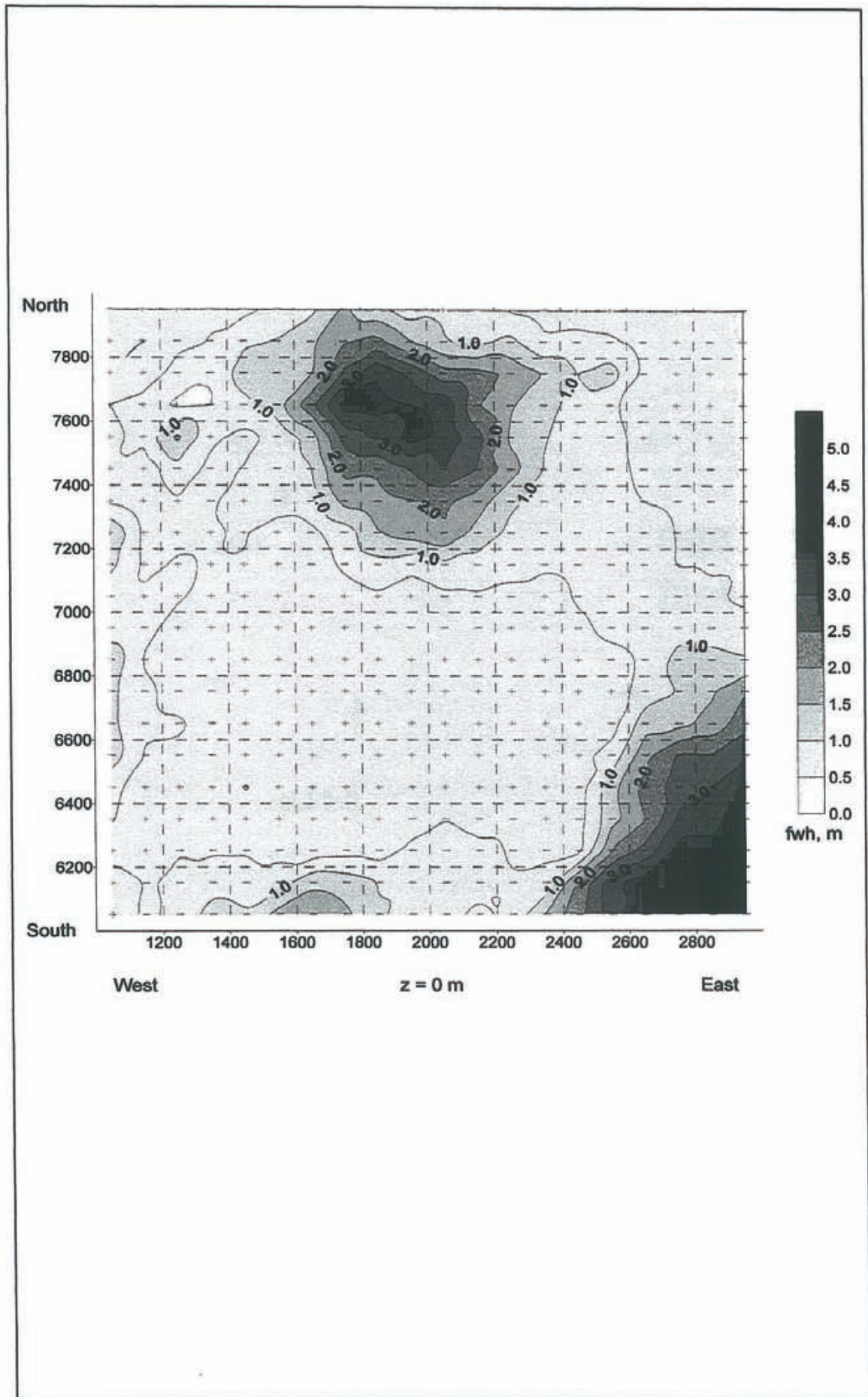


Figure 3-3 Interpolated fresh-water heads for the top boundary based on the results reported by Svensson (1997). The plus and minus signs denote local discharge (+) and recharge (-) areas..

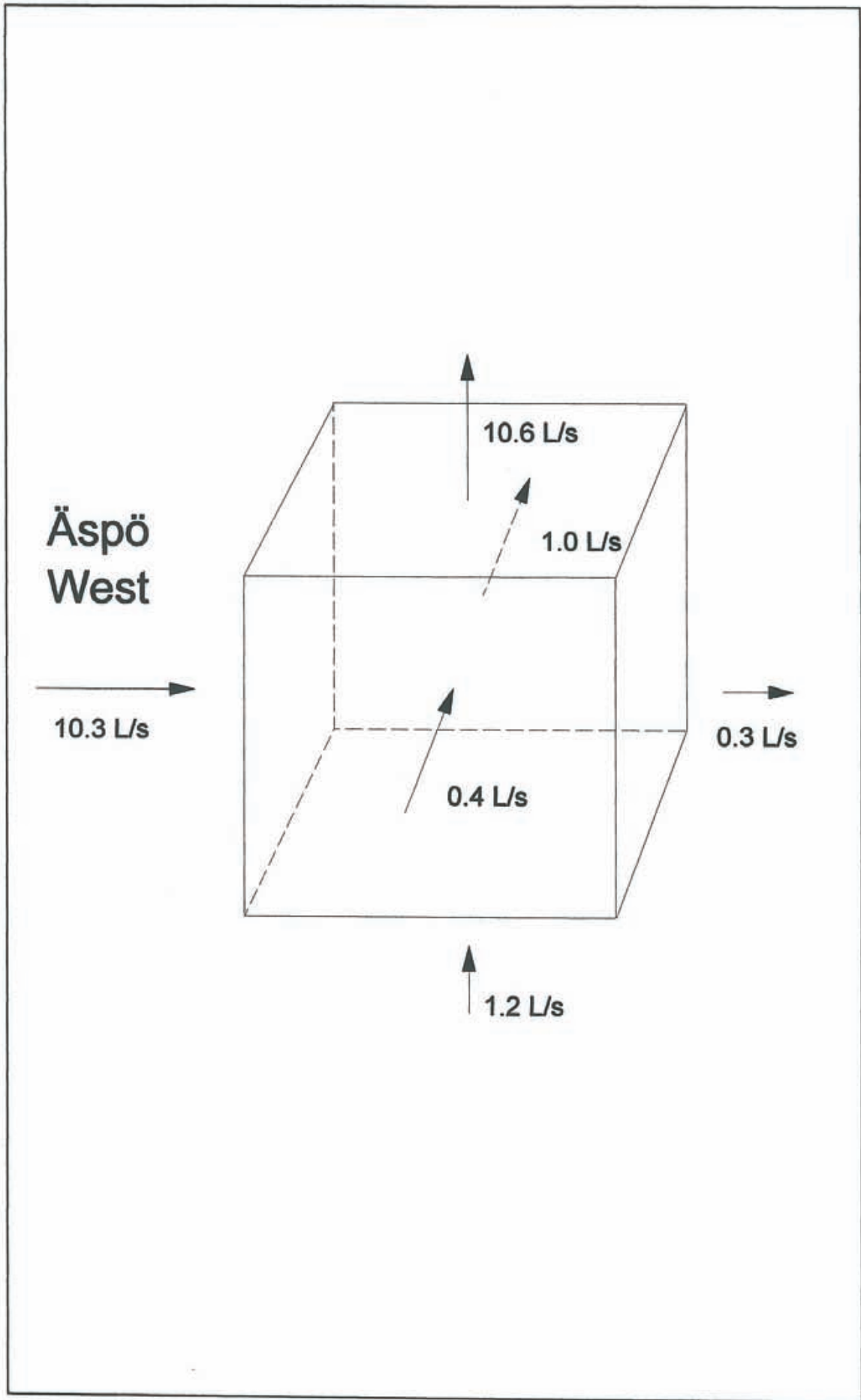


Figure 3-4 Interpolated flow rates for each of six external boundaries (Svensson, 1997).

4

ABERG DFN SITE MODEL

This section describes the Aberg reference FracMan model developed for the AMP of SR 97. At the time of this project model simulations of the hydrogeology at Aberg have been performed on a regional scale by Svensson (1997). Figure 4-1 shows the extent of the regional study as well as the location of the simulation domain for the AMP. The Äspö coordinates of the simulation domain are shown in Table 4-1. The size and location of the domain is chosen so that the discharge areas for the optimized layout (see, Munier et al., 1997) will be in the center.

Table 4-1 Äspö coordinates of the simulation domain to be used in the AMP (Ström and Selroos, 1997).

Coordinate	Positive direction	Minimum	Maximum
x	East	+1000	+3000
y	North	+6000	+8000
z	Up	-1000	0

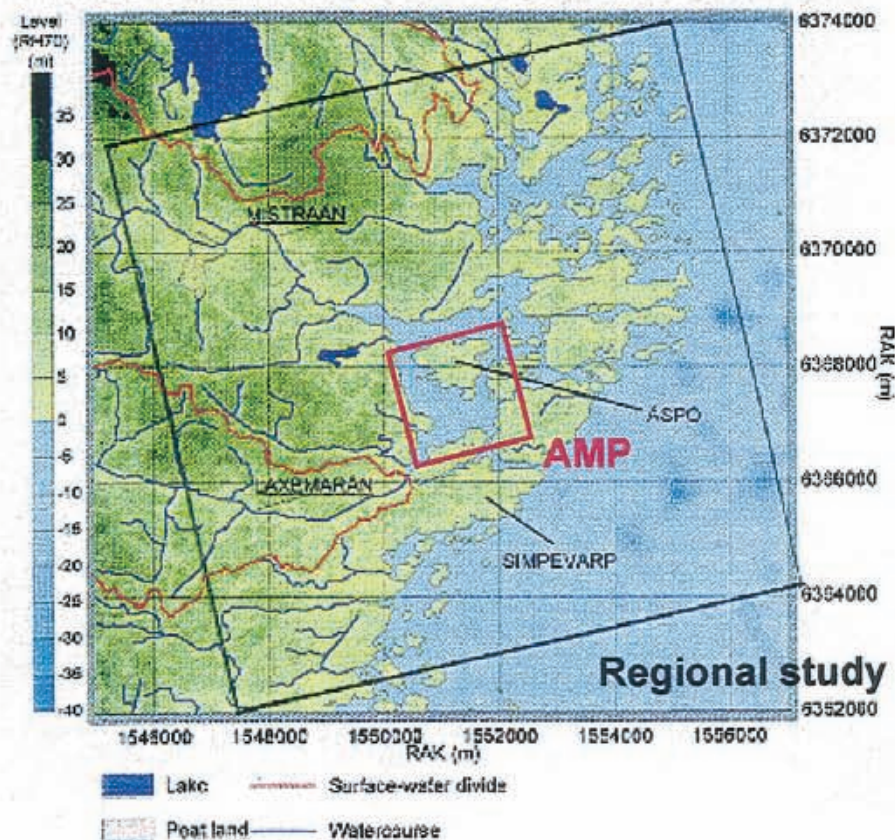


Figure 4-1 Areal extent of the regional study by Svensson (1997) as well as the location of the simulation domain for the AMP.

To facilitate FracMan/PAWorks modeling, the model utilized a detailed region in the direct vicinity of the repository, together with a less detailed region at the Äspö island site scale:

Generation Region: The fracture generation region was established by (Ström and Selroos, 1997) for the sake of the AMP as a 2000 m by 2000 m by 1000 m rock volume (Figure 4-2). Within this region, only fracture zones and the larger stochastic discrete fractures (model scale fractures) are simulated based on Rhén et al. (1997) and Uchida et al. (1994). Smaller stochastic fractures could not be modeled on a model scale due to computational constraints. Sensitivity studies have not been carried out to determine the effect of this truncation.

Repository Regions: A detailed region was defined surrounding each of the three repository sectors in the AMP reference repository (Figure 4-2). The detailed regions were defined to be large enough to provide a realistic representation of the connection from the canister emplacement boreholes to the surrounding fracture zones. This ensures both the correct hydraulic gradient through the repository area, and connectivity from the boreholes to the fracture zones for pathway formation. The repository region fracture statistics are based on Follin and Hermansson (1996). Note that fractures from the larger stochastic fracture generation region also extend through the detailed model region.

The model regions simulated are summarized in Table 4-2.

Table 4-2 Model regions simulated.

Geometric Feature	Generation Region	Repository Region
Model Region	2000 m x 2000 m x 1000 m	Sector 3: 700 x 800 x 50 m Sector 4: 600 x 600 x 50 m Sector 6: 600 x 800 x 50 m
Orientation of Major Axis (Äspö Coordinate System)	Trend $\theta = 0^\circ$ Plunge $\phi = 0^\circ$	all Sectors: Trend $\theta = 0^\circ$ Plunge $\phi = 0^\circ$
Orientation of Minor Axis (Äspö Coordinate System)	Trend $\theta = 90^\circ$ Plunge $\phi = 0^\circ$	all Sectors: Trend $\theta = 0^\circ$ Plunge $\phi = 0^\circ$
Center of Model (Äspö Coordinate System)	$X_c = 2000N$ $Y_c = 7000E$ $Z_c = -500Z$	Sector 3: $X_c = 1850N, Y_c = 7150E, Z_c = -500Z$ Sector 4: $X_c = 2400N, Y_c = 7400E, Z_c = -500Z$ Sector 6: $X_c = 2050N, Y_c = 6850E, Z_c = -500Z$
Features Modeled	Fracture Zones Stochastic Fracture Population with Radius Greater than 20 m	Emplacement Canisters Stochastic Fracture Population with Radius $0.2 \leq R \leq 20$ m

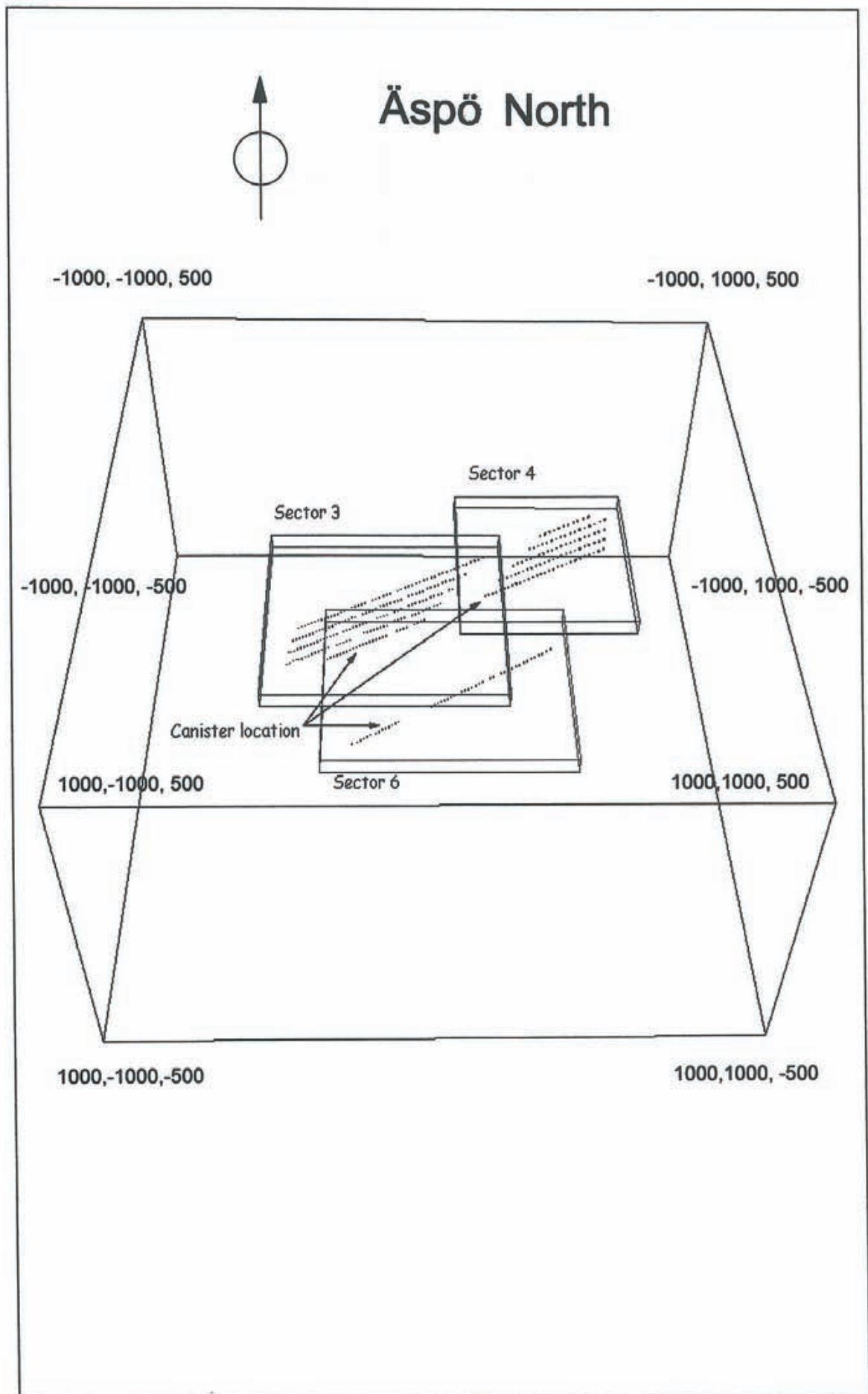


Figure 4-2 Aberg DFN model regions. FracMan coordinates.

4.1 ROCK MASS PARAMETERS

The deterministic fracture zone geometry and transmissivity for this study was based solely on Rhén et al. (1997).

The stochastic fracture geometry for this study was based primarily on TBM fracture statistics (Follin and Hermanson, 1996), supplemented by larger scale outcrop fracture statistics (Uchida and Geier, 1992). It was necessary to combine these two approaches because while significant evidence in the Äspö tunnels supports the Follin and Hermanson parameters, successful site scale modeling for the LPT-2 experiment was carried out using the statistics of Uchida et al. (1995).

In the current model it is assumed that the fracture size statistics of Uchida and Geier (1992) are applicable at the site scale, while the TBM fracture statistics should be applied within the detailed model region around the repository sectors.

The memo by Ström and Selroos (1997) specifies that the three models of the AMP should describe their input data evaluation process or model parameter abstraction process. Table 4-3 summarizes the fracture model parameters considered in the Aberg DFN site model when modeling groundwater flow using FracMan. In FracMan flow and transport through fracture networks is constrained to occur through 3-D networks of interconnected 2-D fractures (planes). However, PAWorks use 1-D pipes (lines) to represent transport. Appendix B describes the simplifications of the topology of the fracture network as applied in this project.

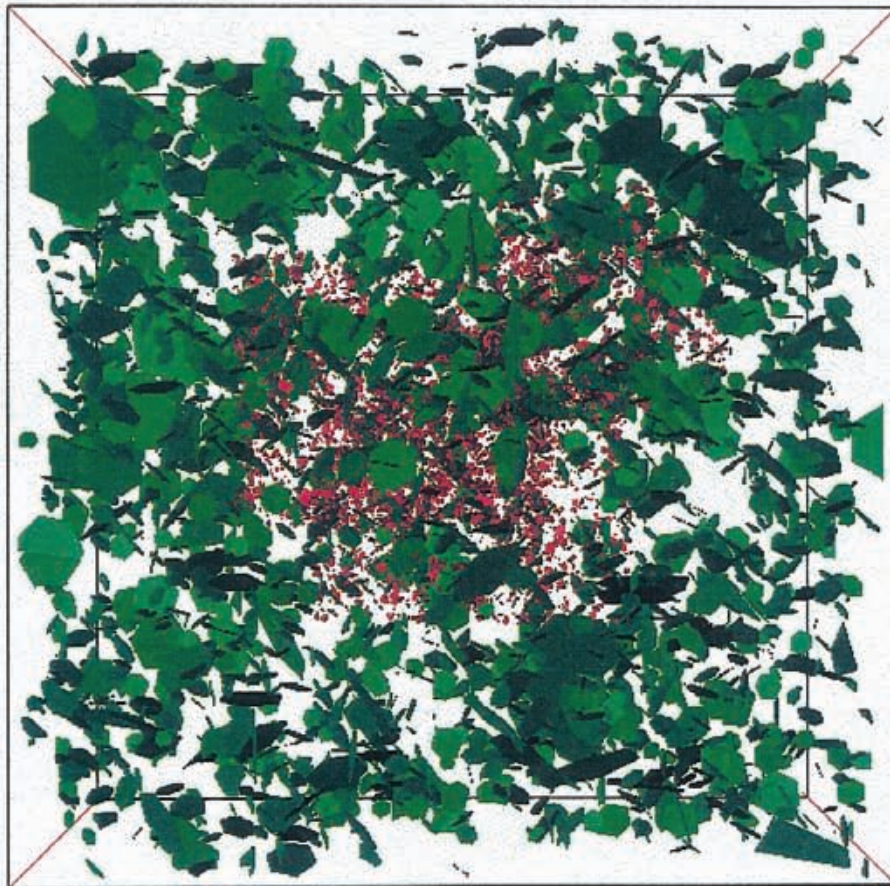
Table 4-3 Rock mass parameters considered in the Aberg DFN site model when modeling groundwater flow using FracMan.

DFN Parameter	Assumption	Basis
Generation Region	Box 2000 x 2000 x 1000 m ³	Ström and Selroos (1997)
Repository Regions (around each sector)	Sector 3: Box 700 x 800 x 50 m Sector 4: Box 600 x 600 x 50 m Sector 6: Box 600 x 800 x 50 m	Aberg repository layout (Munier et al., 1997)
Conceptual Model	BART (Enhanced Baecher)	TBM Trace Maps Follin and Hermanson (1996)
Fracture Orientation Distribution	Bootstrap ($\kappa=300$) based on fractures mapped in the TBM tunnel	TBM Trace Orientations (Terzaghi Corrected) Follin and Hermanson (1996)
Fracture Size Distribution f(R) (Model Region)	Lognormal Mean=13.7 m Std.Dev=12.7 m Truncated to 20 m ≤ R ≤ 1000m	Uchida et al. (1994)
Fracture Size Distribution f(R) (Repository Region)	Lognormal Mean=6 m Std.Dev=3 m Truncated to 0.2 ≤ R ≤ 20 m	TBM Trace Maps Follin and Hermanson (1996)
Termination Probability	37%	TBM Trace Maps Follin and Hermanson (1996)
Fracture Transmissivity Distribution f(T)	Truncated Lognormal Mean= 9.0e-7 m ² /s Std.Dev.= 5.0e-6 m ² /s T _{min} = 1.0e-09 m ² /s	LPT-2 Data Analysis (Uchida et al., 1994)
Conductive Intensity	P ₃₂ = 0.2 m ⁻¹	TBM Trace Maps (Follin and Hermanson, 1996)
Conductive Intensity (above T _{min} and R _{min})	P ₃₂ = 0.038 m ⁻¹ (Model Region) P ₃₂ = 0.2 m ⁻¹ (Repository Region)	Uchida et al. (1995)
Transport Aperture e _t	0.5 T ^{1/2}	Doe (1993)

These fracture models are illustrated in Figures 4-3 and 4-4.

For a detailed explanation of the derivation of the fracture parameters, see the references cited in Table 4-3. The derivation of fracture parameters is summarized as follows:

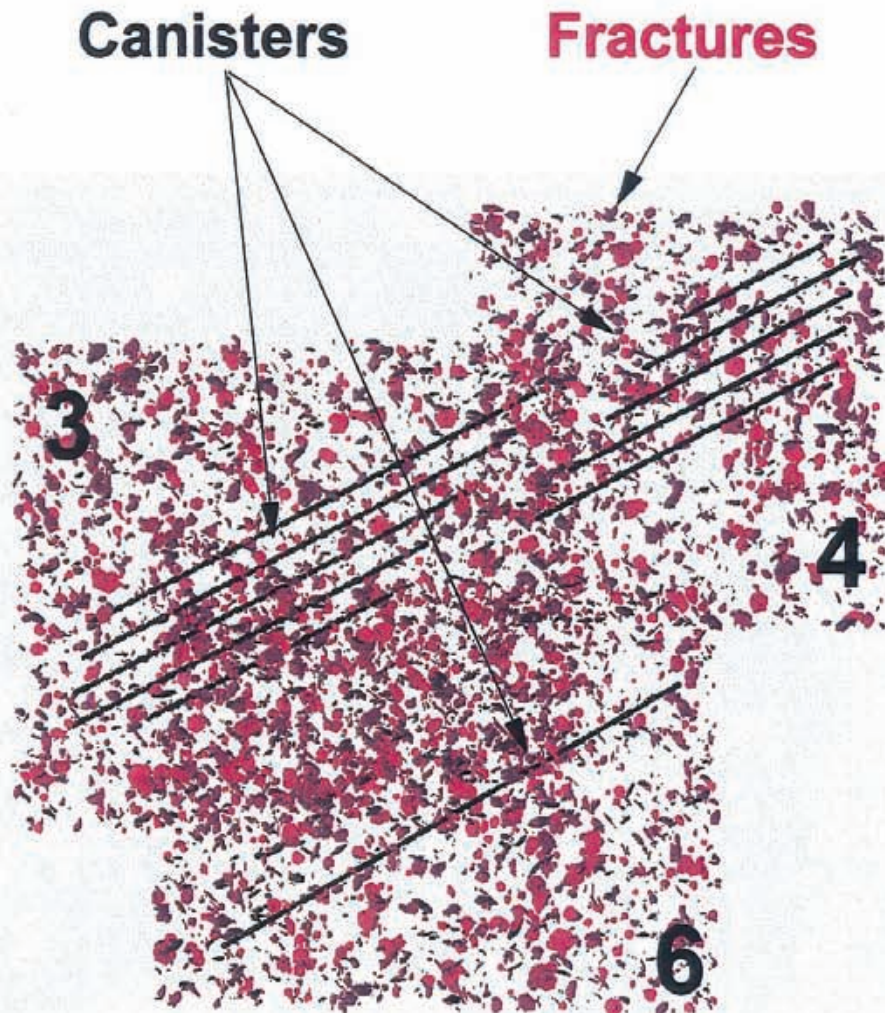
- **Fracture Spatial Pattern:** Follin and Hermansson (1996) demonstrated that 37% of mapped fractures terminate at intersections with other fractures. This can be significant for fracture connectivity and pathway formation. This was incorporated in the DFN model by using the Bart spatial location conceptual model (Dershowitz et al., 1989), which explicitly accounts for the fracture connectivity pattern. Dershowitz et al. (1996) evaluated alternative spatial models based on borehole data from the TRUE-1 area, and concluded that the BART spatial model is generally applicable.
- **Fracture Orientation:** In the absence of data to distinguish sets based on transmissivity, the fractures have been defined as a single set, using the bootstrap approach to match the measured fracture orientation distribution from the TBM tunnels to the synthetic fracture orientations. The bootstrap approach is described in Dershowitz et al. (1996).
- **Fracture Size:** The size distribution of fractures in Äspö has been studied by a number of authors, including Dershowitz et al. (1996), Uchida et al. (1994) and Follin and Hermansson (1996). The statistics of Follin and Hermansson are presumably based on conductive fractures in the TBM tunnel, and are therefore selected to represent the fractures in the repository region. The truncated model for the repository omits only fractures smaller than 0.2 m, and represents 99.73% of the population. In the larger model generation region, computational constraints require that only fractures larger than 20 m scale be included. This portion of the size distribution is not well quantified by intersections with the TBM tunnel, since this is at an extreme tail of the fracture size distribution obtained from the TBM tunnel. To obtain a better indication of this size distribution, we rely on the size distribution from significant structures mapped at the surface by Uchida and Geier (1992).
- **Fracture Intensity:** The conductive fracture intensity was addressed by Dershowitz et al. (1996), LaPointe et al. (1995a) and Uchida et al. (1995). For the present study, the conductive fracture intensity from site scale packer testing (Uchida et al., 1995) was used, rather than the higher intensity from focused testing in the TRUE-1 area (Dershowitz et al., 1996).
- **Fracture Transmissivity:** The fracture transmissivity distribution was derived from packer testing in non-fracture zone intervals, as reported by Uchida et al. (1995).
- **Fracture Transport Aperture:** Two expressions for fracture transport aperture were considered: the “cubic law” and the “Doe law” (Uchida et al., 1994). The cubic law is based on an derivation of aperture from considerations of laminar flow velocities, while the “Doe law” is concerned with the fracture volume available for storage. For transport simulations, the “Doe law” was previously used successfully in transport predictions (Uchida et al., 1994), and is therefore used in the present study.



Green = Uchida et al. (1994)

Red = Follin and Hermanson (1996)

Figure 4-3 Perspective view from the top of the model (green) and repository (red) scale fractures. 10 % of fractures are displayed.



3, 4 AND 6 ARE SECTOR NUMBERS

Figure 4-4 Repository sector scale fractures and canister locations. 10 % of fractures displayed. Sectors modeled separately.

4.2 FRACTURE ZONE PARAMETERS

The fracture zone assumptions used in the Aberg DFN site model of the AMP are based on the SKB structural model for Äspö Island (Rhén et al., 1997). The fracture zones included in the AMP Aberg DFN site model are listed in Table 4-4.

The AMP considers a simplified repository layout described in Section 4.3 and Figure 4-5. A 3-D view of the fracture zone model can be found in Figures 4-6 and 4-7. Figure 4-6 contains the fracture zones as well as the model and repository scale stochastic fracture sets. Figure 4-7 is a close-up which also shows the canister locations.

Table 4-4 Fracture zone model for Aberg AMP (after Rhén et al., 1997).

Zone name	Zones and planes defining the zone	Equation Coefficients				Transmissivity (m ² /s)	Åspö coordinates (constrained by zones, planes or by model domain)																		
		A	B	C	D		Northings	Eastings	Z	Northings	Eastings	Z	Northings	Eastings	Z	Northings	Eastings	Z	Northings	Eastings	Z				
EW-1N	BW03,BW04	-0.4890	0.8717	-0.0328	-5636.18	1.5E-06	6989.1	1000.0	-1000.0	8000.0	2801.9	-1000.0	8000.0	2735.0	0.0	7026.7	1000.0	0.0							
EW-1S	BW01,BW03,BW04	-0.4792	0.8547	-0.1994	-5472.54	2.2E-05	8000.0	2848.9	0.0	8000.0	3000.0	-363.1	7851.4	3000.0	-1000.0	6730.0	1000.0	-1000.0	6963.4	1000.0	0.0				
EW-3	NE-1,BW03	-0.1994	0.9612	-0.1908	-6409.20	2.4E-05	7256.3	2835.0	0.0	6875.7	1000.0	0.0	6677.1	1000.0	-1000.0	6686.9	1047.2	-1000.0							
EW-7	NE-4N,BW01	-0.2557	0.9540	-0.1562	-5606.41	6.8E-05	6377.7	1869.9	0.0	6680.6	3000.0	0.0	6516.8	3000.0	-1000.0										
NE-1	BW03,BW01	-0.4380	0.8472	0.3008	-4905.35	3.0E-04	7341.6	3000.0	0.0	6307.5	1000.0	0.0	6662.5	1000.0	-1000.0	7696.7	3000.0	-1000.0							
NE-2	EW-1S,NE-1,EW-3	-0.7883	0.5727	-0.2250	-2588.86	4.1E-07	8000.0	2528.5	0.0	7049.5	1837.9	0.0	6965.8	1922.7	-510.3	7360.0	2348.9	-1000.0	8000.0	2813.9	-1000.0				
NE-3	BW01,BW02,BW03	-0.4814	0.8337	0.2706	-4462.14	2.9E-04	7084.4	3000.0	0.0	6000.0	1121.9	0.0	6000.0	1000.0	-216.8	6254.3	1000.0	-1000.0	7409.0	3000.0	-1000.0				
NE-4N	BW01,BW03	-0.3851	0.8647	-0.3225	-4794.61	3.0E-05	6000.0	1021.9	0.0	6881.0	3000.0	0.0	6507.9	3000.0	-1000.0	6000.0	1859.4	-1000.0							
NE-4S	NE-4N,BW02	-0.4670	0.8602	-0.2048	-4608.54	3.0E-05	6000.0	1183.6	0.0	6000.0	1361.4	-405.3	6400.9	1922.1	0.0										
NW-1	EW-1N,BW04	0.3677	0.3387	0.8660	-3132.45	1.7E-07	7413.4	1689.2	0.0	8000.0	1148.9	0.0	8000.0	2781.4	-693.2										
NNW-1	EW-3,EW-1S	0.9514	0.3078	0	-4312.29	1.1E-05	7129.9	2225.7	0.0	7570.6	2083.1	0.0	7373.1	2147.0	-1000.0	6943.9	2285.9	-1000.0							
NNW-2	NE-1,EW-1S	0.9160	0.4013	0	-4958.39	5.6E-05	7576.7	2094.0	0.0	7003.1	2345.3	0.0	7292.6	2218.5	-1000.0	7389.4	2176.1	-1000.0							
NNW-3	F2,F3	0.9995	-0.0315	0	-1921.13	2.0E-05	7025.4	2143.6	0.0	6812.9	2136.9	0.0	6812.9	2136.9	-1000.0	7025.4	2143.6	-1000.0							
NNW-4	NE-1,EW-1S	0.9882	0.1256	0.0872	-3176.61	1.5E-04	6993.1	2326.0	0.0	7659.3	2241.3	0.0	7487.7	2351.4	-1000.0	7369.1	2366.4	-1000.0							
NNW-5	NE-4N,F1	0.9988	0.0494	0	-2325.57	2.0E-06	6440.0	2010.0	0.0	7394.1	1962.8	0.0	7394.1	1962.8	-1000.0	6075.1	2028.0	-1000.0							
NNW-6	EW-7,NE-4N,NE-1	0.9901	0.1404	0	-3266.71	1.4E-05	6984.4	2309.1	0.0	6513.3	2375.9	0.0	6444.4	2385.7	-437.0	6246.8	2413.7	-1000.0	7315.2	2262.3	-1000.0				
NNW-7	EW-3,EW-1S	0.9040	0.4186	0.0868	-4915.15	4.8E-06	7112.8	2143.3	0.0	7503.1	1962.6	0.0	7360.6	2124.6	-1000.0	6949.9	2314.8	-1000.0							
NNW-8	EW-1N,A1,A2,BW04	0.7071	0.7071	0	-6788.23	1.0E-05	7584.9	2015.1	-300.0	8000.0	1600.0	-300.0	8000.0	1600.0	-700.0	7575.2	2024.8	-700.0							
SFZ11	NE-1,BW01	0.1978	0.9802	0	-7540.77	1.0E-04	7158.7	2646.3	0.0	7087.3	3000.0	0.0	7087.3	3000.0	-1000.0	7258.4	2152.4	-1000.0							
SFZ14a	BW03,SFZ14b	-0.9900	0.1409	0	-23.42	1.0E-04	7860.0	1095.0	0.0	7192.5	1000.0	0.0	7192.5	1000.0	-1000.0	7860.0	1095.0	-1000.0							
SFZ14b	SFZ14a,BW04	-0.9785	0.2064	0	-550.85	1.0E-04	7860.0	1095.0	0.0	8000.0	1124.5	0.0	8000.0	1124.5	-1000.0	7860.0	1095.0	-1000.0							
Fictive boundary planes		A	B	C	D		Northings	Eastings	Z	Northings	Eastings	Z	Northings	Eastings	Z	Northings	Eastings	Z	Northings	Eastings	Z	Northings	Eastings	Z	
A1	Defines NNW-8 to be below -300 m	0	0	1	300.00																				
A2	Defines NNW-8 to be above -700 m	0	0	1	700.00																				
F1	Defines NNW-5 to be south of 7394 m	0	-1	0	7394.10																				
F2	Defines NNW-3 to be south of 7025 m	0	-1	0	7025.40																				
F3	Defines NNW-3 to be north of 6813 m	0	-1	0	6812.90																				
BW01	Defines Eastern model boundary	1	0	0	-3000.00		8000.0	3000.0	0.0	6000.0	3000.0	0.0	6000.0	3000.0	-1000.0	8000.0	3000.0	-1000.0							
BW02	Defines Southern model boundary	0	1	0	-6000.00		6000.0	1000.0	0.0	6000.0	3000.0	0.0	6000.0	3000.0	-1000.0	6000.0	1000.0	-1000.0							
BW03	Defines Western model boundary	1	0	0	-1000.00		8000.0	1000.0	0.0	6000.0	1000.0	0.0	6000.0	1000.0	-1000.0	8000.0	1000.0	-1000.0							
BW04	Defines Northern model boundary	0	1	0	-8000.00		8000.0	1000.0	0.0	8000.0	3000.0	0.0	8000.0	3000.0	-1000.0	8000.0	1000.0	-1000.0							

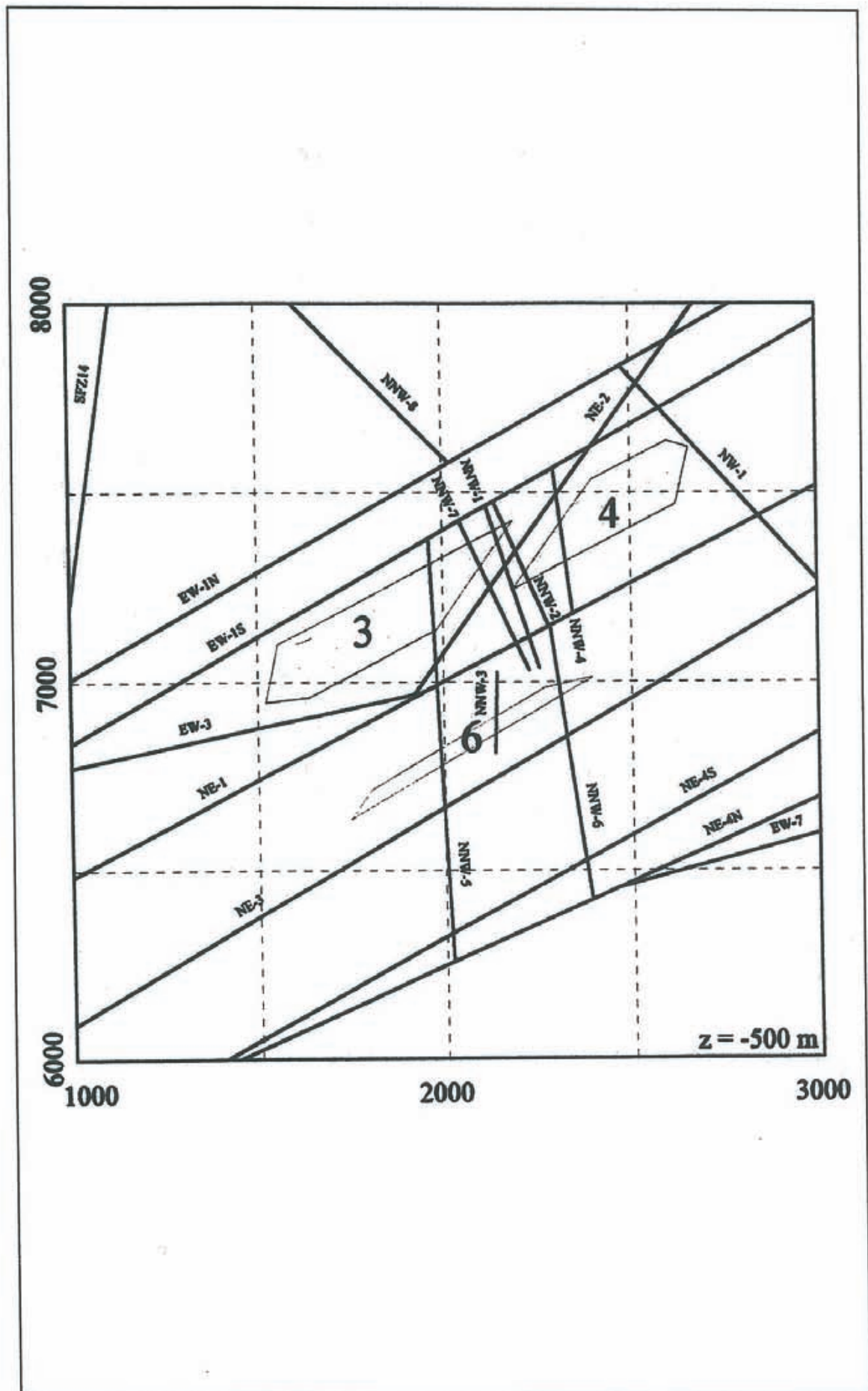


Figure 4-5 Aberg fracture zones at repository depth.



Blue = Rhén et al. (1997)

Green = Uchida et al. (1994)

Red = Follin and Hermanson (1996)

Figure 4-6 Fracture zones as well as the model and repository scale stochastic fracture sets. 10 % of the stochastic fractures are displayed.



Blue = Rhén et al. (1997)

Green = Uchida et al. (1994)

Red = Follin and Hermanson (1996)

Figure 4-7 Closeup showing fracture zones as well as the model and repository scale stochastic fracture sets and the canister locations. 10 % of the stochastic fractures are displayed.

4.3 REFERENCE REPOSITORY LAYOUT

Munier et al. (1997) present an optimized repository layout, which is based on the major hydraulic conductors described in Rhén et al. (1997) and constrained by the discontinuity classification system presented by Almén et al. (1996). The classification system yields that all NNW zones described by Rhén et al. (1997) could be classified as D3 discontinuities and does not influence the layout of the repository. Munier et al. (1997) conclude that zones which could be classified as D1 or D2 discontinuities strongly limit the available space for the repository. To some extent this is a result of the way the D1 and D2 discontinuities have been extrapolated in the work of Munier et al. (1997).

The AMP selected a single level (500 m) and three sectors (3, 4, and 6) for the present study as shown in Figure 4-5. The reference repository includes canister emplacement boreholes only, and does not consider drifts or shafts to have any hydrological significance. This is a key difference from the previous study by Dershowitz et al. (1996). The canister dimensions are summarized in Table 4-5.

Table 4-5 Repository layout

Parameter	Value	Basis
Canister Locations		Canister.xls
Number of Canisters	Sector 3: 500 Sector 4: 319 Sector 6: 126	
Canister Height	7.833 m	
Canister Diameter	1.75 m	
Distance between Canisters	6 m	

The canisters representing the source locations for the pathway search, are modeled using a fracture group which consists of four fractures. The size of the four fractures was chosen so that the box formed by the fractures has the same volume as a canister. The center of the box is identical to the center of the canister.

Due to computational constraints the pathway search could not be carried out for all canister locations. Therefore a representative number of canisters was defined as potential source locations. The distance between the searched canisters is approximately 50 meters in Sectors 4 and 6 and approximately 100 meters in Sector 3. The larger distance for Sector 3 was necessary to reduce computational efforts.

Tables 4-6 summarizes the geometric characteristics of the implementation of the Aberg reference repository design in the current study.

Table 4-6 Repository model geometry.

"Canister" Fractures		
Top	-500 m (Äspö Coordinates)	
No. of fractures per canister	4	
Canister cross sectional area	2.4 m ²	
Equivalent fracture box	1.55 x 1.55 m	
Fracture length	7.833 m	
Transmissivity	1.0 x 10 ⁻²⁰ m ² /s	
Number of Searched Canisters	Spacing (m)	
Sector 3	30 (out of 500)	100
Sector 4	37 (out of 319)	50
Sector 6	14 (out of 126)	50

4.4 BOUNDARY CONDITIONS

Svensson (1997) carried out a regional, steady-state variable-density flow simulation of the Äspö site using the PHOENICS continuum code. The AMP established the results of Svensson's study as the basis for boundary conditions of the present study. For the purpose of this project, however, it was decided to use Svensson's fresh-water solution rather than the variable-density solution.

The results from this study were provided by the AMP (Ström and Selroos, 1997) as fluxes to 100 m by 100 m panels, and as average fresh-water heads to 100 m by 100 m panels.

The discrete fracture network model uses the fresh-water head values (located in the center of the panel) to define constant head boundaries. This is done by assigning fresh-water head to the boundary node using an parabolic distance weighted average of the 3 nearest head values.

5

PATHWAYS ANALYSIS

This section presents the results of the FracMan/PAWorks analysis carried out in support of the AMP. A series of ten (10) stochastic realizations were carried out for each of the three studied sectors of the repository to identify and quantify transport properties of integrated scale pathways from canisters to the biosphere. This analysis integrates conventional near-field and far-field pathway approaches, since pathways are defined from canisters to the environmental release. For the current analysis, we identified the highest flow rate pathways from the repository canisters to the surface, based on the repository design, fracture and fracture zone hydrogeologic conceptual models, and boundary conditions described in Sections 2, 3 and 4.

Table 5-1 presents a summary of the required simulation results (“performance measures”) as established by the AMP (Ström and Selroos, 1997). These “performance measures” constitute statistics based on the base 10 logarithm of the F-factor (F_{path}), travel time (t_{path}) and Darcy flux (q_c).

Table 5-1 AMP required simulation results: $Y = \log_{10}(F_{path}; t_{path}; q_c)$, where F_{path} is the F-factor along a pathway from a canister to the geosphere/biosphere interface (needed by FARF31), t_{path} is the travel time along a pathway from a canister to the geosphere/biosphere interface (needed by FARF31), and q_c is the Darcy flux past each canister location (needed by COMP32).

Parameter	Legend	Parameter	Legend
$\langle Y \rangle$	ensemble mean	\bar{Y}	single realization mean
$var[Y]$	ensemble variance	σ_Y^2	single realization variance
M_Y	ensemble median	Y_{50}	single realization median
U_Y	ensemble range	D_Y	single realization range
$\langle \bar{Y} \rangle$	ensemble mean of realization means	$var[\bar{Y}]$	ensemble variance of realization means
$\langle \sigma_Y^2 \rangle$	ensemble mean of realization variances	$var[\sigma_Y^2]$	ensemble variance of realization variances
$M_{Y_{50}}$	ensemble median of realization medians	$U_{Y_{50}}$	ensemble range of realization medians
M_{D_Y}	ensemble median of realization ranges	U_{D_Y}	ensemble range of realization ranges
$(x, y, z)_{path}$	Coordinates of all pathway discharge points in each realization		

It is noted here that the “performance measures” in Table 5-1 have been slightly modified from the original specification by Ström and Selroos (1997) due to the following reasons:

- the number of realizations is limited to 10,
- pathway search is limited to a subset of all canisters (81 out of 945),
- in each DFN realization there may exist canisters which do not have any pathways to the geosphere/ biosphere, and
- in each DFN realization there may exist canisters which may have more than one pathway to the geosphere/ biosphere.

The following modifications are made:

- The “performance measures” in each realization are based on all existing pathways for each canister. Hence, canisters without pathways are excluded in the calculations.
- In addition to the requested ensemble statistics (see Table 5-1) we also provide pooled statistics (all canisters and realizations combined). Besides the obvious pooled statistics based on all existing pathways for each canister we also provide pooled statistics based on pathway with the smallest F-factor for each canister and realization.
- The range (= maximum value - minimum value) is used to estimate the dispersion interval in each result rather than using the width of the interval between the 95% and the 5% percentiles.
- The most typical realization in this study is the one which is closest to the ensemble median and the ensemble median variance of $Y = \log_{10}(q_c; F_{\text{path}}; t_{\text{path}})$.
- The most typical canister in this study is the one which is closest to the ensemble median and the ensemble median variance of $Y = \log_{10}(q_c; F_{\text{path}}; t_{\text{path}})$.

5.1 SIMULATION RESULTS

Ten simulations were carried out to create realizations of the Aberg hydrogeological conceptual model described in Section 4. Due to computational limitations each of the three repository sectors had to be modeled separately. However, the same model scale stochastic fracture network was used for all three sectors within one realization. For all realizations the pathway search was carried out on a canister-by-canister basis. The maximum number of pathways (per canister) was not limited.

Pathways were identified using the “flow rate weighted” pathway search algorithm described in Section 2, and using the steady-state flow field derived by MAFIC 1-D based on the boundary conditions described in Section 4.4.

Figure 5-1 illustrates the results of the PAWorks approach. Figure 5-1 shows how the stochastic fracture network provides the “inter fracture” pathway away from the canister. Both fracture sets (i.e. model and repository scale) are shown here as well as the fracture zones.

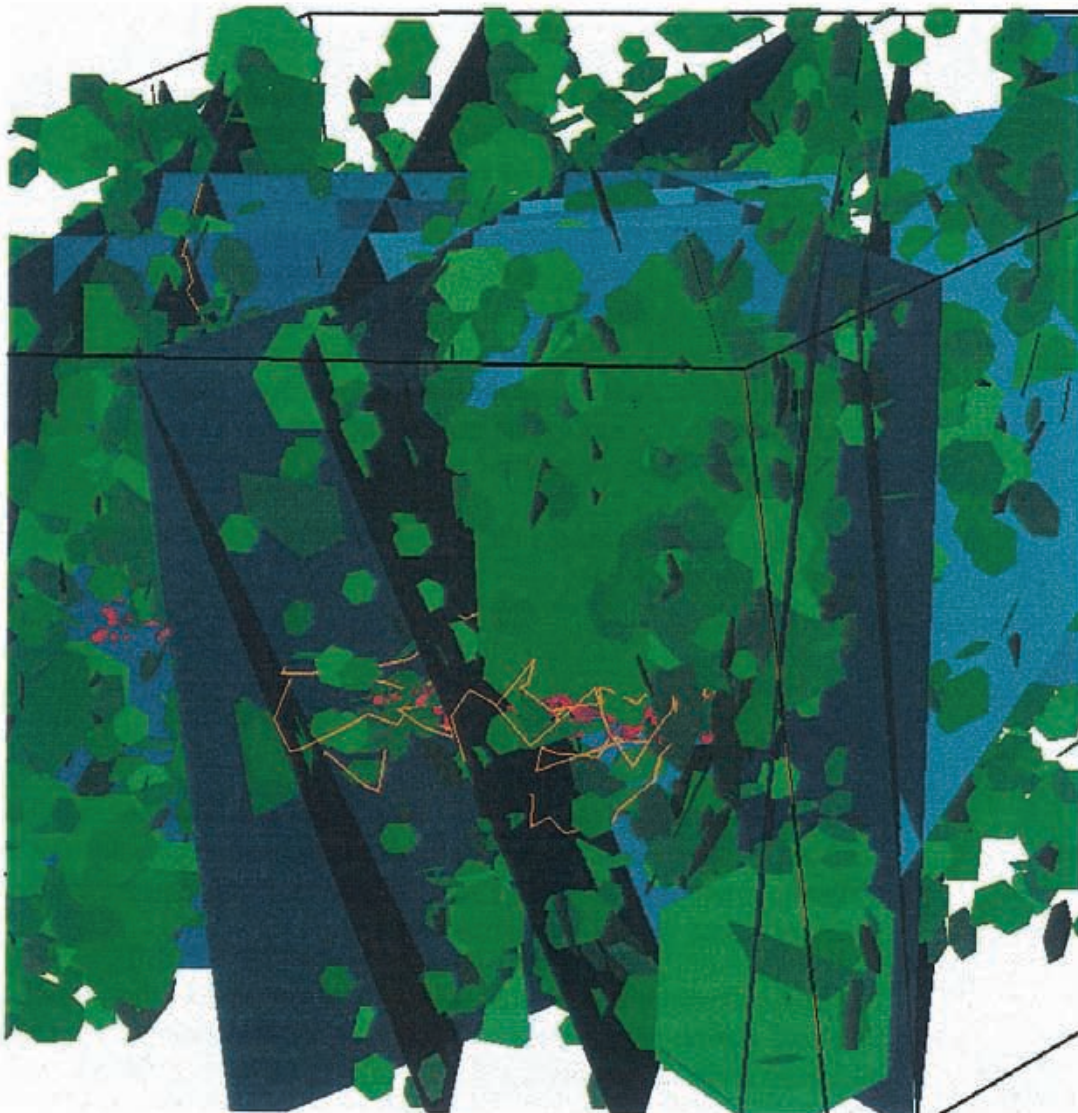
Some of the following statistics were derived by averaging over all pathways of a realization (i.e. all effective pathway properties like travel time and F-Factor), others are calculated by combining all pathways of one canister and then averaging over the canisters (i.e., flow rate and Darcy flux at the canister). By stating the number of pathways or canisters used, each table indicates which possibility was applied.

The tables shows the results for each repository sector and summarized for the repository as a whole.

5.2 PATHWAY SEARCH

As mentioned before the pathway search was conducted on a subset of all canister locations and the search was carried out separately for the three different repository sectors. Table 5-2 gives some general results of the pathway search for the ten realizations.

Appendix D provides a visualization of the outcome of the pathway search. Pathway discharge points are shown for all realizations. In addition, all pathways from all sectors are shown in 3-D for two of the ten realizations, namely 1 and 9. Table 5-3 gives the Äspö coordinates of each discharge point. As shown in Appendix D discharge occurs at a few specific points. The reason for this locus effect is due primarily to the combination of boundary conditions and major fracture zones, which resulted in particular preferred discharge locations.



Blue = Rhén et al. (1997)

Green = Uchida et al. (1994)

Red = Follin and Hermanson (1996)

Orange = Discrete fracture pathways

Figure 5-1 3-D visualization view of the discrete fracture pathways approach. Orange lines are pathways between the canisters and the discharge points. 10 % of the stochastic fractures are displayed.

Table 5-2 Pathway search results by realization and sector.

Realization	# of canisters searched	# of pathways found	# of canisters w/o pathway	average # of pathways per canister	no pathway canister percentage
Sector 3					
1	30	66	15	4.40	50.00%
2	30	100	5	4.00	16.67%
3	30	68	8	3.09	26.67%
4	30	49	15	3.27	50.00%
5	30	56	12	3.11	40.00%
6	30	48	16	3.43	53.33%
7	30	64	11	3.37	36.67%
8	30	66	14	4.13	46.67%
9	30	50	13	2.94	43.33%
10	30	41	13	2.41	43.33%
Sector 4					
1	37	67	19	3.72	51.35%
2	37	105	10	3.88	27.03%
3	37	91	14	3.96	37.84%
4	37	76	12	3.04	32.43%
5	37	63	15	2.86	40.54%
6	37	95	13	3.96	35.14%
7	37	90	11	3.46	29.73%
8	37	78	16	3.71	43.24%
9	37	59	14	2.57	37.84%
10	37	75	15	3.41	40.54%
Sector 6					
1	14	27	8	4.50	21.62%
2	14	13	5	1.44	13.51%
3	14	34	5	3.78	13.51%
4	14	27	6	3.38	16.22%
5	14	30	5	3.33	13.51%
6	14	39	4	3.90	10.81%
7	14	48	5	5.33	13.51%
8	14	17	7	2.43	18.92%
9	14	20	6	2.50	16.22%
10	14	27	6	3.38	16.22%
All Sectors*					
1	111	226	57	4.19	51.35%
2	111	318	25	3.70	22.52%
3	111	261	35	3.43	31.53%
4	111	201	48	3.19	43.24%
5	111	205	44	3.06	39.64%
6	111	230	49	3.71	44.14%
7	111	266	38	3.64	34.23%
8	111	227	51	3.78	45.95%
9	111	179	46	2.75	41.44%
10	111	184	47	2.88	42.34%

* Sector 3 has double weight because of the larger spacing between the analyzed canisters in this sector.

Table 5-3 Pathway discharge point results by realization and sector. The pathway discharge points are shown for all realizations in Appendix D.

Realization	Sector	# of pathways found	Discharge at Äspö x	Discharge at Äspö y	Discharge at Äspö z
1	3	66	2061	6542	-1
	4	67	2000	6825	-1
	6	27	2061	6542	-1
2	3	22	2000	6825	-1
	3	78	2061	6542	-1
	4	105	2061	6542	-1
	6	13	2061	6542	-1
3	3	68	2061	6542	-1
	4	1	3000	7640	-96
	4	90	2061	6542	-1
	6	34	2000	6825	-1
4	3	49	2061	6542	-1
	4	55	2061	6542	-1
	4	21	2925	8000	-182
	6	27	2061	6542	-1
5	3	56	2061	6542	-1
	4	63	2061	6542	-1
	6	5	2061	6542	-1
	6	25	2000	6825	-1
6	3	48	2061	6542	-1
	4	34	2061	6542	-1
	4	61	3000	7519	-500
	6	39	2000	6825	-1
7	3	64	2061	6542	-1
	4	90	2061	6542	-1
	6	28	2061	6542	-1
	6	20	2000	6825	-1
8	3	66	2061	6542	-1
	4	53	3000	7519	-500
	4	25	2061	6542	-1
	6	17	2000	6825	-1
9	3	50	2061	6542	-1
	4	36	2925	8000	-182
	4	7	3000	7519	-500
	4	16	2061	6542	-1
	6	1	2436	6529	-1
	6	19	2823	7123	-1
10	3	41	2061	6542	-1
	4	71	2061	6542	-1
	4	4	3000	7519	-500
	6	27	2061	6542	-1

5.3 PATHWAY STATISTICS

5.3.1 Sector 3

Table 5-4 Basic numbers for all statistical calculations of Sector 3.

Number of Sector	3
Total number of canisters in this sector:	500
Total number of searched canisters:	30
Total number of realizations:	10

Table 5-5 Number of canisters that connect to the biosphere (out of 30) in Sector 3.

Realization	Number	Realization	Number
1	13	6	8
2	17	7	10
3	9	8	8
4	10	9	8
5	10	10	17
Average canister-biosphere connectivity:		11	36.7 %

Table 5-6 Ensemble statistics for all realizations of Sector 3.

Parameter	$\log_{10}(F_{\text{path}})$	$\log_{10}(t_{\text{path}})$	$\log_{10}(q_c)$
$\langle \bar{Y} \rangle$	6.00	1.31	-2.44
$\text{var}[\bar{Y}]$	0.13	0.13	0.08
$\langle \sigma_Y^2 \rangle$	0.30	0.12	0.58
$\text{var}[\sigma_Y^2]$	0.03	0.005	0.08
$M_{Y_{50}}$	6.09	1.24	-2.45
$U_{Y_{50}}$	0.65	0.22	0.52
M_{D_Y}	1.61	1.05	2.55
U_{D_Y}	0.99	0.52	1.61

Table 5-7 Pooled statistics for Y in Sector 3 (all realizations and canisters combined).

Parameter	$\log_{10}(F_{\text{path}})$	$\log_{10}(t_{\text{path}})$	$\log_{10}(q_c)$
$\langle Y \rangle$	5.95	1.28	-2.46
$\text{var}[Y]$	0.39	0.22	0.56
M_Y	5.88	1.20	-2.43
U_Y	2.90	1.83	3.76

Table 5-8 Pooled statistics for Y in Sector 3 based on the pathways with the smallest F -factors ($F_{\text{path,min}}$) (all realizations and canisters combined).

Parameter	$\log_{10}(F_{\text{path,min}})$	$\log_{10}(t_{\text{path}})$	$\log_{10}(q_c)$
$\langle Y \rangle$	5.83	1.25	-2.25
$\text{var}[Y]$	0.40	0.24	0.66
M_Y	5.75	1.17	-2.24
U_Y	2.78	1.99	3.96

Table 5-9 Statistics for the realization of Sector 3 that is closest to the ensemble median and ensemble median variance.

Parameter	$\log_{10}(F_{\text{path}})$	$\log_{10}(t_{\text{path}})$	$\log_{10}(q_c)$
# of the Realization	7	8	10
# of Canisters	10	8	17
\bar{Y}	6.03	1.36	-2.53
σ_Y^2	0.34	0.16	0.60
Y_{50}	6.02	1.32	-2.41
D_Y	1.60	1.11	3.29

Table 5-10 Statistics for the canister in Sector 3 that is closest to the ensemble median and ensemble median variance. The connectivity percentage is based on ten realizations.

Parameter	$\log_{10}(F_{\text{path}})$	$\log_{10}(t_{\text{path}})$	$\log_{10}(q_c)$
# of the Canister	9	22	3
Connectivity %	80	70	80
\bar{Y}	6.00	1.24	-2.51
σ_y^2	0.22	0.21	0.40
Y_{50}	6.00	1.21	-2.48
D_y	1.36	1.31	1.93

5.3.2 Sector 4

Table 5-11 Basic numbers for all statistical calculations of Sector 4.

Number of Sector	4
Total number of canisters in this sector:	319
Total number of searched canisters:	37
Total number of realizations:	10

Table 5-12 Number of canisters that connect to the biosphere (out of 37) in Sector 4.

Realization	Number	Realization	Number
1	13	6	18
2	18	7	15
3	16	8	11
4	15	9	12
5	15	10	22
Average canister-biosphere connectivity:		15.5	41.9 %

Table 5-13 Ensemble statistics for all realizations of Sector 4.

Parameter	$\log_{10}(F_{\text{path}})$	$\log_{10}(t_{\text{path}})$	$\log_{10}(q_c)$
$\langle \bar{Y} \rangle$	6.52	1.72	-2.75
$\text{var}[\bar{Y}]$	0.14	0.08	0.05
$\langle \sigma_Y^2 \rangle$	0.31	0.15	0.71
$\text{var}[\sigma_Y^2]$	0.03	0.003	0.17
$M_{Y_{50}}$	6.47	1.76	-2.59
$U_{Y_{50}}$	1.47	1.22	0.63
M_{D_T}	1.78	1.30	2.95
U_{D_T}	1.72	0.99	3.08

Table 5-14 Pooled statistics for Y in Sector 4 (all realizations and canisters combined).

Parameter	$\log_{10}(F_{\text{path}})$	$\log_{10}(t_{\text{path}})$	$\log_{10}(q_c)$
$\langle Y \rangle$	6.55	1.75	-2.73
$\text{var}[Y]$	0.40	0.20	0.75
M_Y	6.54	1.77	-2.64
U_Y	3.66	2.41	5.62

Table 5-15 Pooled statistics for Y in Sector 4 based on the pathways with the smallest F -factors ($F_{\text{path,min}}$) (all realizations and canisters combined).

Parameter	$\log_{10}(F_{\text{path,min}})$	$\log_{10}(t_{\text{path}})$	$\log_{10}(q_c)$
$\langle Y \rangle$	6.46	1.71	-2.58
$\text{var}[Y]$	0.39	0.22	0.77
M_Y	6.46	1.75	-2.56
U_Y	3.05	2.08	5.77

Table 5-16 Statistics for the realization of Sector 4 that is closest to the ensemble median and ensemble median variance.

Parameter	$\log_{10}(F_{\text{path}})$	$\log_{10}(t_{\text{path}})$	$\log_{10}(q_c)$
# of the Realization	6	6	8
# of Canisters	18	18	11
\bar{Y}	6.35	1.79	-2.74
σ_Y^2	0.18	0.21	0.44
Y_{50}	6.49	1.76	-2.54
D_Y	1.92	1.48	2.09

Table 5-17 Statistics for the canister in Sector 4 that is closest to the ensemble median and ensemble median variance. The connectivity percentage is based on ten realizations.

Parameter	$\log_{10} (F_{\text{path}})$	$\log_{10} (t_{\text{path}})$	$\log_{10} (q_c)$
# of the Canister	18	23	14
Connectivity %	50	50	70
\bar{Y}	6.72	1.67	-2.80
σ_Y^2	0.31	0.05	0.42
Y_{50}	6.54	1.75	-2.62
D_Y	1.44	0.55	1.59

5.3.3

Sector 6

Table 5-18 Basic numbers for all statistical calculations of Sector 6.

Number of Sector	6
Total number of canisters in this sector:	126
Total number of searched canisters:	14
Total number of realizations:	10

Table 5-19 Number of canisters that connect to the biosphere (out of 14) in Sector 6.

Realization	Number	Realization	Number
1	4	6	6
2	5	7	5
3	6	8	4
4	7	9	4
5	6	10	8
Average canister-biosphere connectivity:		5.5	39.3 %

Table 5-20 Ensemble statistics for all realizations of Sector 6.

Parameter	$\log_{10}(F_{\text{path}})$	$\log_{10}(t_{\text{path}})$	$\log_{10}(q_c)$
$\langle \bar{Y} \rangle$	5.73	0.97	-2.47
$\text{var}[\bar{Y}]$	0.11	0.07	0.05
$\langle \sigma_Y^2 \rangle$	0.51	0.15	0.73
$\text{var}[\sigma_Y^2]$	0.18	0.01	0.45
$M_{Y_{50}}$	5.57	0.86	-2.42
$U_{Y_{50}}$	0.91	0.79	0.85
M_{D_Y}	1.34	1.02	1.81
U_{D_Y}	1.88	0.70	3.65

Table 5-21 Pooled statistics for Y in Sector 6 (all realizations and canisters combined).

Parameter	$\log_{10}(F_{\text{path}})$	$\log_{10}(t_{\text{path}})$	$\log_{10}(q_c)$
$\langle Y \rangle$	5.58	0.95	-2.47
$\text{var}[Y]$	0.52	0.19	0.74
M_y	5.72	0.93	-2.48
U_y	3.76	2.05	4.76

Table 5-22 Pooled statistics for Y in Sector 6 based on the pathways with the smallest F -factors ($F_{\text{path,min}}$) (all realizations and canisters combined).

Parameter	$\log_{10}(F_{\text{path,min}})$	$\log_{10}(t_{\text{path}})$	$\log_{10}(q_c)$
$\langle Y \rangle$	5.49	0.86	-2.16
$\text{var}[Y]$	0.52	0.20	0.62
M_y	5.58	0.89	-2.24
U_y	3.95	2.12	3.95

Table 5-23 Statistics for the realization of Sector 6 that is closest to the ensemble median and ensemble median variance.

Parameter	$\log_{10}(F_{\text{path}})$	$\log_{10}(t_{\text{path}})$	$\log_{10}(q_c)$
# of the Realization	1	3	2
# of Canisters	4	6	5
\bar{Y}	5.68	0.92	-2.69
σ_y^2	0.31	0.12	0.53
Y_{50}	5.55	0.89	-2.43
D_y	1.23	0.84	1.84

Table 5-24 Statistics for the canister in Sector 6 that is closest to the ensemble median and ensemble median variance. The connectivity percentage is based on ten realizations.

Parameter	$\log_{10}(F_{\text{path}})$	$\log_{10}(t_{\text{path}})$	$\log_{10}(q_c)$
# of the Canister	2	1	2
Connectivity %	50	20	50
\bar{Y}	5.72	1.04	-2.17
σ_y^2	0.17	0.12	0.33
Y_{50}	5.59	1.04	-2.43
D_y	1.07	0.50	1.23

5.3.4 Sample histograms

According to Tables 5-4 through 5-24, the three sectors 3, 4 and 6 appear to have similar statistical properties concerning the base 10 logarithm of the F-factor (F_{path}), travel time (t_{path}) and Darcy flux (q_c).

In order to keep the number of pages at a reasonable level, we present plots for Sector 6 only. Sector 6 has the smallest pooled F-factors, shortest pooled travel times and highest pooled Darcy fluxes, thus making it the most interesting sector from a safety performance point of view.

Figures 5-2 through 5-13 show frequency and cumulative relative frequency histograms based on the results for Sector 6.

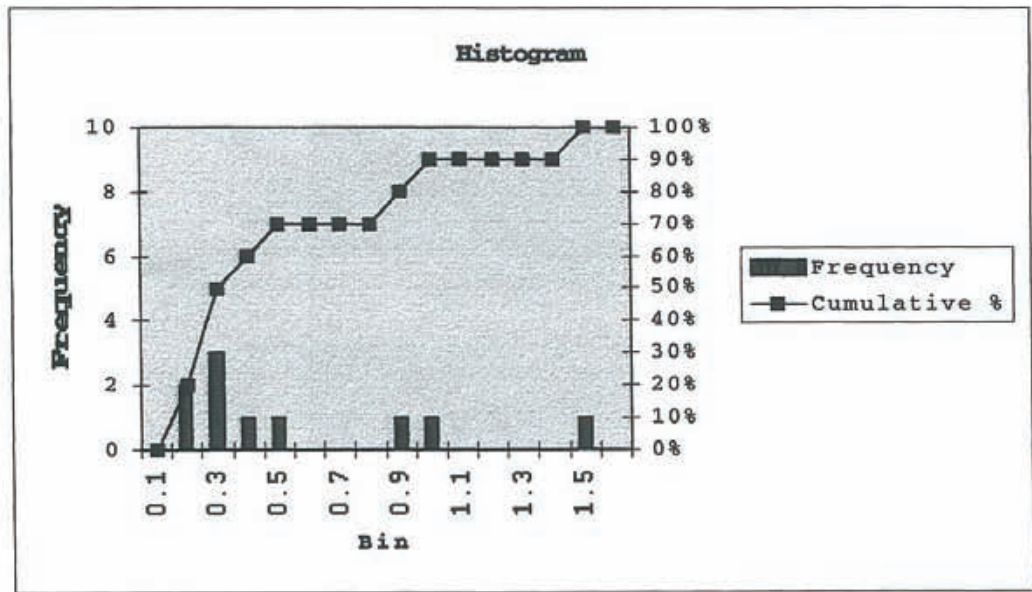
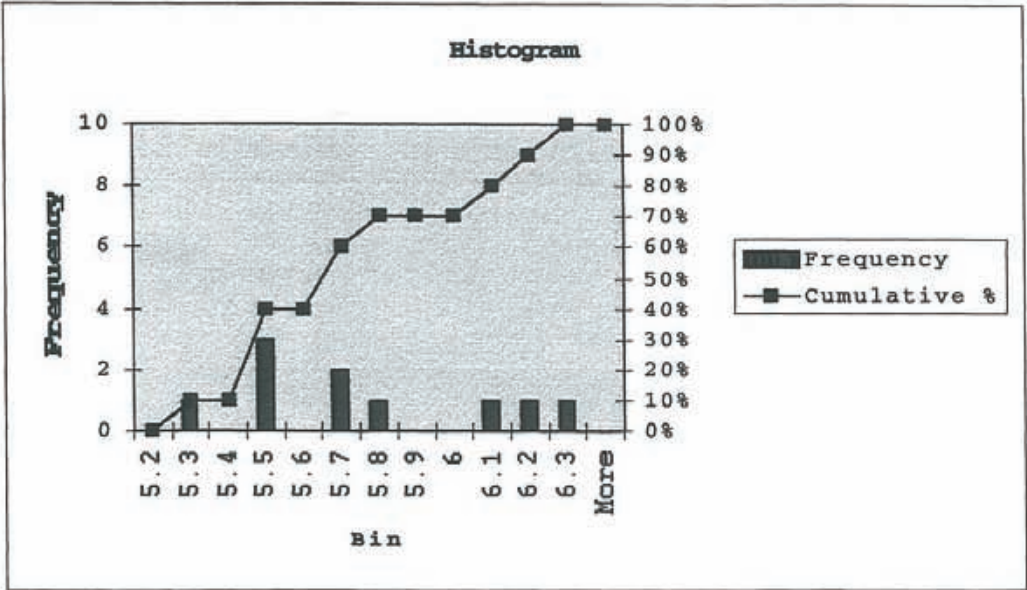


Figure 5-2 Ensemble histograms for $\log(F)$ in Sector 6 based on all realizations. Top: Realization means. Bottom: Realization variances. Reference table: Table 5-20.

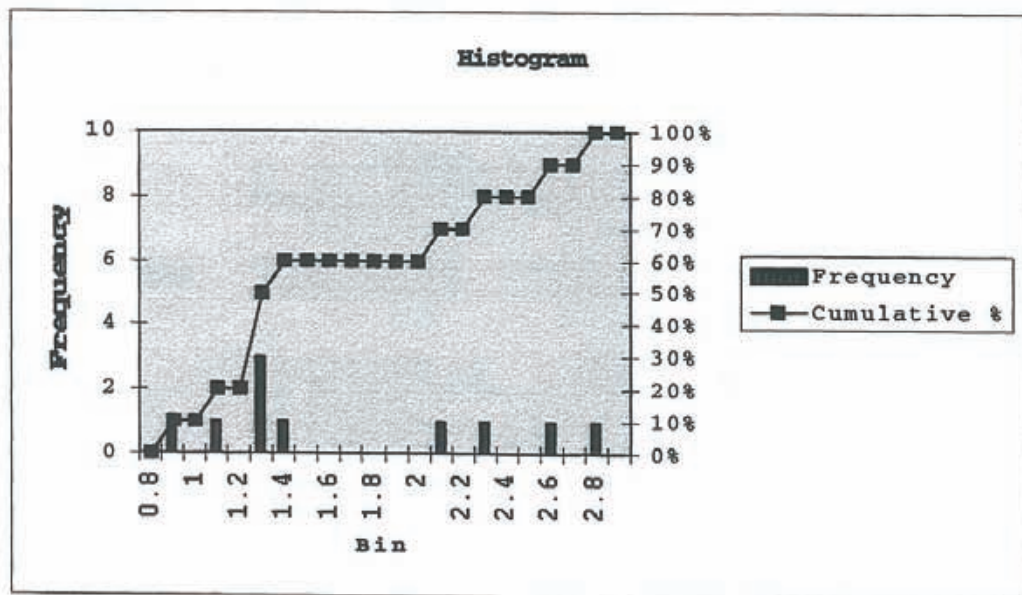
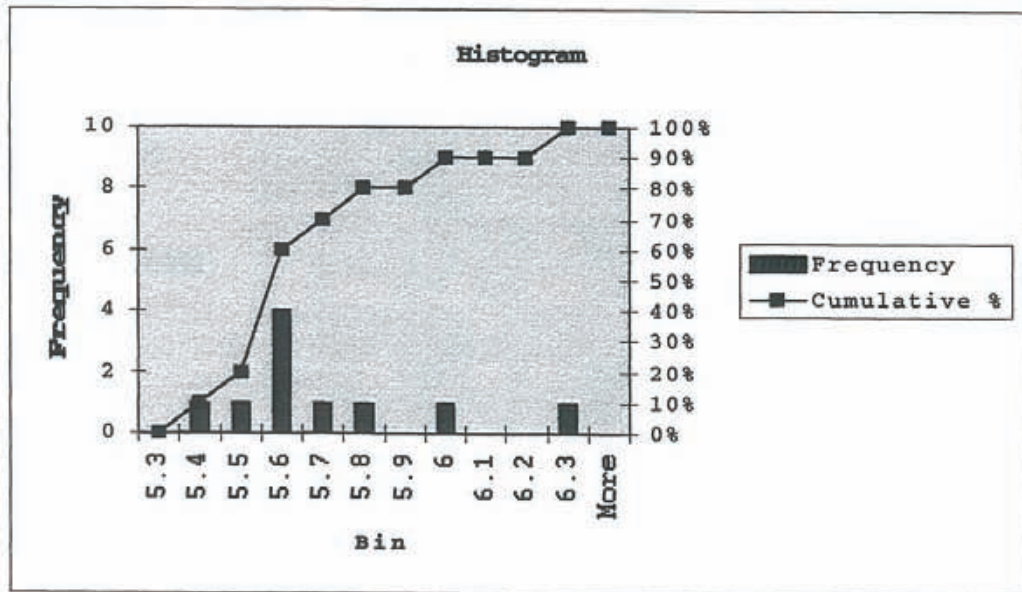


Figure 5-3 Ensemble histograms for $\log(F)$ in Sector 6 based on all realizations. Top: Realization medians. Bottom: Realization ranges. Reference table: Table 5-20.

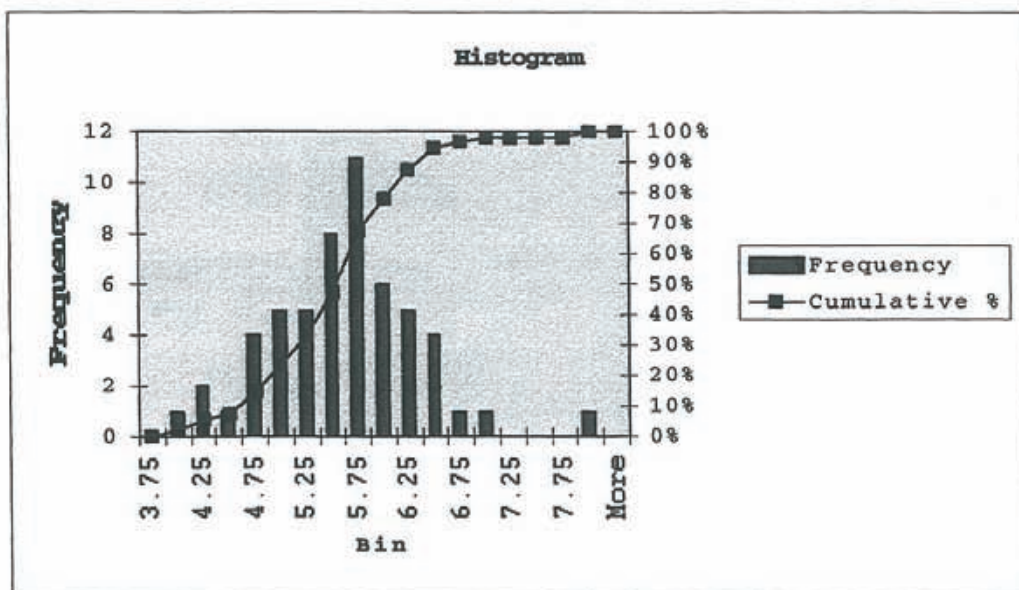
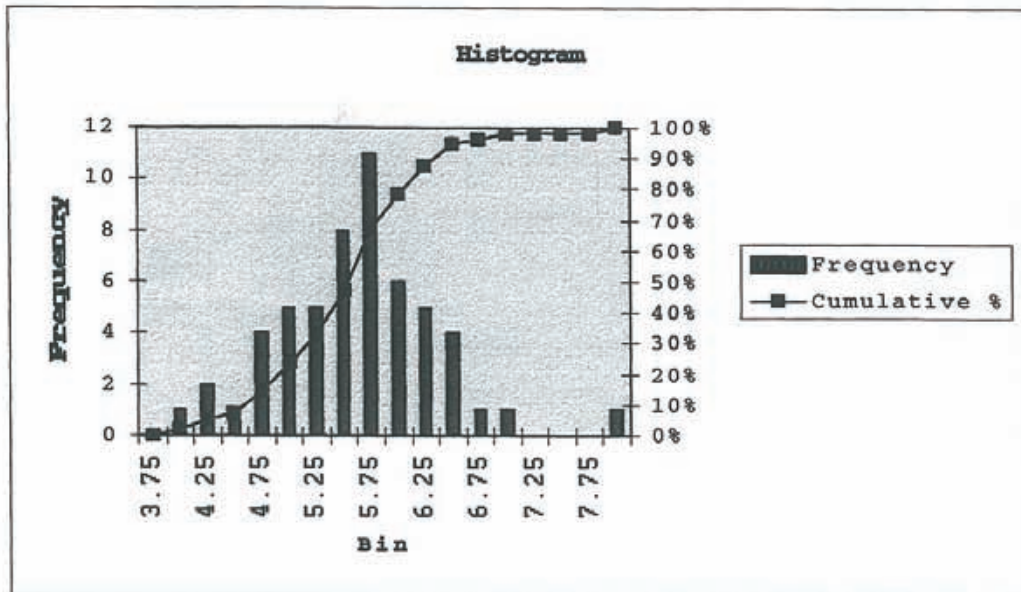


Figure 5-4 Pooled histograms for $\log(F)$ in Sector 6 (all realizations and all canisters combined). Top: $Y = \text{Average } \log(F)$ for each canister. Bottom: $Y = \text{min } \log(F)$ of each canister. Reference tables: Table 5-21 and 5-22.

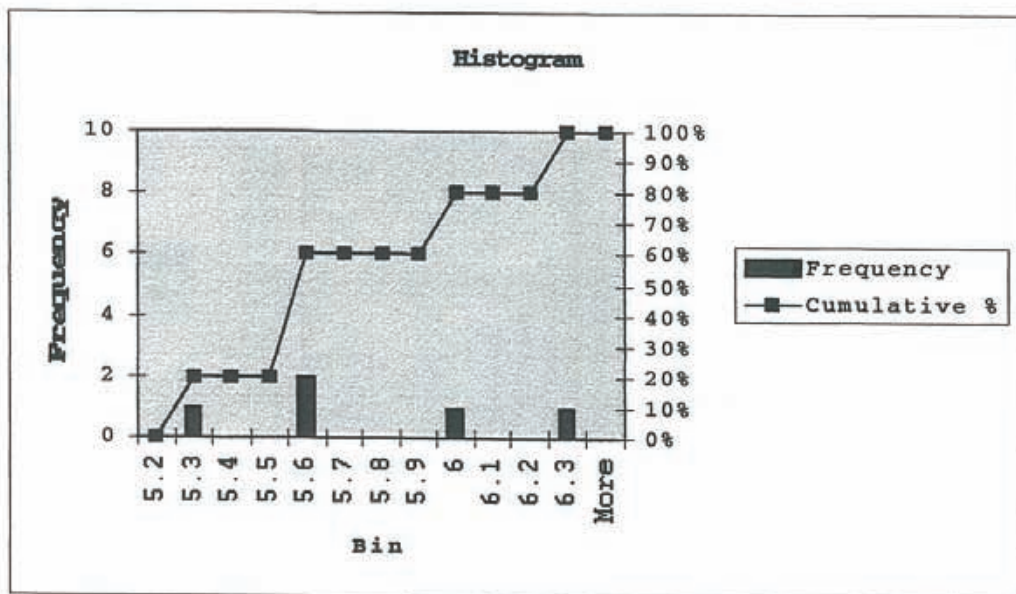
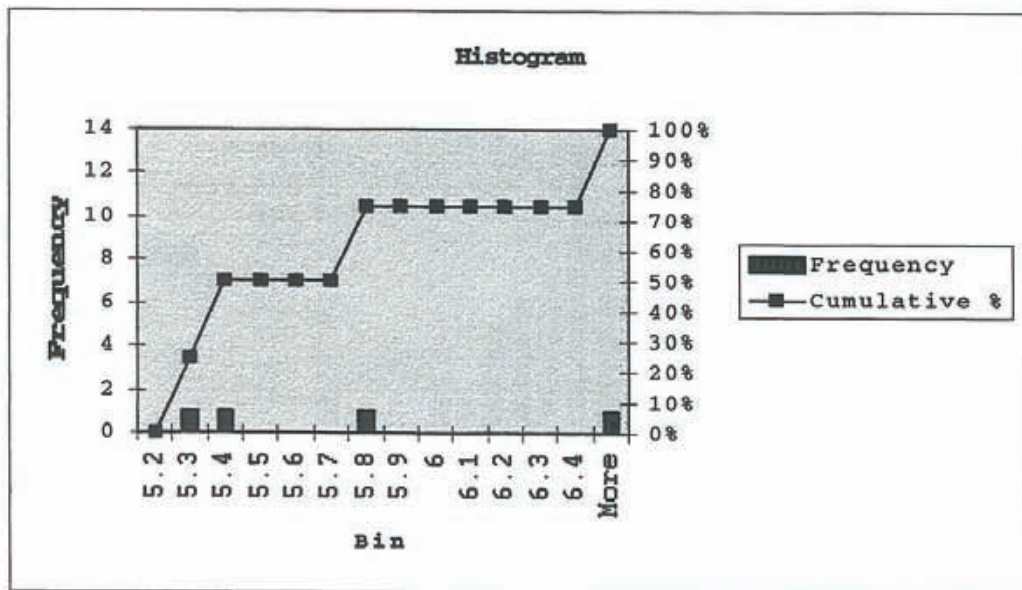


Figure 5-5 Histograms for the realization (top) and the canister (bottom) of Sector 6 that are closest to the ensemble median and ensemble median variance for $\log(F)$. Reference tables: Table 5-23 and 5-24.

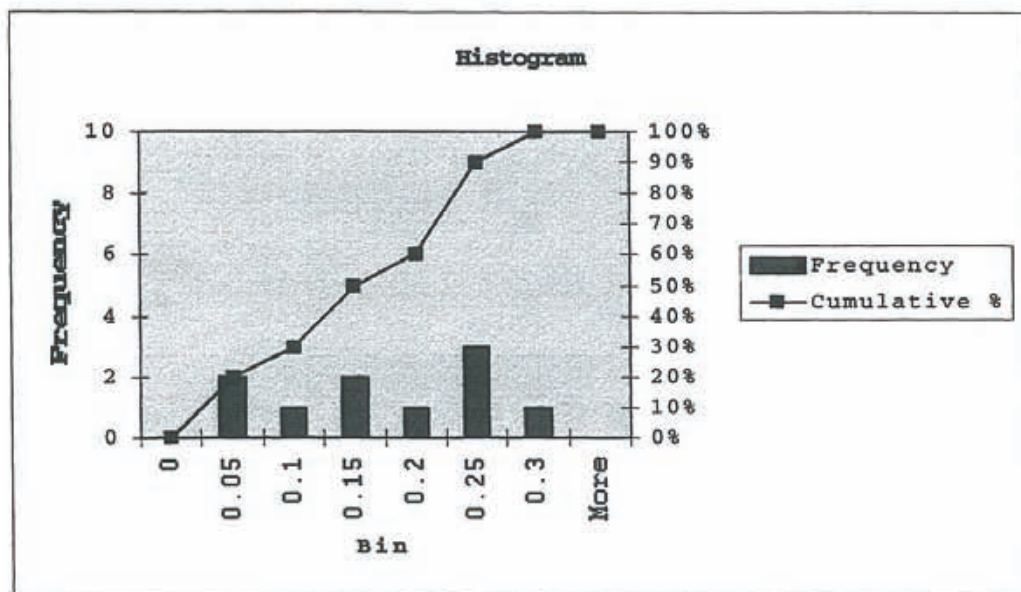
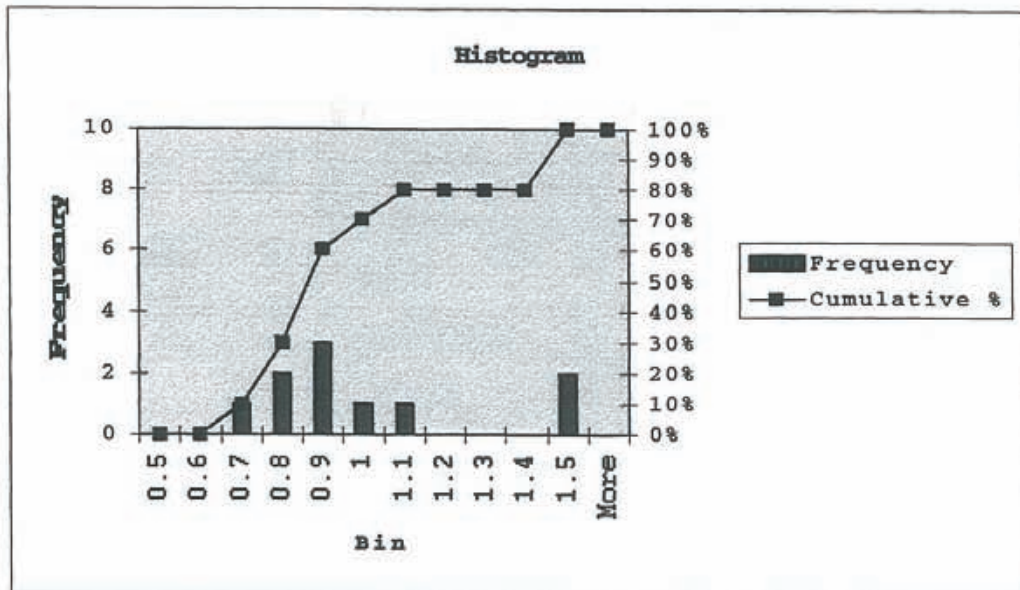


Figure 5-6 Ensemble histograms for $\log(t)$ in Sector 6 based on all realizations. Top: Realization means. Bottom: Realization variances. Reference table: Table 5-20.

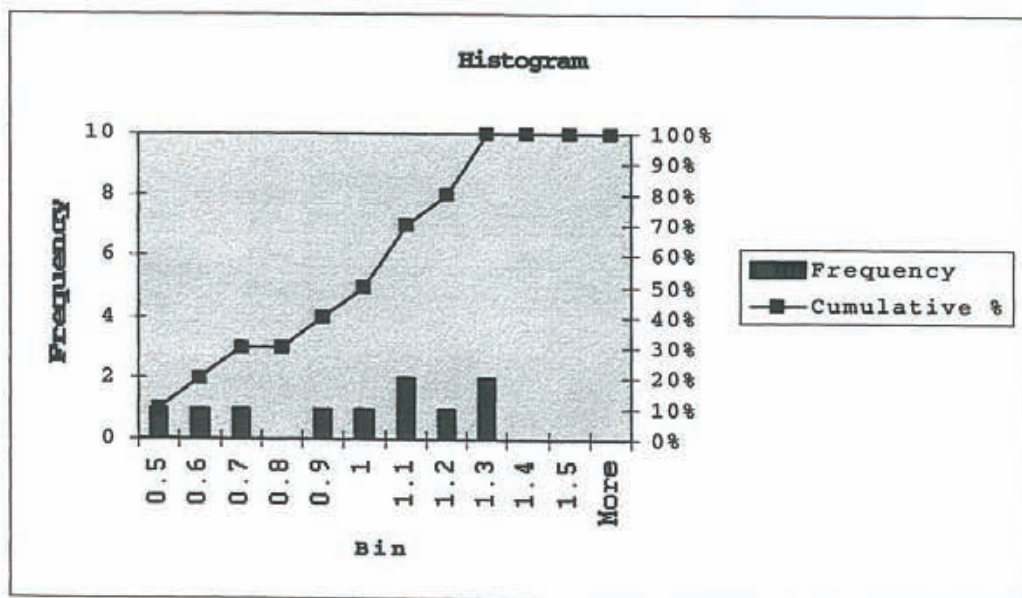
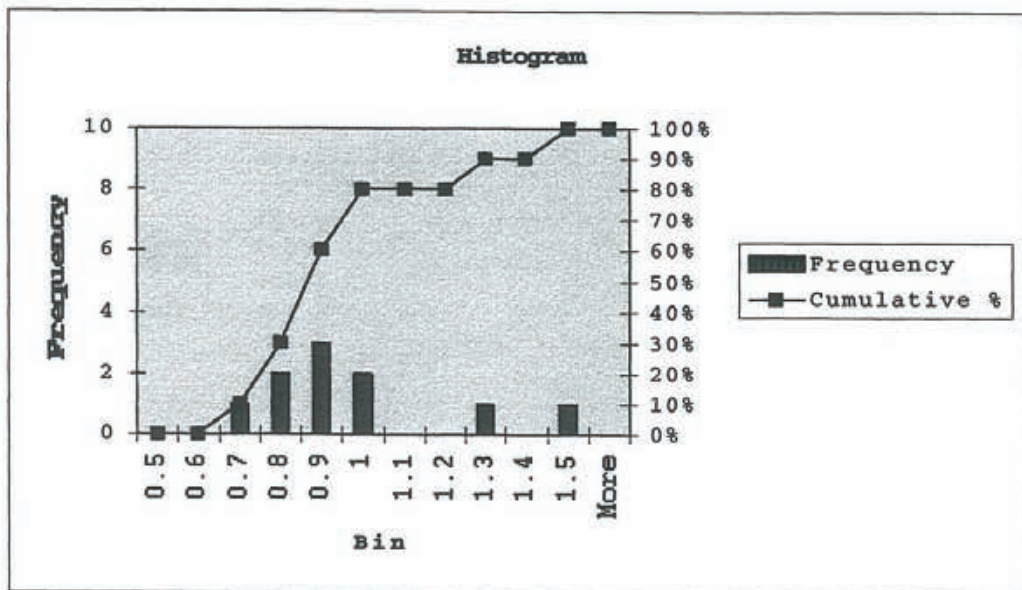


Figure 5-7 Ensemble histograms for $\log(t)$ in Sector 6 based on all realizations. Top: Realization medians. Bottom: Realization ranges. Reference table: Table 5-20.

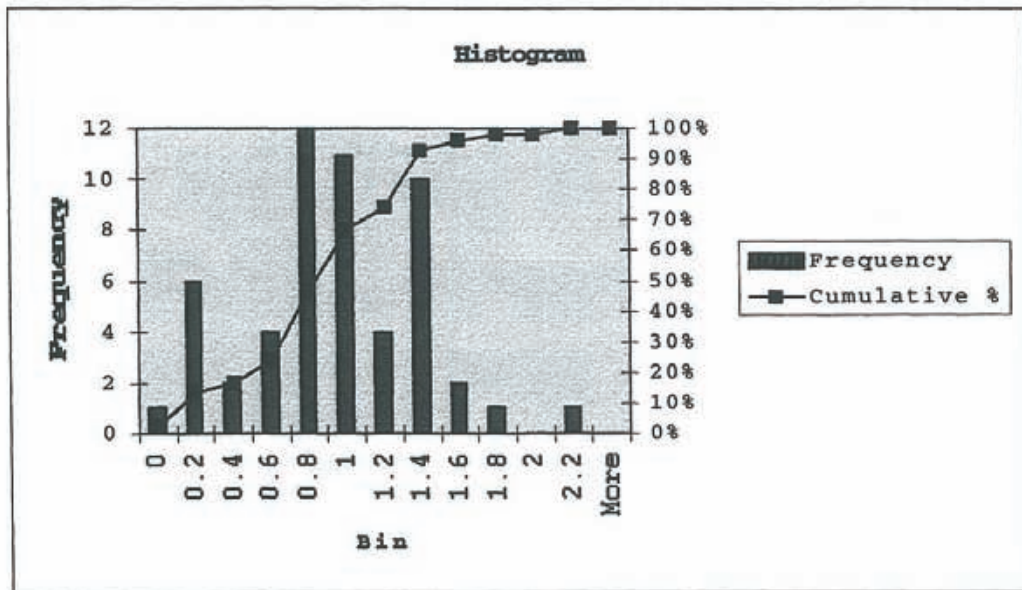
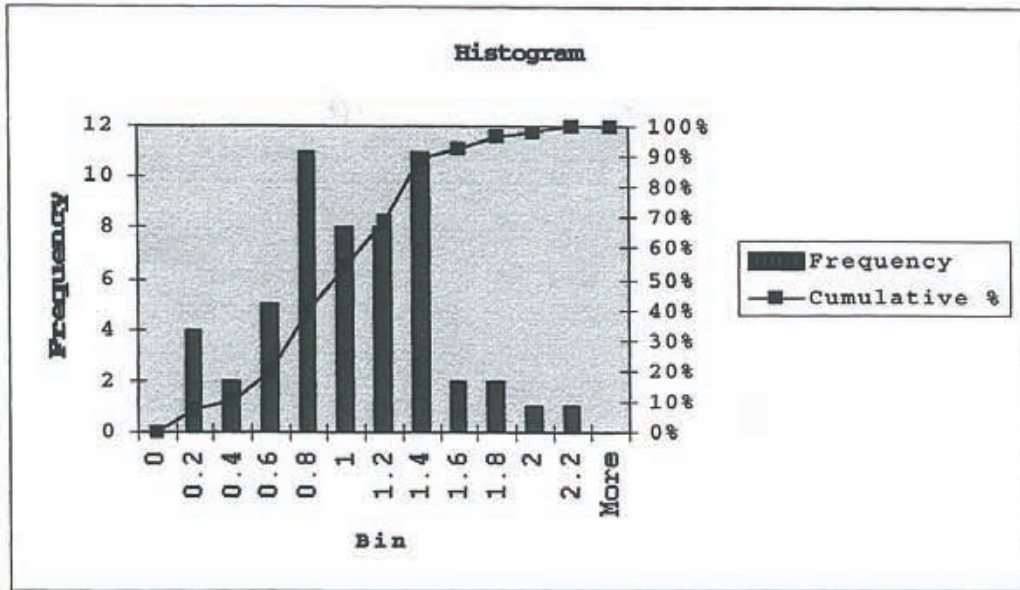


Figure 5-8 Pooled histograms for $\log(t)$ in Sector 6 (all realizations and all canisters combined). Top: $Y = \text{Average } \log(t)$ for each canister. Bottom: $Y = \log(t)$ for $\min \log(F)$ of each canister. Reference tables: Table 5-21 and 5-22.

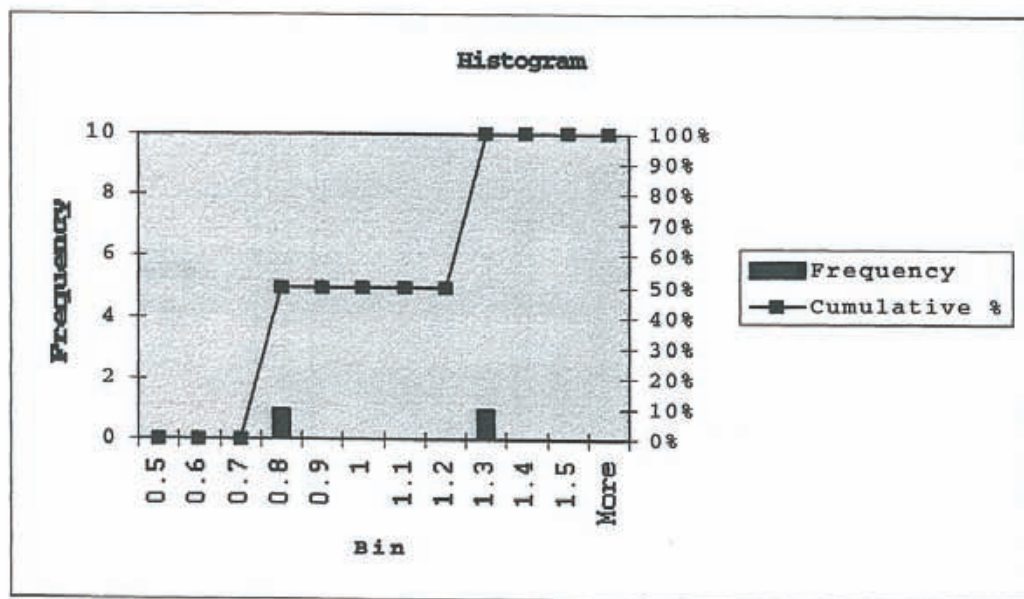
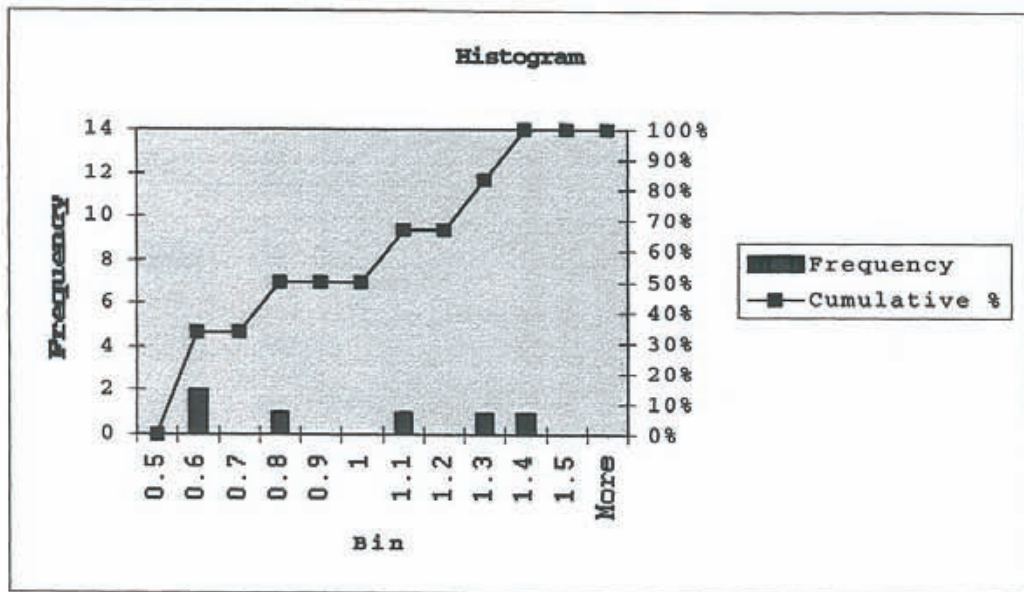


Figure 5-9 Histograms for the realization (top) and the canister (bottom) of Sector 6 that are closest to the ensemble median and ensemble median variance for $\log(t)$. Reference tables: Table 5-23 and 5-24.

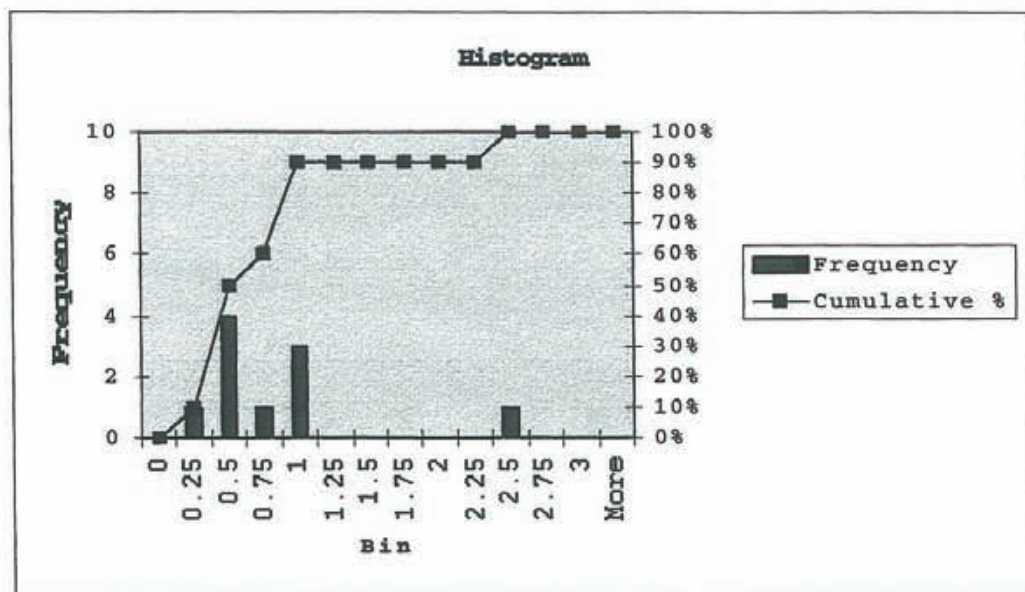
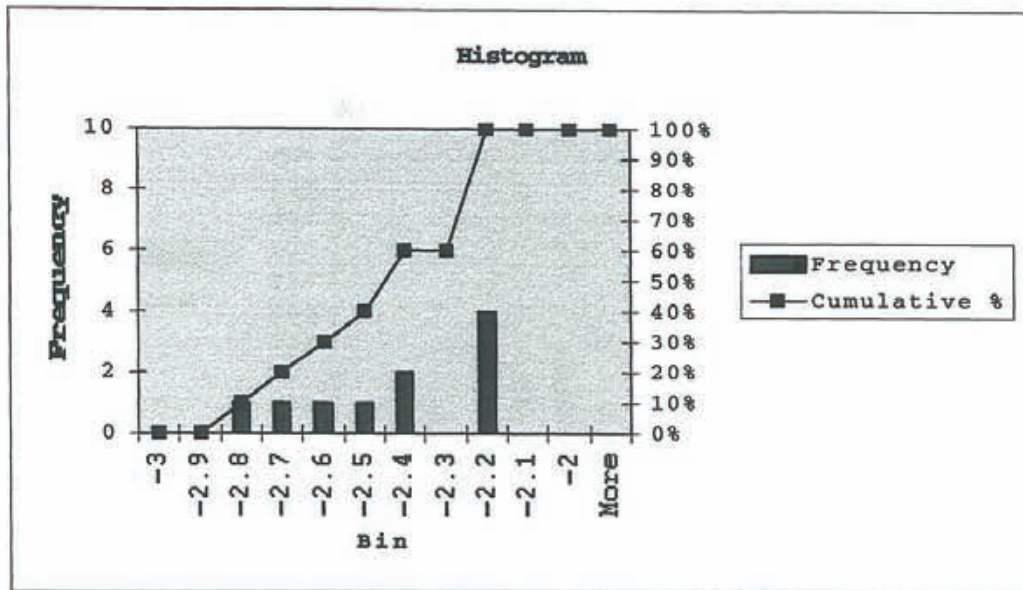


Figure 5-10 Ensemble histograms for $\log(q)$ in Sector 6 based on all realizations. Top: Realization means. Bottom: Realization variances. Reference table: Table 5-20.

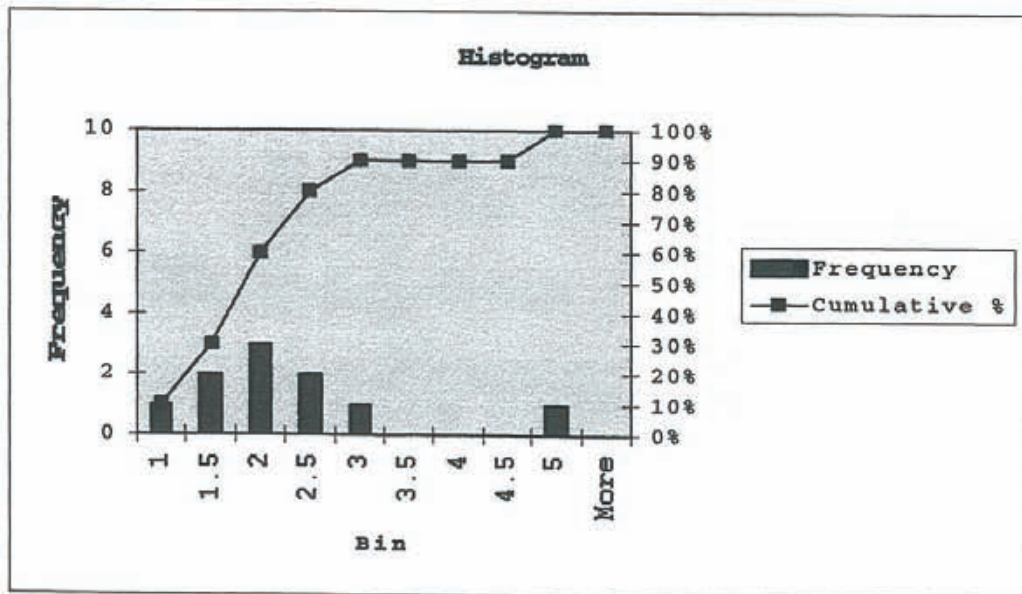
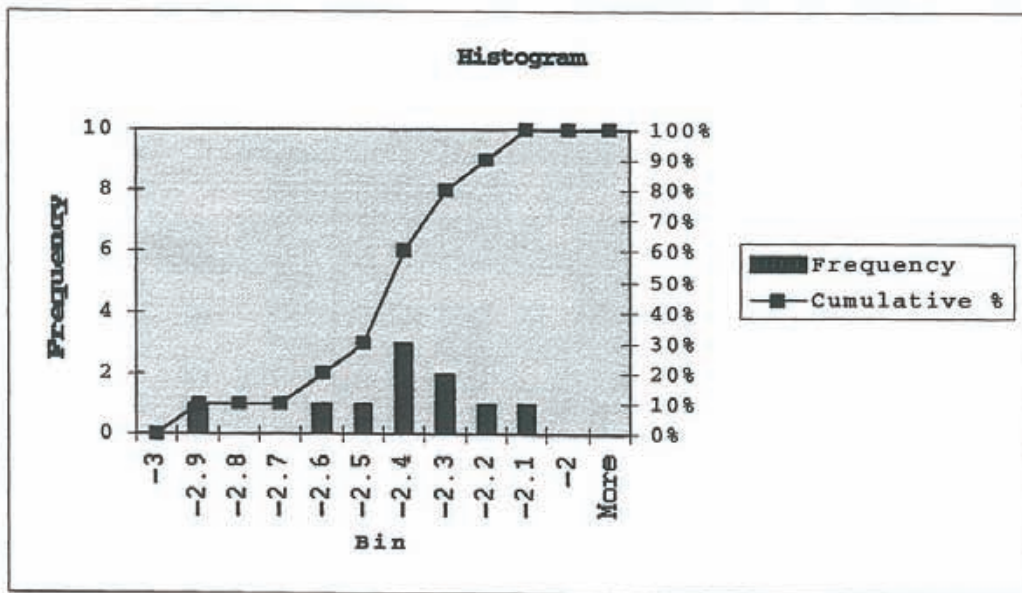


Figure 5-11 Ensemble histograms for $\log(q)$ in Sector 6 based on all realizations. Top: Realization medians. Bottom: Realization ranges. Reference table: Table 5-20.

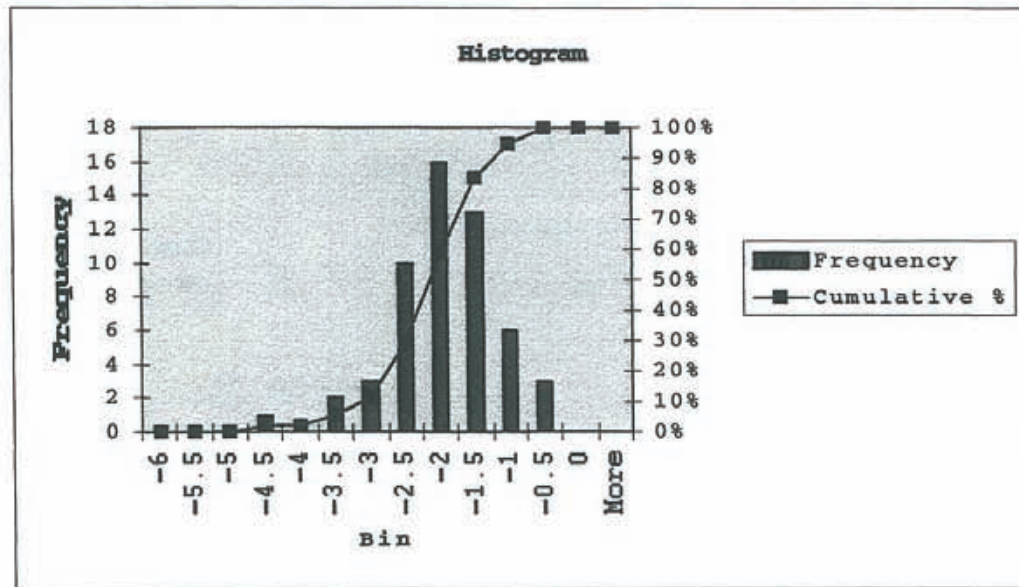
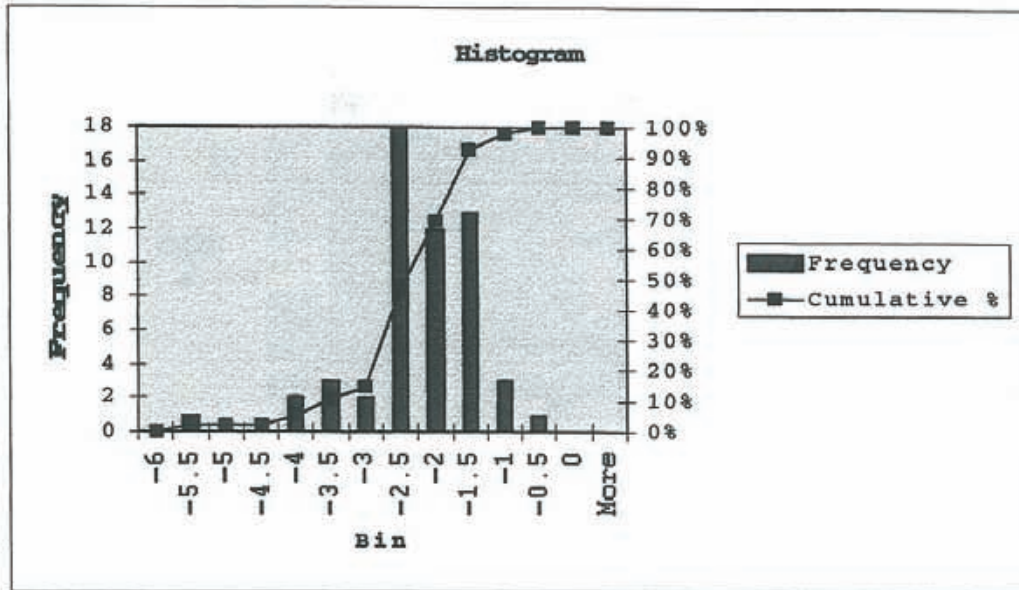


Figure 5-12 Pooled histograms for $\log(q)$ in Sector 6 (all realizations and all canisters combined). Top: $Y = \text{Average } \log(q)$ for each canister. Bottom: $Y = \log(q)$ for $\min \log(F)$ of each canister. Reference tables: Table 5-21 and 5-22.

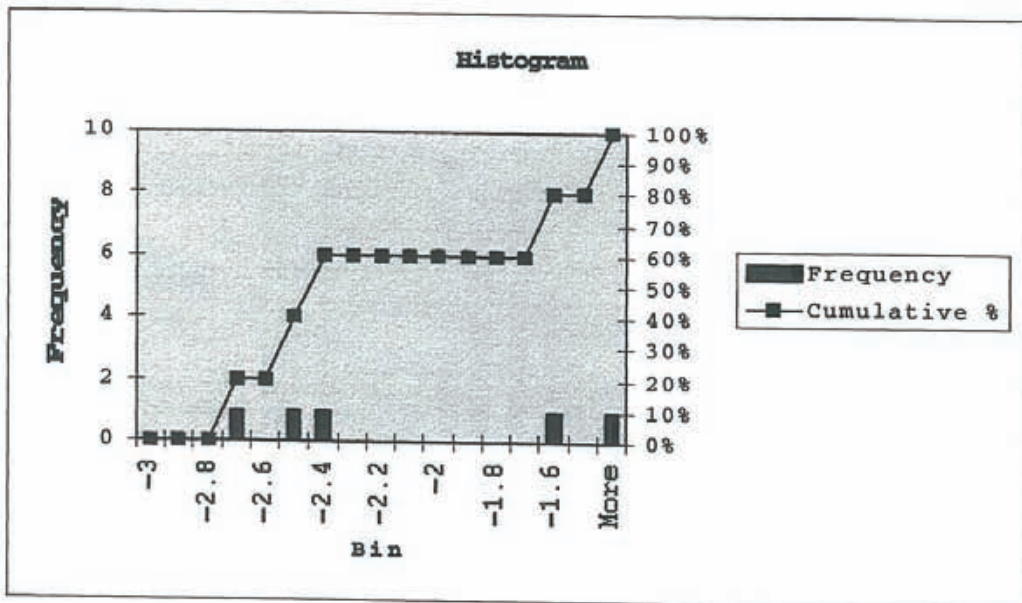
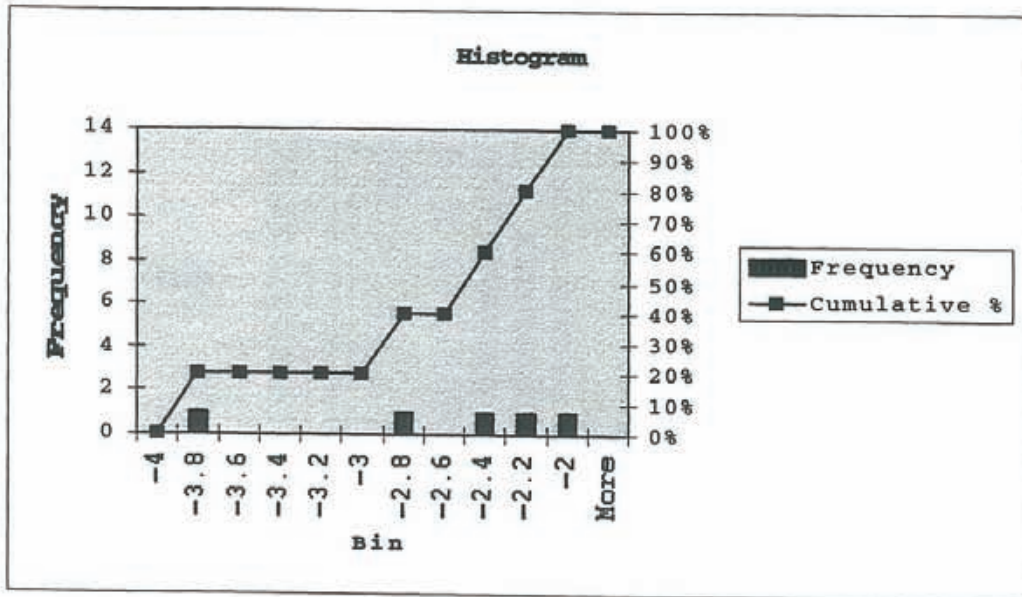


Figure 5-13 Histograms for the realization (top) and the canister (bottom) of Sector 6 that are closest to the ensemble median and ensemble median variance for $\log(q)$. Reference tables: Table 5-23 and 5-24.

5.4

CONSISTENCY OF BOUNDARY FLUXES

Ström and Selroos (1997) have specified that all of the AMP models are to rely on boundary conditions derived from the regional groundwater flow modeling study of Svensson (1997). Svensson used a finite difference continuum model, PHOENICS, to study ground water recharge and regional flow patterns. The results included steady-state heads and fluxes along the limits of the site-scale model domain. Ström and Selroos (1997) specified that these head values should be used as constant head (Dirichlet) boundary conditions by all three of the AMP studies.

Due to differences between the connecting structures of DFN and SC implementations, different results are obtained using prescribed head boundary conditions than would have been obtained using flux boundary conditions. For the input data given by Ström and Selroos (1997) this project yields a median boundary flow rate across the site-scale domain that is approximately 10 times smaller than that of the subdomain of the single realization regional model reported by Svensson (1997), see Figure 5-14 and Table 5-25. The flow rates for the Aberg DFN site model in Figure 5-14 are median values for 10 realizations. The variability between realizations is small since the flow occurs mainly along the more transmissive deterministic Äspö fracture zones.

As shown in Figure 5-14, both models indicate that the majority of the integrated inflow to the AMP model domain comes from the west (Äspö coordinates), and the majority of the outflow is directed out of the upper surface of the model to the Baltic Sea. This is consistent with the regional pattern of recharge and discharge. The differences shown in Figure 5-14 between the porous representation and the discontinuous Aberg DFN site model are a consequence of the boundary conditions used (specified heads). Table 5-25 summarizes the net flow rates in the positive x, y, z directions (north, east and upward in the Äspö coordinate system). Appendix D provides an enhanced resolution of the outflow pattern.

Table 5-25 Consistency of boundary flow rates, regional model (Svensson, 1997) versus Aberg DFN site model. Positive values indicate net outflow and negative values indicate net inflow in the considered direction.

Direction (Äspö)	Net Flow Rate through Subdomain ($\text{m}^3/\text{s} \times 10^3$)	
	Regional Model	Aberg DFN Site Model
X (easting)	-9.95	-0.77
Y (northing)	0.48	-0.59
Z (upward)	9.47	1.36
Sum of flow rates	0.00	0.00

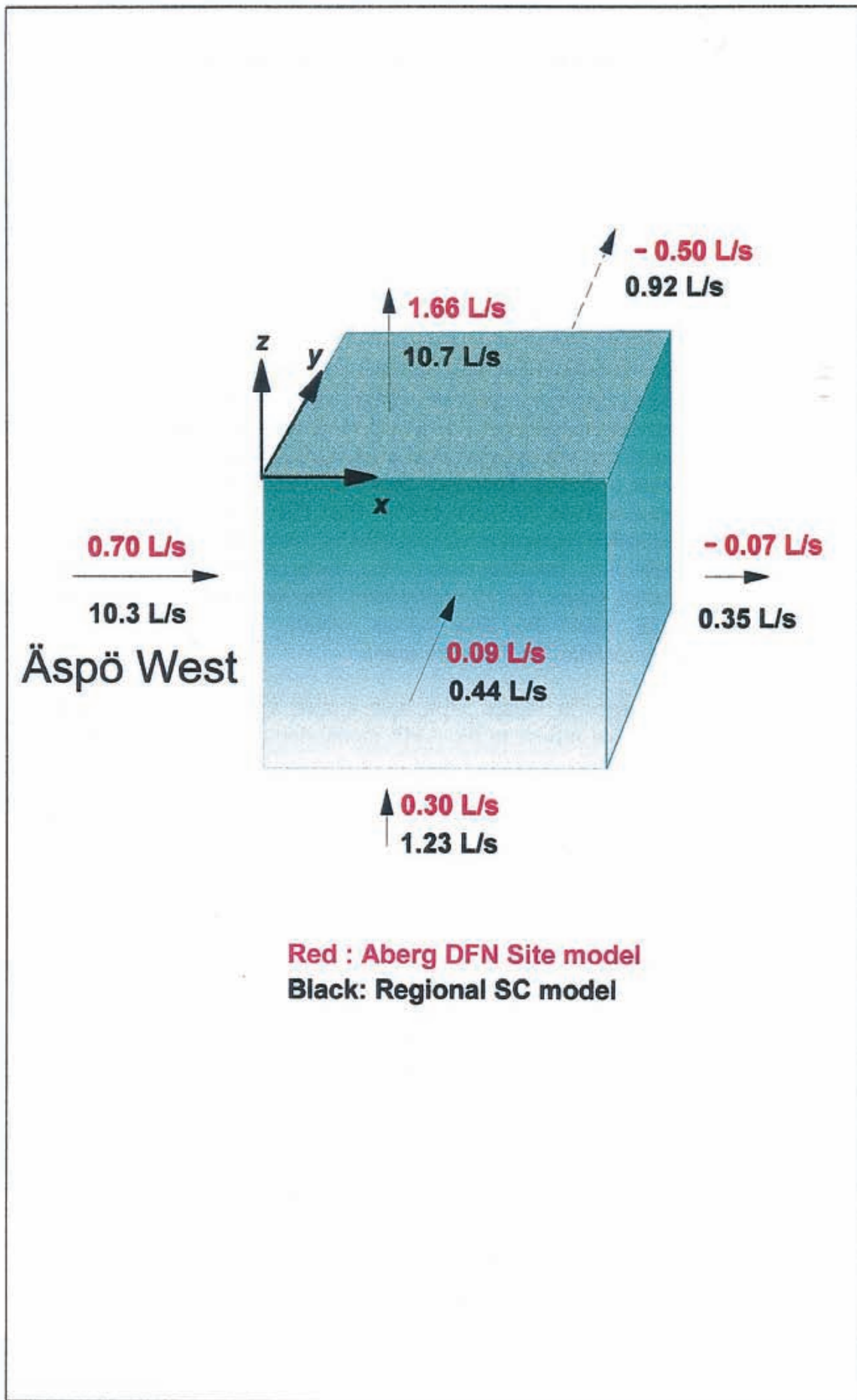


Figure 5-14 Consistency of boundary flow rates.

5.5

SUPPLEMENTARY PERFORMANCE PLOTS

Figures 5-15 through 5-18 are example plots which demonstrate the conceptual and computational power of the discrete fracture pathways approach. The cross-plots are chosen arbitrarily, thus it is impossible to say whether Figures 5-15 through 5-18 are representative examples for the ensemble of pathways. Nevertheless, the different plots demonstrate some key features of interest for SR 97 concerning near-field and far-field safety performance correlation.

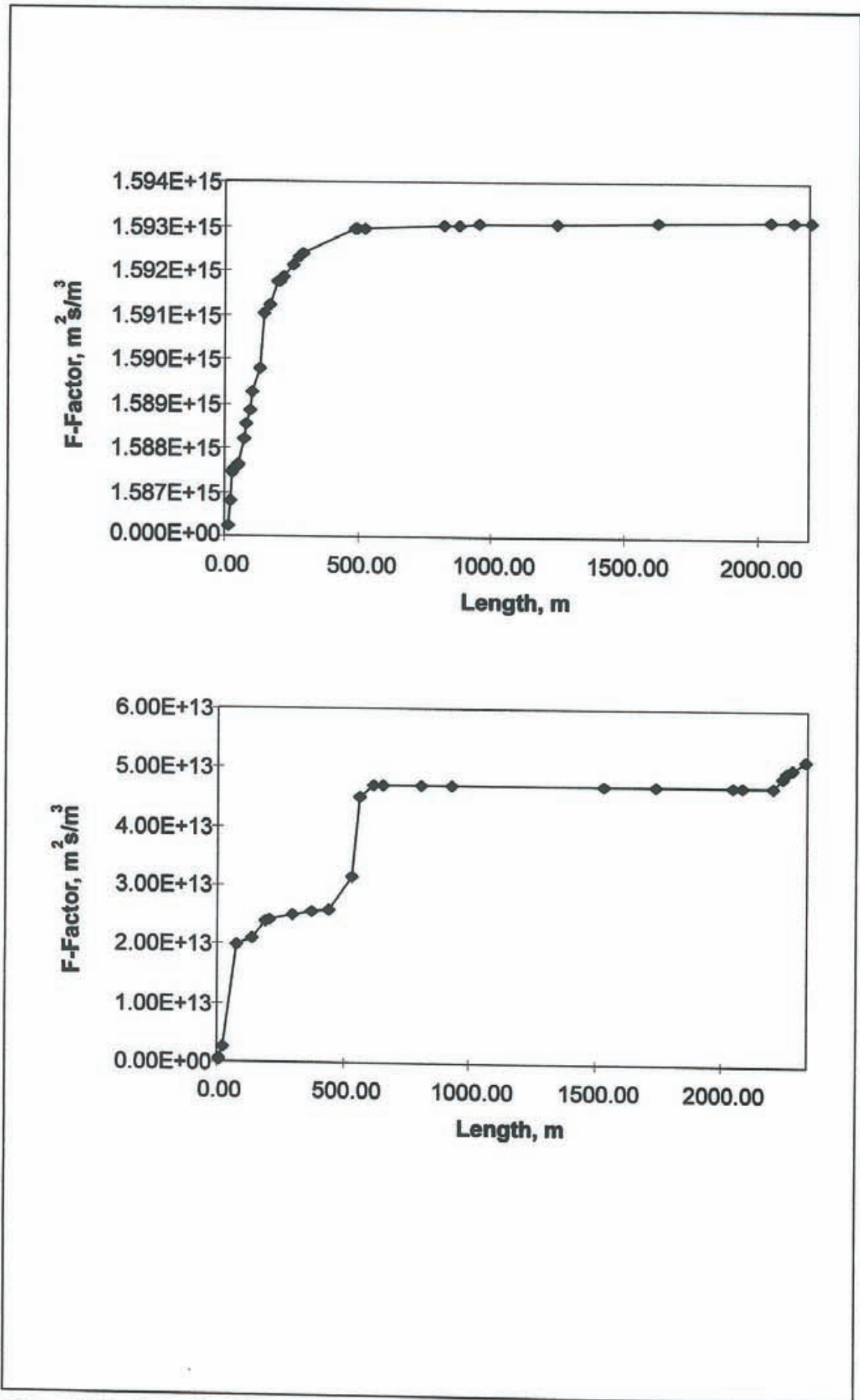


Figure 5-15 Example of F-factor growth with length of pathway.

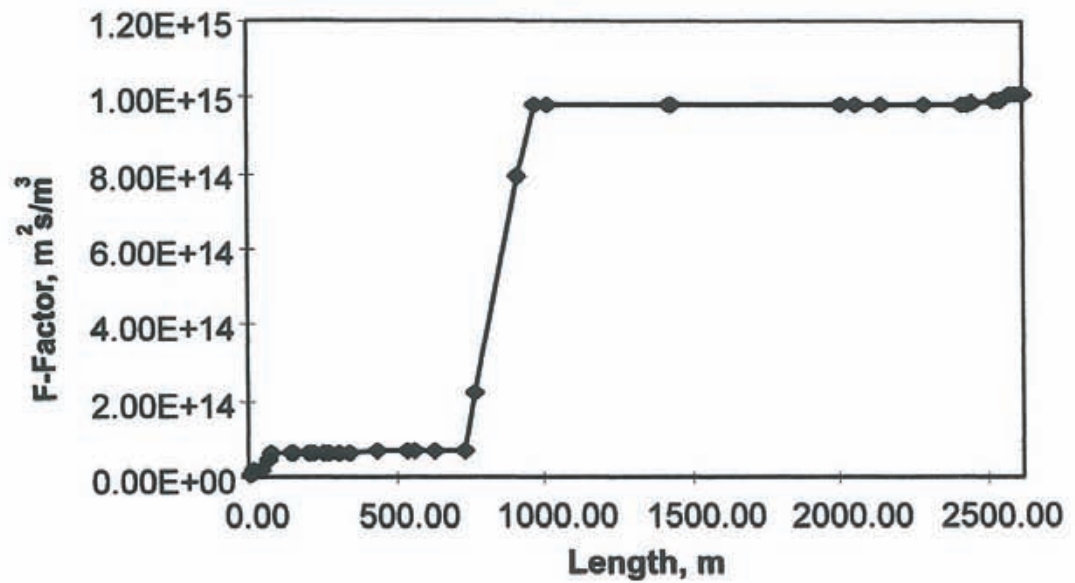
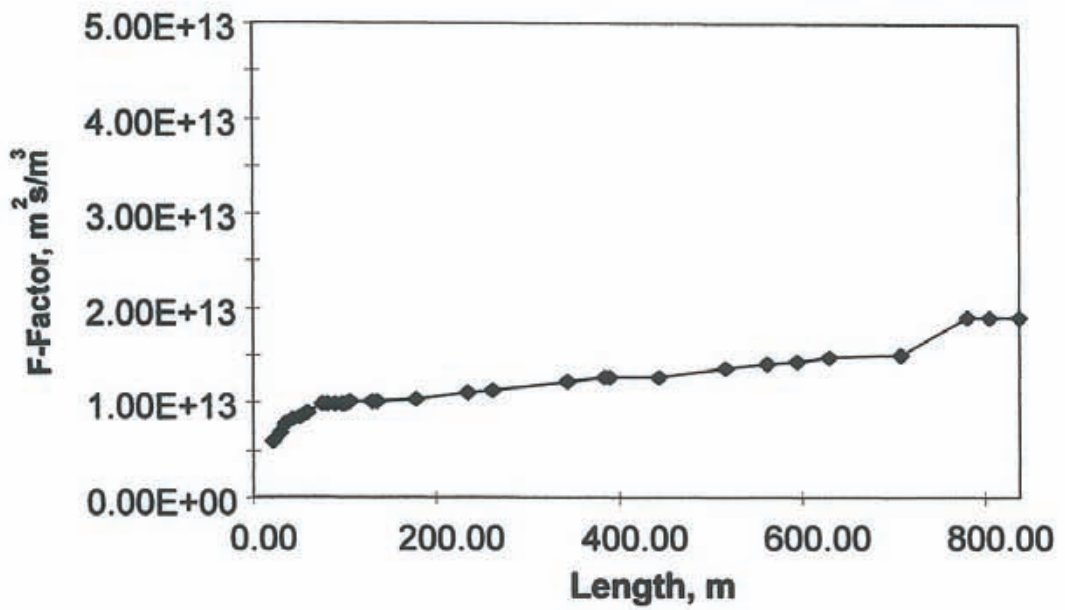


Figure 5-15 (cont.) Example of F-factor growth with length of pathway.

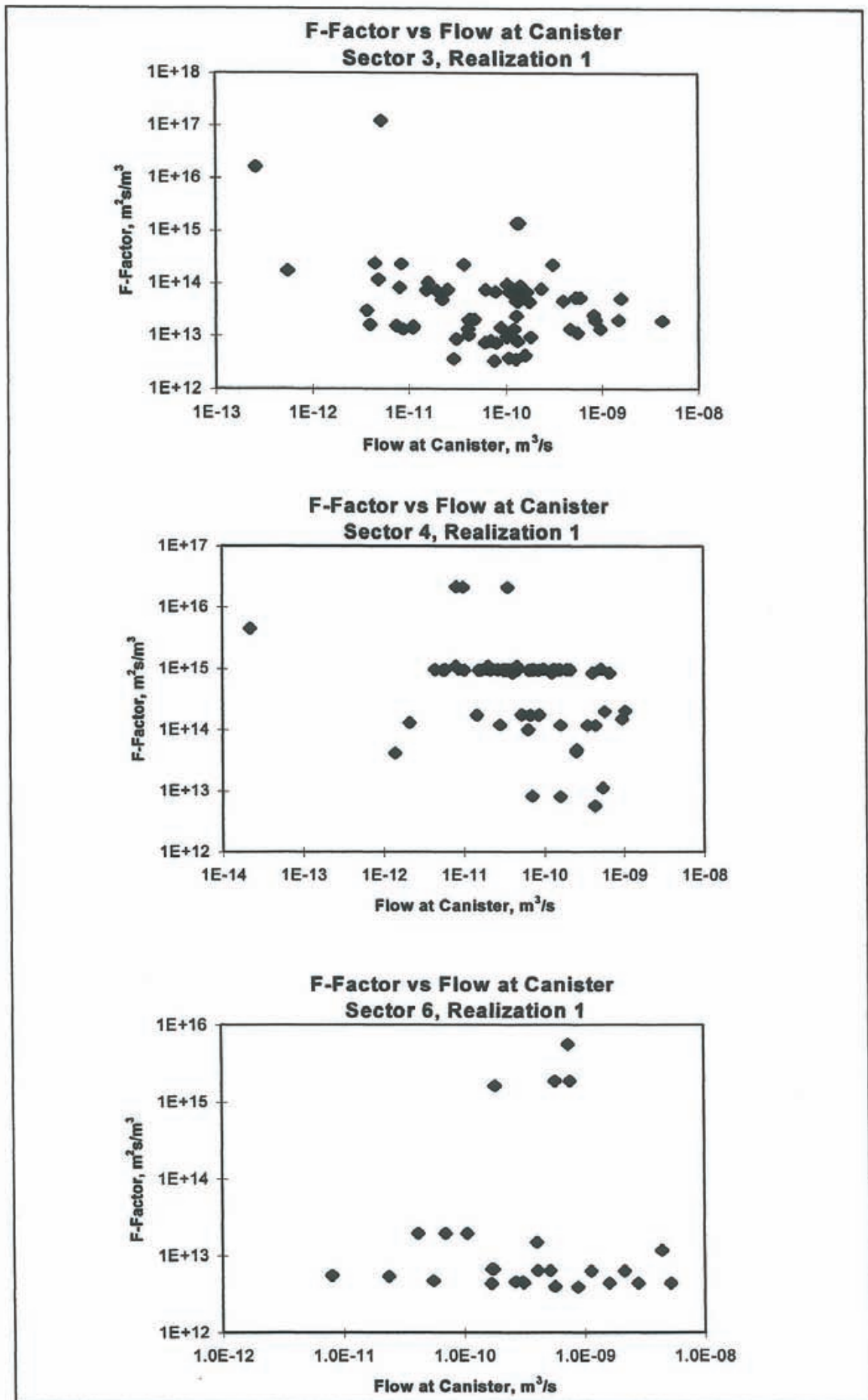


Figure 5-17 Example crossplots of F-factor versus canister flow rates.

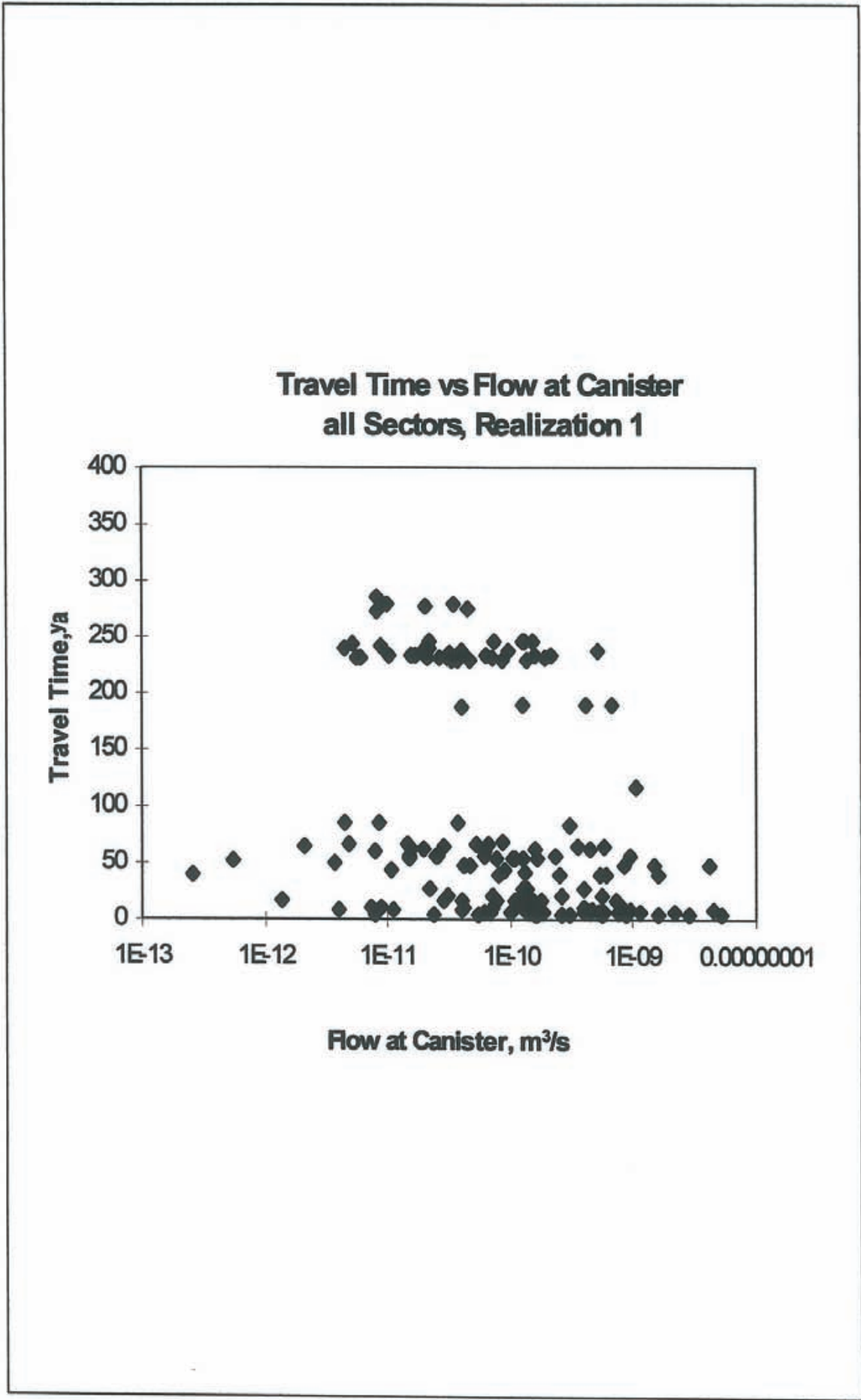


Figure 5-18 Example crossplot of travel times versus canister flow rates.

6 CONCLUSIONS

This report presents the discrete fracture network (DFN) approach within the context of the SR 97 Alternative Models Project (AMP). Parallel projects are providing results by stochastic continuum and channel network approaches.

The DFN model in this report consists of deterministic fracture zones, two sets of stochastic fractures at different scales and the canister locations of the preliminary repository layout. The hydrogeological model is defined by constant head boundary conditions on the edges of a $2000 \times 2000 \times 1000 \text{ m}^3$ rock block.

The model used the PAWorks flow rate weighted pathway search algorithm to identify pathways build by the fracture network between the canister locations and the model boundaries. For each pathway effective pathway properties were calculated to be used with SKB's FARF31 and COMP23 performance assessment codes. The pathway analysis also provides additional pathway parameters (pathway length, pathway width, transport aperture, reactive surface area, pathway transmissivity), canister statistics (average number of pathways per canister, percentage of canister locations with pathways) and visualization of pathways. However, due to editorial reasons only a subset of all this information is treated in this report.

This project demonstrates that the DFN approach can be used to directly obtain the parameters for SKB's performance assessment codes FARF31 and COMP23. More importantly, it demonstrates that the DFN approach can provide key information concerning the formation of transport pathways, including:

- pathway geometry,
- the variation in flow rates, travel times, and reactive surface areas along transport pathways,
- variability in pathways between different canister locations,
- identification of canister sites without transport pathways,
- identification of pathways based on flux (as in the current study), or alternatively based on advective travel time, F-factor, or other key PA concerns, and
- definition of heterogeneous pathways which can be analyzed directly using PA codes featuring heterogeneous pathways.

7

ACKNOWLEDGEMENTS

The authors acknowledge the support of Power Reactor and Nuclear Fuel Development Corporation (PNC), and in particular Masahiro Uchida, for development of the initial PAWorks code. The authors also acknowledge our colleagues Paul LaPointe, Todd Foxford, and Jan Hermanson for key technical contributions. Paul LaPointe was the technical reviewer for this report. Finally, the authors acknowledge the Swedish Nuclear Fuel and Waste Management for ongoing support for application of discrete feature approaches within the Swedish radioactive waste management program.

- Almén, K-E., R. Stanfors and C. Svemar.** (1996). *Nomenklatur och klassificering av geologiska strukturer vid platsundersökningar för SKB:s djupförvar*. SKB PR D-96-029, Swedish Nuclear Fuel and Waste Management Company, Stockholm.
- Dershowitz, W., J. Geier and K. Lee,** 1989. *Field Validation of Conceptual Models for Fracture Geometry*. Submitted to Rock Mechanics and Rock Engineering.
- Dershowitz, W., G. Lee, J. Geier, T. Foxford, P. LaPointe and A. Thomas,** 1995. *FracMan Interactive Discrete Feature Data Analysis, Geometric Modeling, and Exploration Simulation: User Documentation Version 2.5*. Golder Associates Inc., Redmond, Washington.
- Dershowitz, W., A. Thomas and R. Busse,** 1996. *Discrete Fracture Analysis in Support of the Äspö Tracer Retention Understanding Experiment (TRUE-1)*. SKB International Cooperation Report ICR-96-05. SKB, Stockholm.
- Dershowitz, W., S. Follin, P. Wallmann and D. Shuttle,** 1997. *Canister and Far-Field Demonstration of the Discrete Fracture Analysis Approach for Performance Assessment*, unpublished, Golder Associates Inc., Seattle.
- Doe, T.,** 1993. *Derivation of Fracture Transport Aperture*. Unpublished MS. Golder Associates Inc., Seattle.
- Follin, S, and J. Hermanson,** 1996. *A Discrete Fracture Network Model of the Äspö TBM Tunnel Rock Mass*. SKB Report, In press.
- Follin, S.,** 1995. *Geohydrological Simulation of a Deep Coastal Repository*. SKB Technical Report TR-95-33, SKB, Stockholm.
- LaPointe, P, P. Wallmann, and S. Follin,** 1995a. *Estimation of Effective Block Conductivities Based on Discrete Network Analysis Using Data from the Äspö Site*. SKB Technical Report TR-95-15, SKB, Stockholm.
- LaPointe, P., S. Follin, J. Hermanson, and P. Wallmann,** 1995b. *A Method for Identifying and Analyzing Conductive Pathways in Fractured Rock Masses for Performance Assessment Transport Models*. SKB Arbetsrapport AR-95-28, SKB, Stockholm.
- Miller, I, G. Lee, W. Dershowitz, and G. Sharp,** 1994. *MAFIC - Matrix/Fracture Interaction Code with Solute Transport. User Documentation, Version 1.5*. Golder Associates Inc. Report 923-1089. Golder Associates Inc., Seattle.

Munier, R., H. Sandstedt and L. Niland, 1997. *Förslag till principiella utformningar av förvar enligt KBS-3 för Aberg, Beberg och Ceberg.* SKB R 97-09, SKB, Stockholm.

Norman, S. and N. Kjellbert, 1990. *FARF31 - A Far-field Radionuclide Migration Code for Use with PROPERT.* SKB Technical Report TR-90-01, SKB, Stockholm.

Rhén, I., G. Gustafson, R. Stanfors and P. Wikberg, 1997. *Äspö Hard Rock Laboratory - Geoscientific Evaluation 1997/5, Models based on Site Characterization.* SKB Technical Report TR 97-06, SKB, Stockholm.

Romero L., L. Moreno and I. Neretenieks, 1995. *Model Validity Document. NUSTRAN: a Computer Program to Calculate Radionuclide transport in the near field of a repository.* SKB Arbetsrapport AR 95-14, SKB, Stockholm.

Segdewick, R. *Algorithms*, Second Edition; Addison-Wesley, 1988

Ström, A. and J.-O. Selroos (1997) *SR 97 - Use of Alternative Models for describing flow and transport in the far field (CN, SC, and DFN)*, SKB PM 1997-04-25, SKB, Stockholm.

Svensson, U., 1997. *A regional groundwater model of the Äspö area.* SKB Technical Report TR 97-05, SKB, Stockholm.

Uchida, M. and J. Geier, 1992. *Fracture Mapping on Äspö Island.* SKB SICADA Database, SKB, Stockholm.

Uchida, M., T. Doe, W. Dershowitz, A. Thomas, P. Wallmann and A. Sawada, 1994. *Discrete-fracture Modeling of the Äspö LPT-2, large-scale Pumping and Tracer Test.* SKB International Cooperation Report ICR 94-09, SKB, Stockholm.

Uchida, M, T. Doe, A. Sawada, W. Dershowitz and P. Wallmann, 1995. *FracMan Discrete Fracture Modeling for the Äspö Tunnel Drawdown Experiment.* International Cooperation Report ICR-96-XX (In production). SKB, Stockholm.

Walker, D., I. Rhén and I. Gurban, 1997. *Summary of hydrogeologic Conditions at Aberg, Beberg and Ceberg.* SKB Technical Report TR 97-23, SKB, Stockholm.

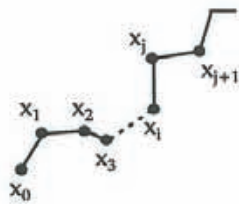
APPENDICES

Appendix A Governing Flow Equations

The governing equations assumed for flow in fracture planes are described in detail in the MAFIC User's Manual (Miller et al., 1994). PAWorks uses 1-D finite elements in order to describe the pipe network.

A.1 Pipe Element

The approximate head solution, \hat{h}^e , of a pipe element, e , can be expressed in a simple linear form:



$$\hat{h}^e = a + bx \quad (A-1)$$

The coefficients a and b are determined from two nodal heads, h_i and h_j of the element, e , that has two ends at $x=x_i$ and $x=x_j$.

$$\begin{cases} h_i = a + bx_i \\ h_j = a + bx_j \end{cases} \quad (A-2)$$

$$\Rightarrow \begin{cases} a = \frac{x_j}{x_j - x_i} h_i - \frac{x_i}{x_j - x_i} h_j \\ b = \frac{-1}{x_j - x_i} h_i + \frac{1}{x_j - x_i} h_j \end{cases} \quad (A-3)$$

Equation A-1 can be rewritten as:

$$\hat{h}^e = \xi_i h_i + \xi_j h_j \quad (A-4)$$

$$\text{with } \xi_i(x) = \frac{x_j - x}{x_j - x_i} \quad \text{and} \quad \xi_j(x) = \frac{-x_i + x}{x_j - x_i} \quad (A-5)$$

The function $\xi_i(x)$ is a linear basis function of the node i .

A quadratic basis function usually provides a better solution than a linear function. Starting from a quadratic polynomial of \hat{h}^e , the similar derivations from Equation A-1 to Equation A-4 will lead to the following solution:

$$\hat{h}^e = \xi_i h_i + \xi_m h_m + \xi_j h_j \quad (\text{A-6})$$

$$\begin{aligned} \xi_i &= 2 \frac{x - x_m}{x_j - x_i} \frac{x - x_j}{x_j - x_i} \\ \text{with } \xi_m &= -4 \frac{x - x_i}{x_j - x_i} \frac{x - x_j}{x_j - x_i} \\ \xi_j &= 2 \frac{x - x_m}{x_j - x_i} \frac{x - x_i}{x_j - x_i} \end{aligned} \quad (\text{A-7})$$

where:

x_m = the midpoint of the pipe = $\frac{1}{2}(x_i + x_j)$,

h_m = Nodal head at $x = x_m$, and

ξ_m = basis function at $x = x_m$

In general, we can express the approximate solution as:

$$\hat{h}^e = \sum_{k=0}^M \xi_k h_k \quad (\text{A-8})$$

The summation index M represents the degree of polynomial used in the basis functions.

A.2 Derivation of Equations using Galerkin Method

Using the same notions as in MAFIC User's Manual (Miller et al., 1994), Section 2.2, the approximate solution, Equation A-3, will be derived for 1-D pipe flow.

Starting from the governing equation for the transient pipe flow:

$$S \frac{\partial h}{\partial t} - T \frac{\partial^2 h}{\partial x^2} = q \quad (\text{A-3})$$

Apply the Galerkin method to the governing equation (Equation A-9):

$$\int_L \left(S \frac{\partial \hat{h}}{\partial t} - T \frac{\partial^2 \hat{h}}{\partial x^2} - q \right) \xi_n dx = 0, \quad n = 1, 2, \dots, N. \quad (\text{A-4})$$

where:

\hat{h} = the approximate solution of head,

N = total number of nodes, and

L = length of the domain.

In the Galerkin method, the residues of the governing equation, i.e., the term $\left(S \frac{\partial \hat{h}}{\partial t} - T \frac{\partial^2 \hat{h}}{\partial x^2} - q \right)$ in Equation A-10, weighted by each basis function, ξ_n , $n=1, 2, \dots, N$, must be zero when integrated over the entire domain, L .

The second derivative term in Equation A-10 can be reduced to a first derivative by applying integration by parts:

$$\int_L -T \frac{\partial^2 \hat{h}}{\partial x^2} \xi_n dx = \int_L T \frac{\partial \hat{h}}{\partial x} \frac{d\xi_n}{dx} dx - \int_{\Gamma} T \left(\frac{\partial \hat{h}}{\partial x} u_x \right) \xi_n d\sigma \quad (\text{A-5})$$

where:

Γ = the boundary of the problem domain,

u_x = the component of a unit vector normal to the boundary, and

σ = an integration variable representing distance along the boundary.

Insert Equation A-11 into Equation A-10, the equation becomes:

$$\int_L \left(S \frac{\partial \hat{h}}{\partial t} \xi_n + T \frac{\partial \hat{h}}{\partial x} \frac{d\xi_n}{dx} \right) dx = \int_L q \xi_n dx + \int_{\Gamma} T \left(\frac{\partial \hat{h}}{\partial x} u_x \right) \xi_n d\sigma = Q_n, \quad n=1, 2, \dots, N \quad (\text{A-6})$$

The terms on the right-hand side of Equation A-12 represent the flow source term, q , weighted by ξ_n over the domain and the normal flux term, $T \left(\frac{\partial \hat{h}}{\partial x} u_x \right)$, weighted by ξ_n over the boundary. The total flux weighted by ξ_n is denoted by Q_n on the right-hand side of Equation A-12.

The integration over the entire domain L can be done element by element, i.e., the summation of integrals over individual element in the domain:

$$\sum_e \left[\int \left(S_e \frac{\partial \hat{h}^e}{\partial t} \xi_n + T_e \frac{\partial \hat{h}^e}{\partial x} \frac{d\xi_n}{dx} \right) dx \right] = Q_n \quad n = 1, 2, \dots, N \quad (\text{A-7})$$

where:

S_e = Storativity of the element e , and

T_e = Transmissivity of the element e .

Introduce the approximate solution \hat{h}^e , derived in Equation A-5 into Equation A-13, the equation becomes:

$$\sum_{e=1}^E \int_{\ell^e} \left\{ S_e \left[\sum_{k=0}^M \xi_k \frac{dh_k}{dt} \right] \xi_n + T_e \left[\sum_{k=0}^M \frac{d\xi_k}{dx} h_k \right] \frac{d\xi_n}{dx} \right\} dx = Q_n \quad n = 1, 2, \dots, N. \quad (\text{A-14})$$

where:

ℓ^e = the subdomain of the element e , and

E = total number of pipe elements.

In terms of the matrix notation Equation A-14 can be transformed to:

$$\sum_{e=1}^E D_{k,n}^e \frac{dh_k}{dt} + A_{k,n}^e h_k = Q_n \quad (\text{A-8})$$

where D^e is the element storage matrix and A^e the element conductance matrix:

$$D_{k,n}^e = \int_{\ell^e} S_e \xi_k \xi_n dx$$

$$A_{k,n}^e = \int_{\ell^e} T_e \frac{d\xi_k}{dx} \frac{d\xi_n}{dx} dx$$
(A-9)

The individual terms of $D_{k,n}^e$ and $A_{k,n}^e$ are found by evaluating the integration over element e in Equation A-16. The global matrices D and A are simply assembled from the sum of each individual element matrix, D^e and A^e . Equation A-15 in terms of the global matrices is:

$$\sum_{m=1}^N \left[D_{nm} \frac{dh_m}{dt} + A_{nm} h_m \right] = Q_n \quad n = 1, 2, \dots, N$$
(A-10)

This is same as the Equation 2-3 in the MAFIC manual.

Appendix B Pipe Approximation for Fracture Network Topology

Flow and transport through fracture networks is constrained to occur through 3-D networks of interconnected 2-D fractures (planes). However, PAWorks use 1-D pipes (lines) to represent transport, which requires a significant simplification of the topology of the fracture network. This appendix describes the simplifications of the topology of the fracture network as applied in this project.

The approximation made here assumes that fractures (2-D) can be represented topologically as a system of pipes (1-D) interconnecting the fracture intersections on that fracture (Figure B-1b). The errors which result from this approximation illustrated in Figure B-1 include:

- double counting of conductance of portions of the fracture network where pipes intersect,
- ignoring portions of the fracture surface area which are not directly between fracture intersections,
- double counting of flow area for overlapping pipes, and
- channeling and spreading in each pipe is controlled by trace sizes, not by pressure streamlines within the fracture planes.

These errors have been assessed through comparison of plate flow MAFIC simulations to the pipe flow approximations (Shuttle et al., 1997) and the conclusions have been implemented in the algorithm for generating networks of pipes from the plate fracture network. The algorithm as used in this project is as follows (Figure B-2):

1. Calculate intersections (traces) between all fractures in the fracture network and develop a linked list of fracture connections.
2. Within each fracture, define pipes depending on chosen criteria a), b), c) or d) (Figure B-3).
 - a) All pipes that can be formed from the midpoints of the traces. The only restriction is that a new pipe cannot cross an existing one. Note that this algorithm is somewhat dependent on the sequence in which pipes are formed.
 - b) Pipe generation identical to (a) apart from the additional restriction that pipes are not allowed to cross traces, and that each node (located at the mid-point of each trace) has at least one pipe connected.
 - c) Pipes from (b) plus additional pipes to ensure that all pipes on the same fracture are connected to each other.

- d) Pipes from (c) plus effective pipes. An effective pipe will be formed when the pipe pathway distance between two nodes is greater than an effective pipe factor, N , times the cartesian distance between the nodes. The effective factor, N , is only used for Option d. The recommended range for N is between 1.2 to 3.0.

In the present study, option d) is used with an effective factor of 1.3.

3. For each resulting pipe the following properties are calculated:

- a) Pipe length L : the distance between the trace centers.

- b) Pipe width W : $W = X_{\min} \cdot L_{\min} + X_{\max} \cdot L_{\max}$

where:

L_{\min} = length of the shorter trace

L_{\max} = length of the longer trace

X_{\min} = factor for the shorter trace (usually in the range 0-1)

X_{\max} = factor for the longer trace (usually in the range 0-1)

For the present study, $X_{\min} = X_{\max} = 0.75$ is used based on the conclusions of Shuttle et al. (1997).

- c) Pipe transport aperture a : $a = a_1 \cdot (T)^{a_2}$

where:

T = Transmissivity of fracture

For the present study, $a_1 = 0.1$ and $a_2 = 0.5$ where used (Doe, 1993).

- d) Pipe surface area A : the surface area available for flow ($W \cdot L$).

- e) Pipe conductance C : the conductance for the pipe ($W \cdot T$).

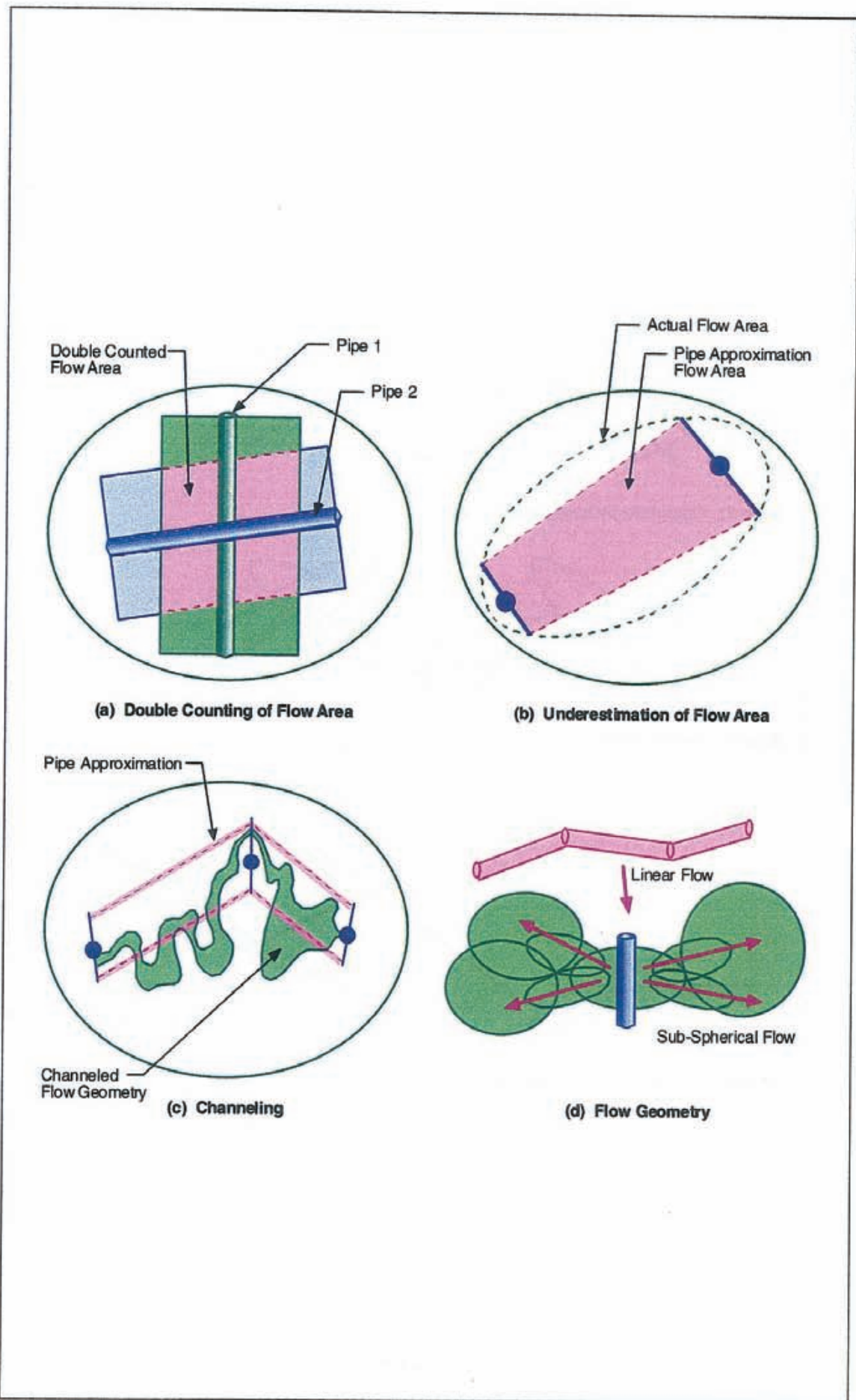
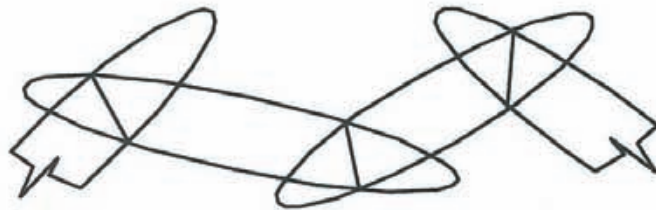
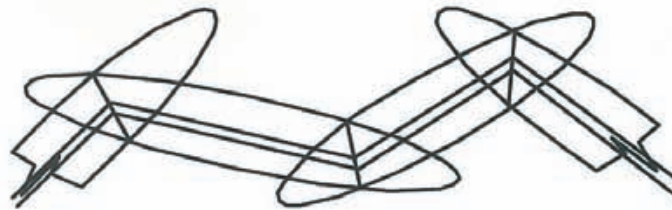


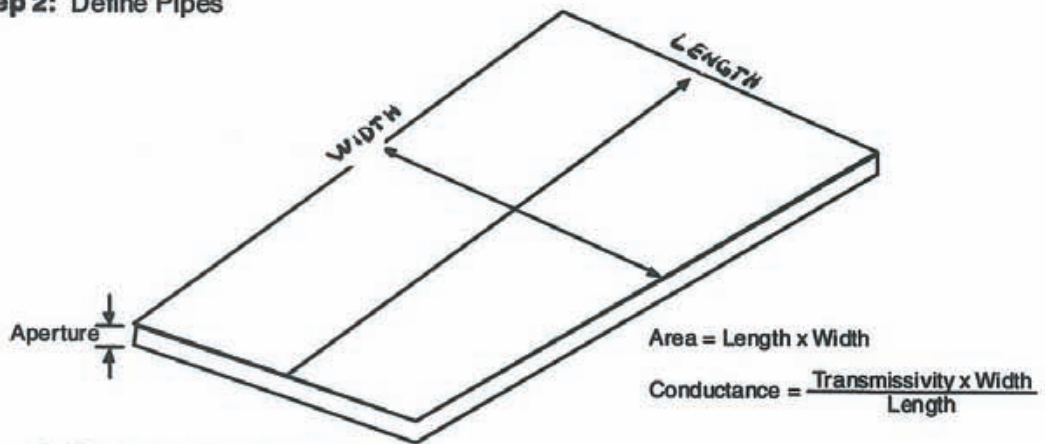
Figure B-1 Pipe approximation limitations.



Step 1: Calculate Intersections



Step 2: Define Pipes



Step 3: Calculate Pipe Properties

Figure B-2 Pipe generation algorithm.

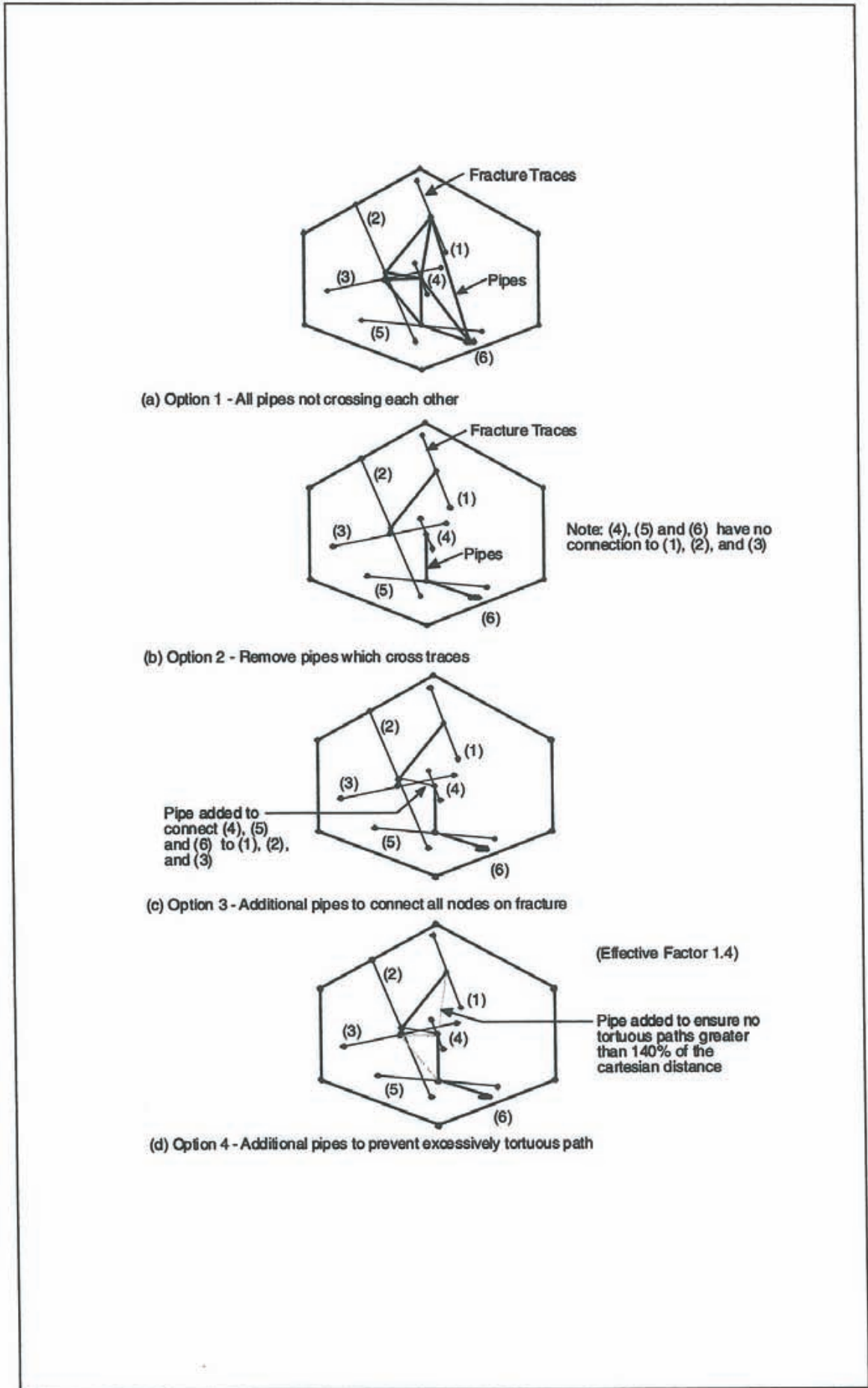


Figure B-3 Pipe connectivity.

Appendix C Effective Pathway Properties

One goal of PAWorks is to estimate the conductance, transmissivity, conductivity, and geometric properties of a representative pipe connecting source to sink. PAWorks can calculate these properties using two models:

1. The individual and representative pathways are rectangular pipe channels (idealized to be between two parallel surfaces) of specific length, width, and aperture (Figure C-1), or
2. The individual and representative pathways are cylindrical tubes of specific length and radius.

In this study, effective pathway properties are calculated and reported based on the rectangular pipe model (Figure C-1).

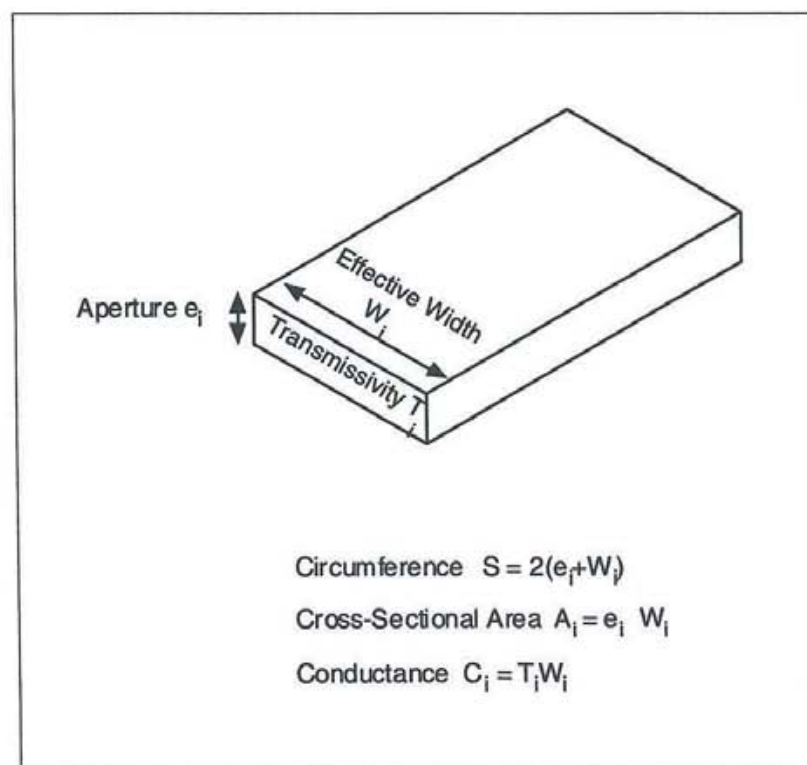


Figure C-1 Rectangular Pipe geometry schematic.

Given Parameters

After the intersections and pipes are generated and the head values calculated, the following parameters are given for each pipe that is part of an identified pathway:

L_{pipe}	Length of each pipe, m
W_{pipe}	Width of each pipe, m
T_{pipe}	Transmissivity of each pipe, m^2/s
ΔH_{pipe}	Head drop over each pipe, m
ΔH_{path}	Head drop over entire pathway, m
t_{pipe}	Travel time of each pipe, s
Q_{pipe}	Flow rate in each pipe, m^3/s

Step #1: Calculate First Order Geometric Parameters

The effective path length is sum of the lengths of each component pipe:

$$L_{path} = \sum L_{pipe} \quad (C-1)$$

The effective path travel time is sum of the travel times of each component pipe:

$$t_{path} = \sum t_{pipe} \quad (C-2)$$

The effective pathway width, however, can obviously not simply be calculated as a sum of the pipe widths. Instead a weighted average is used:

$$W_{path} = \frac{\sum (W_{pipe} \cdot \text{weighting_property}_{pipe})}{\sum \text{weighting_property}_{pipe}} \quad (C-3)$$

The weighting property used here depends on the user assigned pathway search criterion (e.g., flow rate).

Step #2: Calculate Pipe Hydraulic Gradients

The hydraulic gradient in each pipe as well as the entire pathway is the head drop per length:

$$i_{pipe} = \frac{\Delta H_{pipe}}{L_{pipe}} \quad (C-4)$$

$$i_{path} = \frac{\Delta H_{path}}{L_{path}} \quad (C-5)$$

Step #3: Calculate path conductivity

Knowing the pathway travel time, the pathway conductivity [m/s] is calculated as:

$$K_{\text{path}} = \frac{L_{\text{path}}}{t_{\text{path}} i_{\text{path}}} \quad (\text{C-6})$$

Step #4: Calculate aperture, transmissivity and flow rate

This calculation is critical to the pathway property calculation. The three properties aperture, transmissivity and flow rate are interrelated, and which is computed first affects the overall pathway properties.

In the current study, the pathway aperture [m] is calculated first, as a flow rate weighted average:

$$a_{\text{path}} = \frac{\sum(a_{\text{pipe}} \cdot Q_{\text{pipe}})}{\sum Q_{\text{pipe}}} \quad (\text{C-7})$$

Having computed the aperture, the transmissivity [m²/s] and flow rate [m³/s] are computed as follows:

$$T_{\text{path}} = K_{\text{path}} \cdot a_{\text{path}} \quad (\text{C-8})$$

$$Q_{\text{path}} = K_{\text{path}} \cdot i_{\text{path}} \cdot W_{\text{path}} \cdot a_{\text{path}} \quad (\text{C-9})$$

Alternative solutions are available in which transmissivity, pathway flow rate, or the flow rate at the exit element are calculated first:

The “transmissivity” option computes the pathway transmissivity first by weighting the transmissivity by the traversal property:

$$T_{\text{path}} = \frac{\sum (T_{\text{pipe}} \cdot \text{weighting_property}_{\text{pipe}})}{\sum \text{weighting_property}_{\text{pipe}}} \quad (\text{C-10})$$

Again, one of the triad of properties is defined the others follow from substitution:

$$a_{\text{path}} = T_{\text{path}} / K_{\text{path}} \quad (\text{C-11})$$

$$Q_{\text{path}} = K_{\text{path}} \cdot i_{\text{path}} \cdot W_{\text{path}} \cdot a_{\text{path}} \quad (\text{C-12})$$

The “flow rate” option computes the pathway flow first by weighting the flow by the traversal property:

$$Q_{path} = \frac{\sum (Q_{pipe} \cdot weighting_property_{pipe})}{\sum weighting_property_{pipe}} \quad (C-13)$$

The apertures are then computed using the equation:

$$a_{path} = \frac{Q_{path}}{K_{path} \cdot i_{path} \cdot W_{path}} \quad (C-14)$$

where W_{path} is the pathway width, K_{path} is the hydraulic conductivity for the pathway, and i_{path} is the hydraulic gradient.

The “flow rate out” option computes the effective pathway aperture from the last value of flow rate on the pathway, using the equation:

$$a_{path} = \frac{Q_{out}}{K_{path} \cdot i_{path} \cdot W_{path}} \quad (C-15)$$

with W_{path} as the pathway width, K_{path} as the hydraulic conductivity for the pathway, and i_{path} as the hydraulic gradient.

Step #5: Calculate reactive surface area

For calculation of the path surface area [m^2], three options are available (Figure C-2). The first is as the sum of all the individual fracture areas $A_{fracture}$ along the pathway:

$$RSA_{path} = \sum A_{fracture} \quad (C-16)$$

The second is as the sum of pipe areas A , i.e. the area calculated from the pipe width and length:

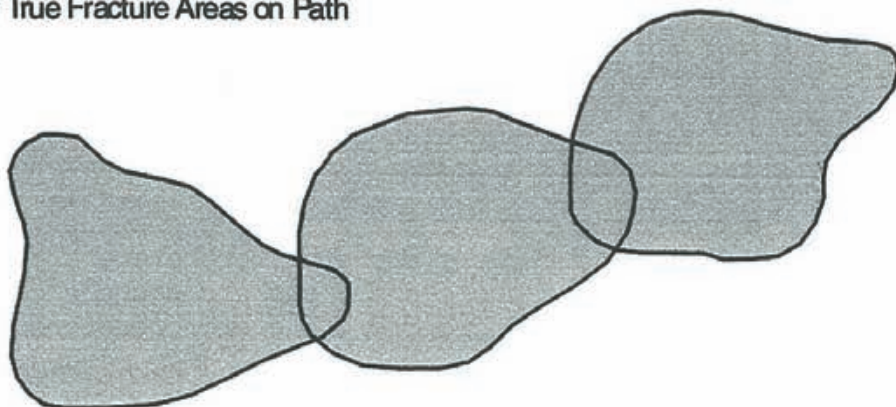
$$RSA_{path} = \sum (W_{pipe} \cdot L_{pipe}) \quad (C-17)$$

The third form of the fracture area is as:

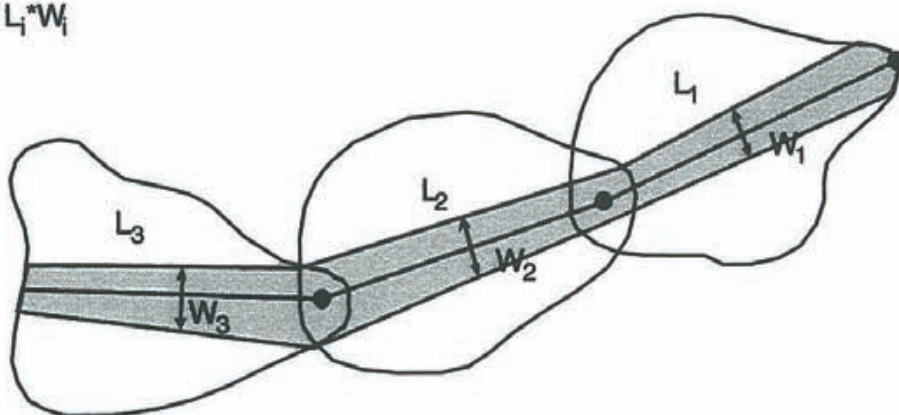
$$RSA_{path} = \frac{\sum (W_{pipe} \cdot weighting_property_{pipe})}{\sum (weighting_property_{pipe} \cdot L_{pipe})} \quad (C-18)$$

In the current study, the pipe area is calculated using the second option.

(a) Sum of True Fracture Areas on Path



(b) Sum of $L_i \cdot W_i$



(c) Weighted Width * L

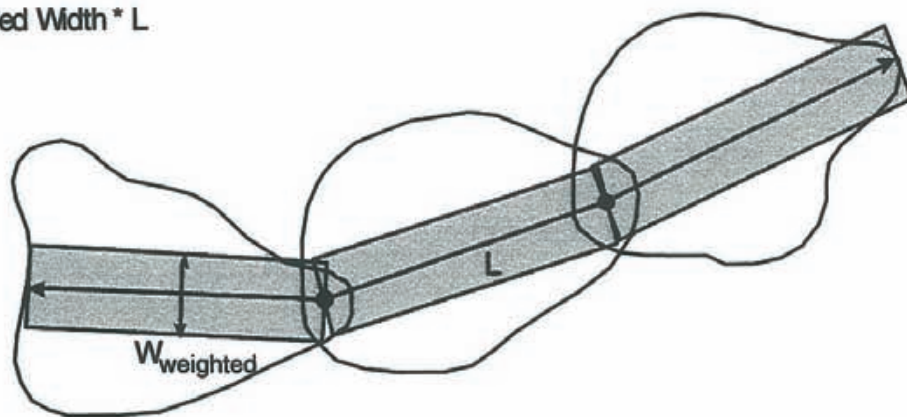


Figure C-2 Reactive surface area options.

Appendix D Graphical Display of Pathway Discharge Points

This appendix shows the pathway discharge points for the modeled canisters of Sectors 3, 4 and 6. The pathway discharge points are plotted on a map which shows the outcrop of the deterministic Äspö fracture zone model (Rhén et al., 1997) at $z = 0$, together with a transparent view of the canister positions of the three sectors. The pathway discharge points are shown for all ten realizations. In addition, we also provide two figures which demonstrate the 3-D envelope of each pathway for realizations # 1 and # 9.

The pathway discharge points are plotted as green dots and labeled with the associated section number. The canister positions are plotted as blue markers and the outcrops are plotted as red lines (Figure D-1).

The figures indicate that the pathway discharge points have very little spatial dispersion and that they are strongly influenced by:

- 1) the hydraulic boundary conditions, and
- 2) the deterministic Äspö fracture zone model.

The small differences between the ten figures are by and large due to differences in the connectivity between the probabilistic rock mass fracture model and the deterministic Äspö fracture zone model. The most deviating realization is # 9.

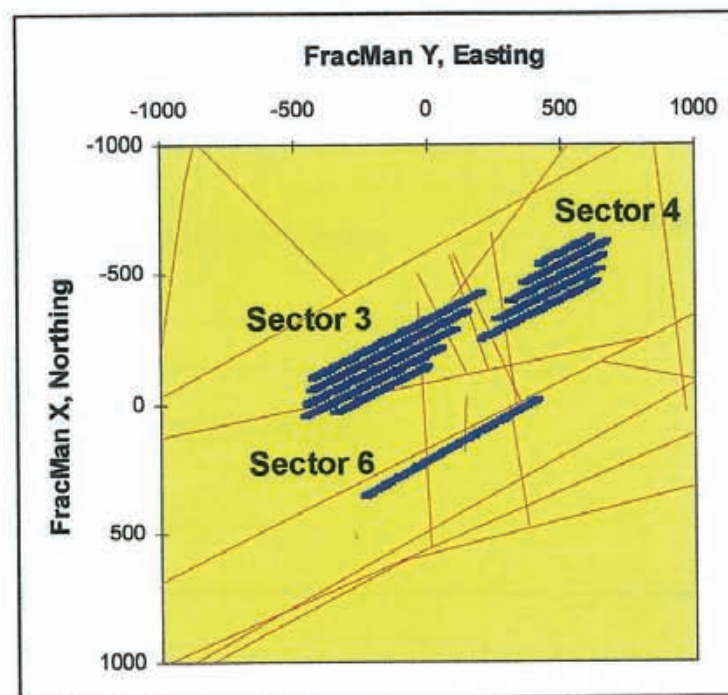


Figure D-1 Outcrop of the deterministic Äspö fracture zone model at $z = 0$ masl together with a transparent view of the modeled canisters of Sectors 3, 4 and 6.

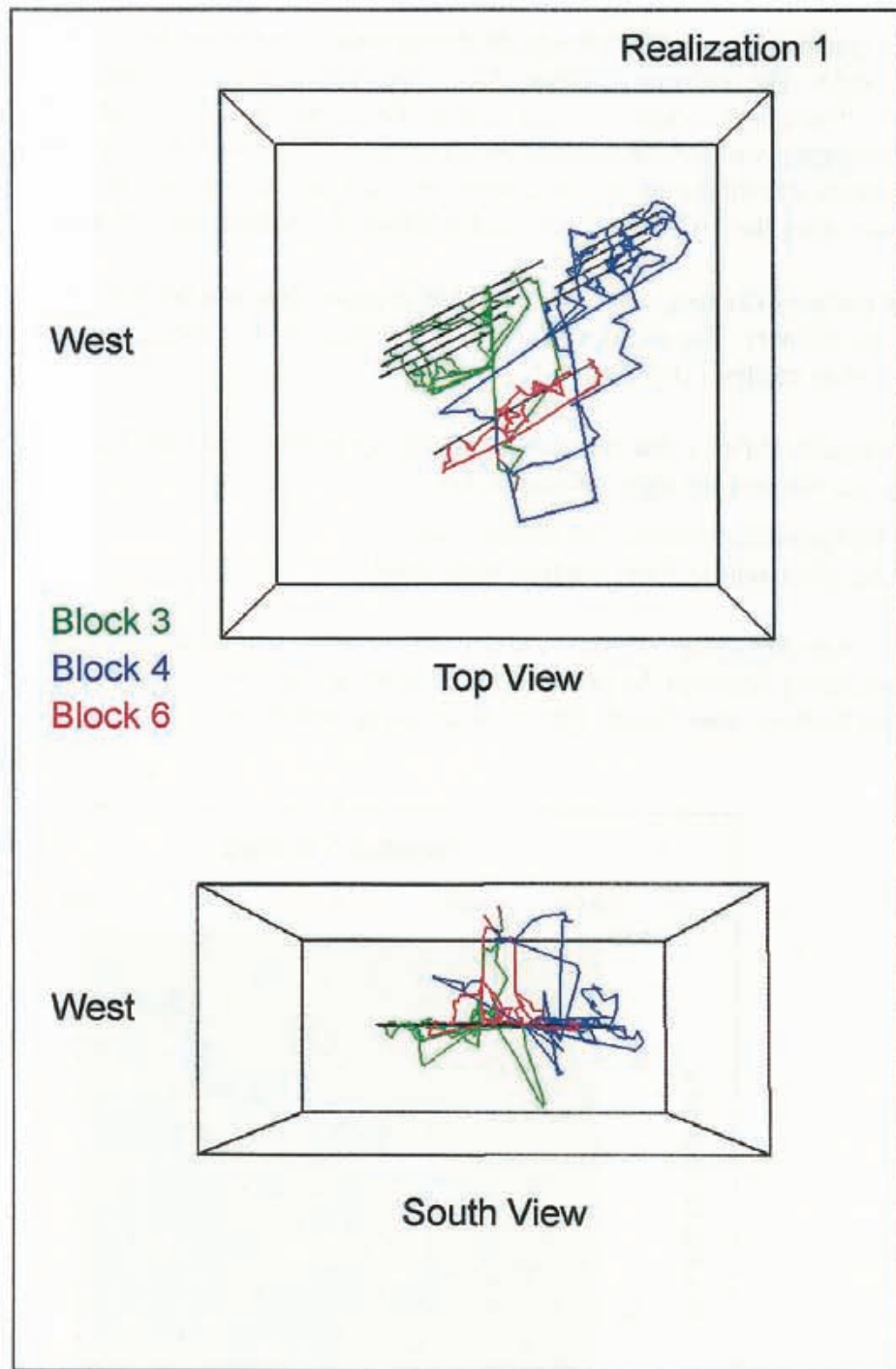


Figure D-2 Particle pathways for realization 1 between the modeled canisters of Sectors 3, 4 and 6 and the external boundaries of the model domain. Section view from south.

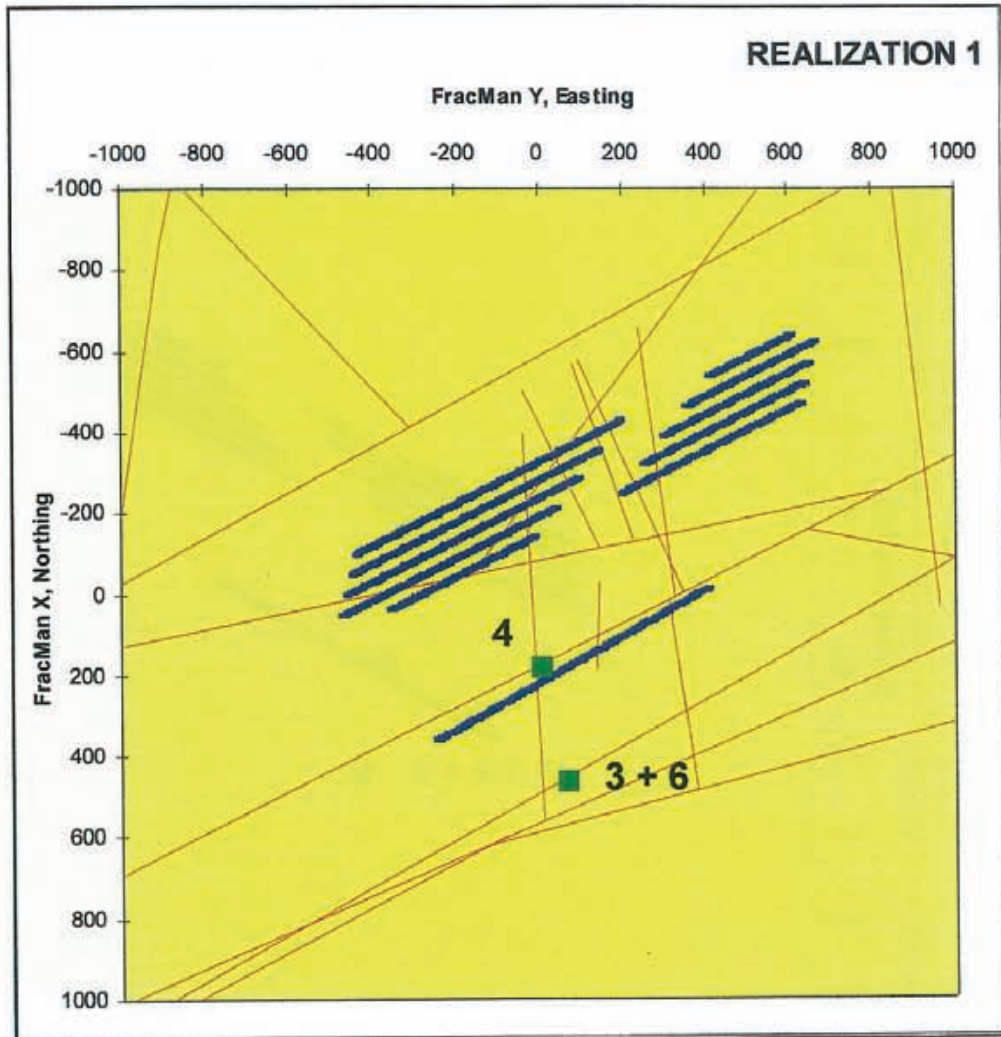


Figure D-3 Plane view of the pathway discharge points of realization 1.

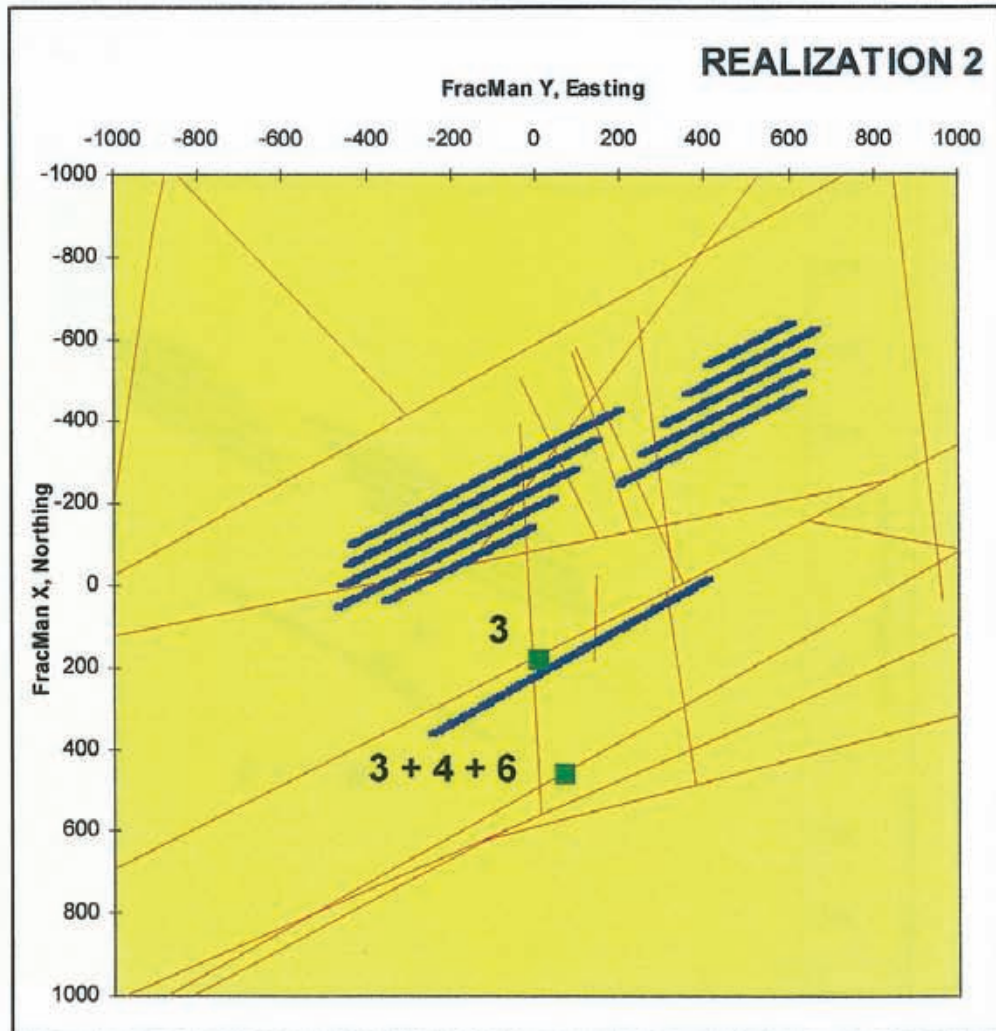


Figure D-4 Plane view of the pathway discharge points of realization 2.

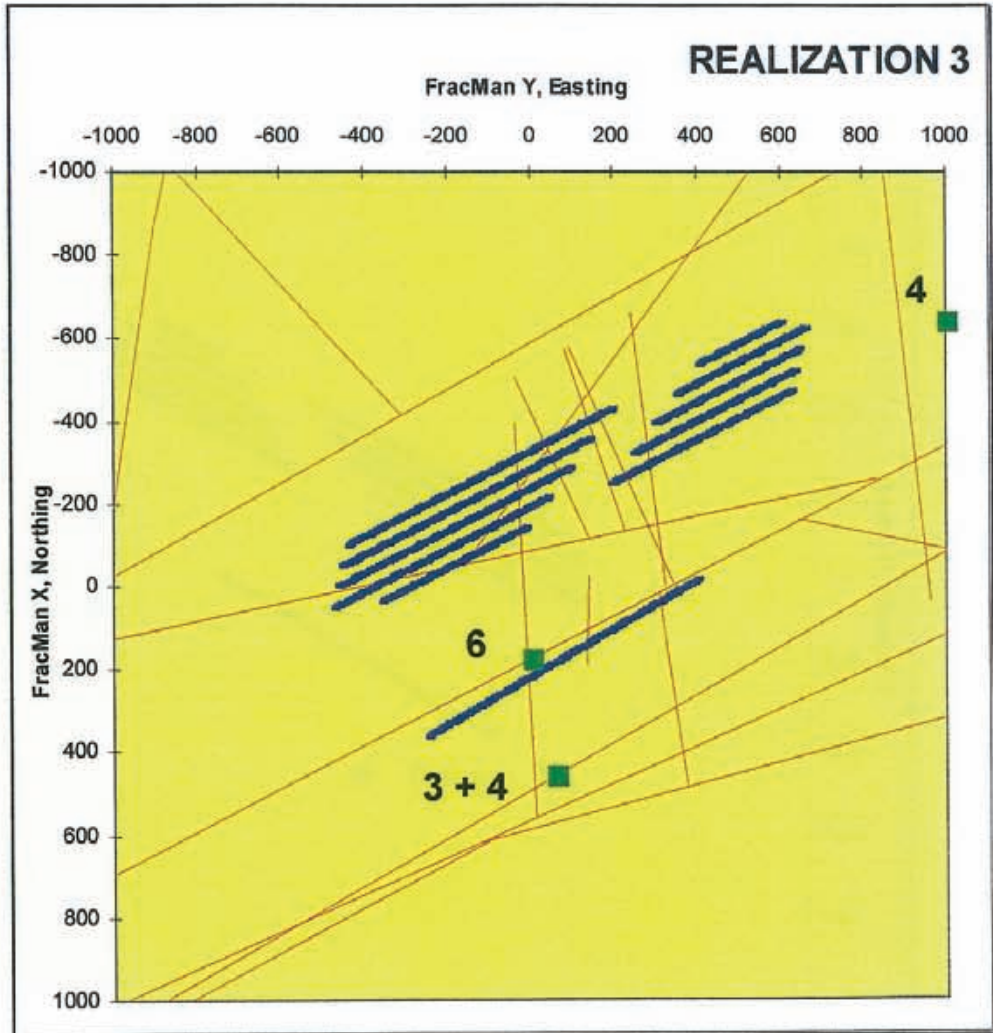


Figure D-5 Plane view of the pathway discharge points of realization 3.

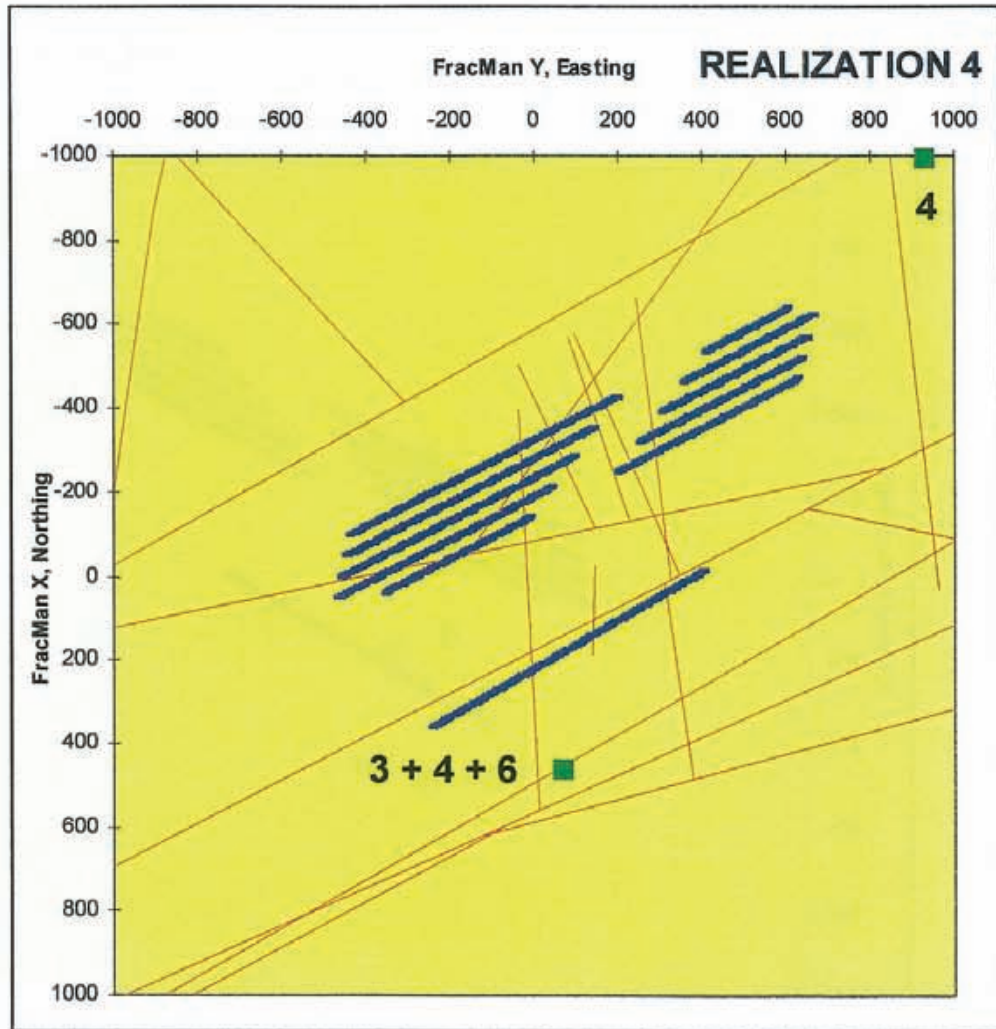


Figure D-6 Plane view of the pathway discharge points of realization 4.

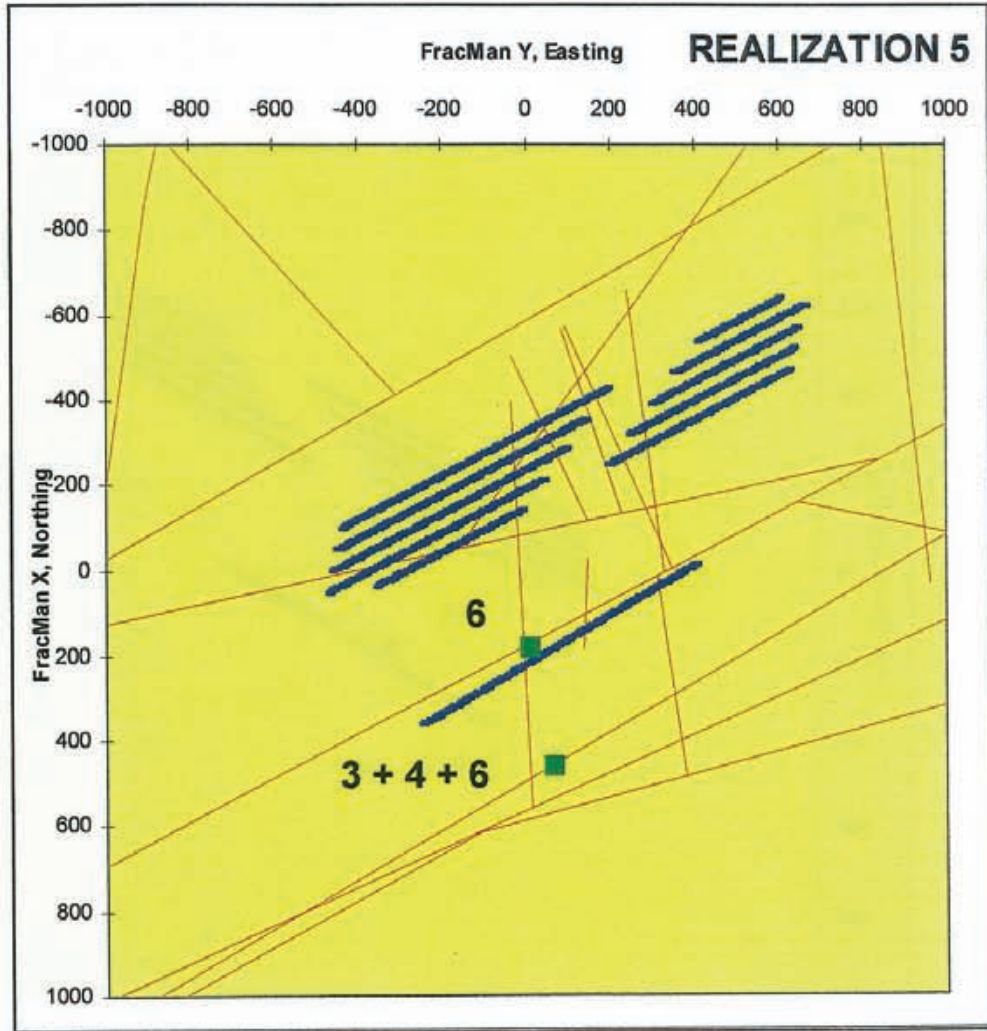


Figure D-7 Plane view of the pathway discharge points of realization 5.

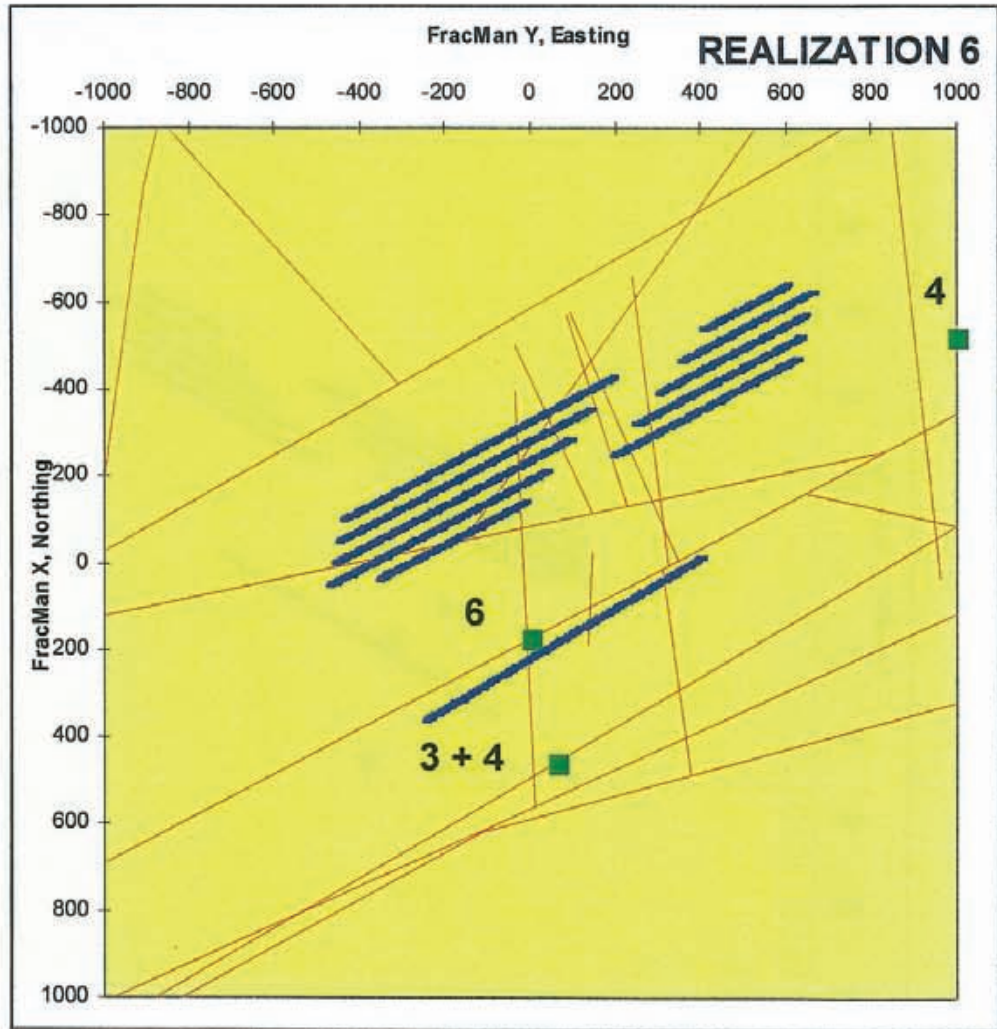


Figure D-8 Plane view of the pathway discharge points of realization 6.

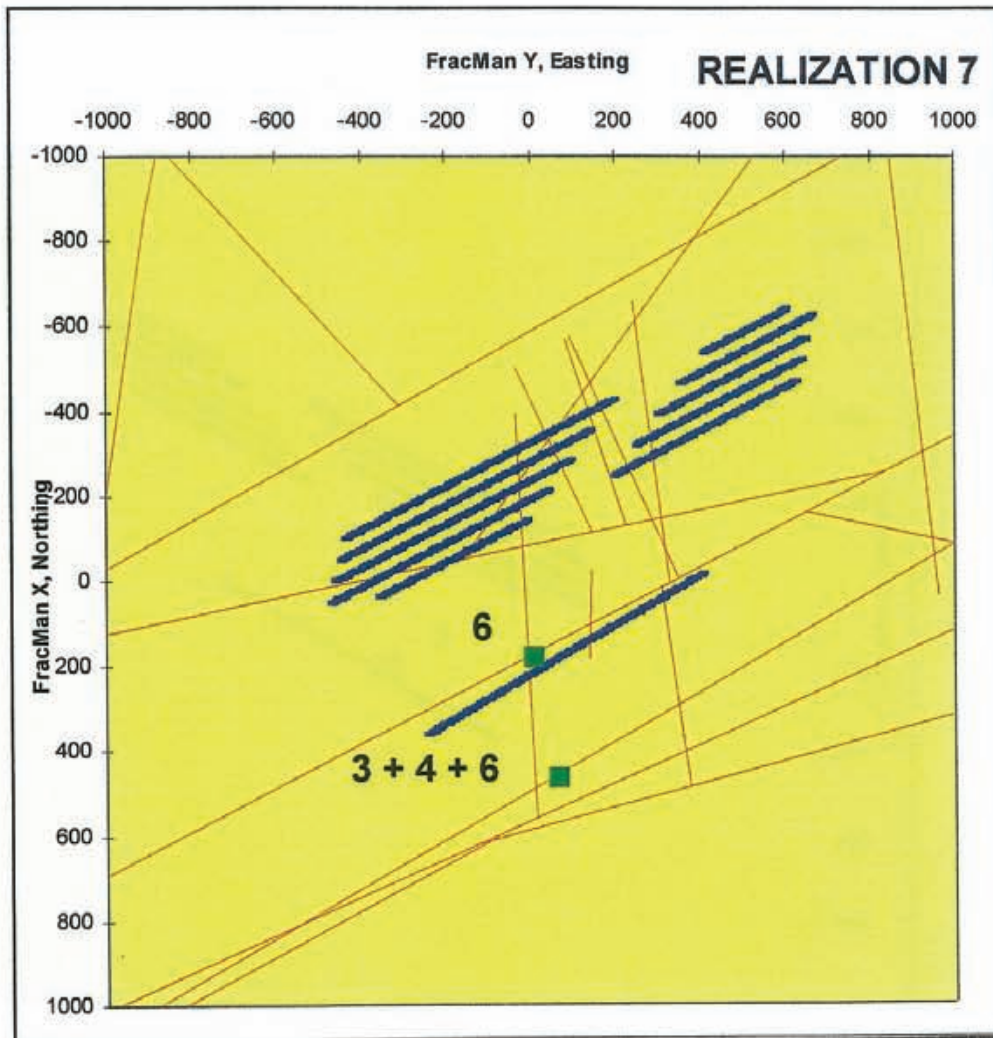


Figure D-9 Plane view of the pathway discharge points of realization 7.

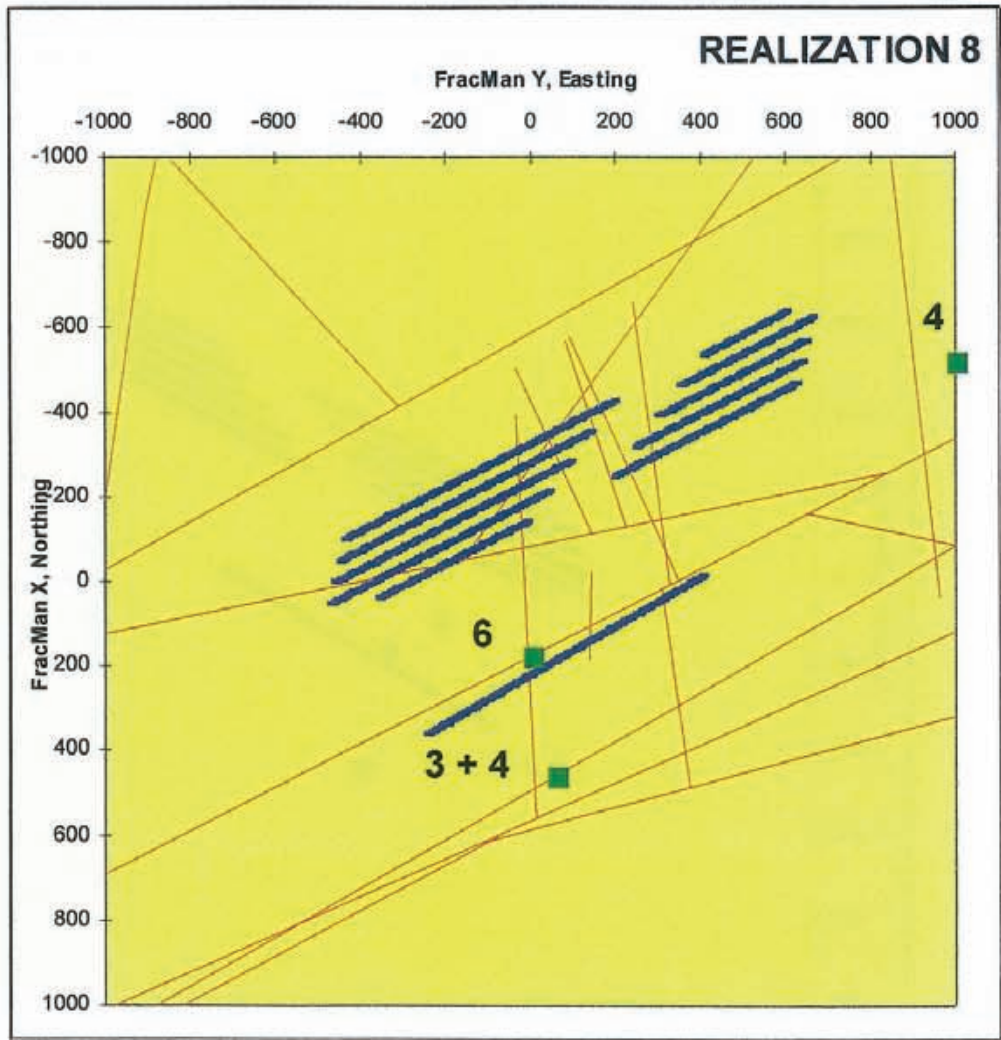


Figure D-10 Plane view of the pathway discharge points of realization 8.

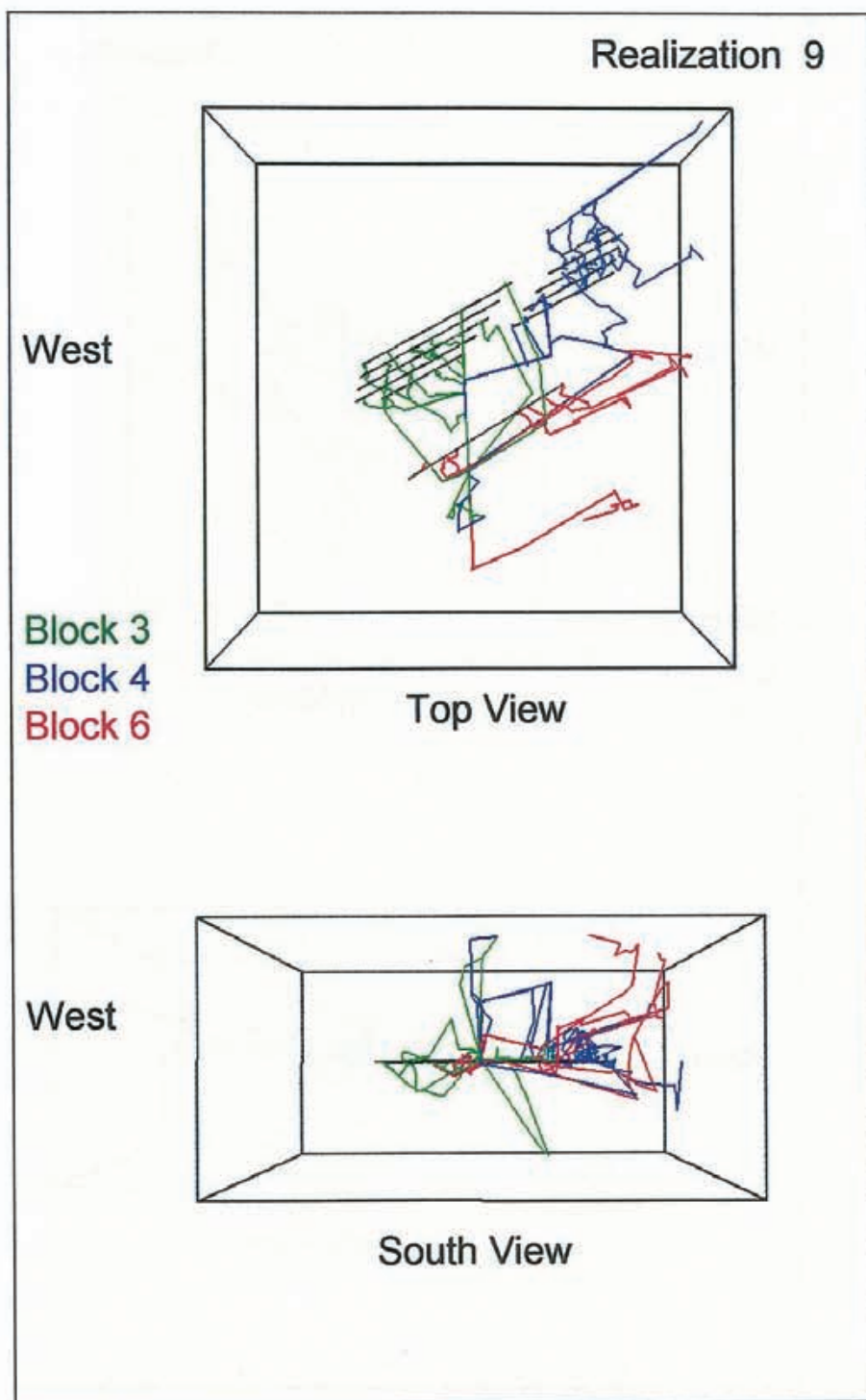


Figure D-11 Particle pathways for realization 9 between the modeled canisters of Sectors 3, 4 and 6 and the external boundaries of the model domain. Section view from south.

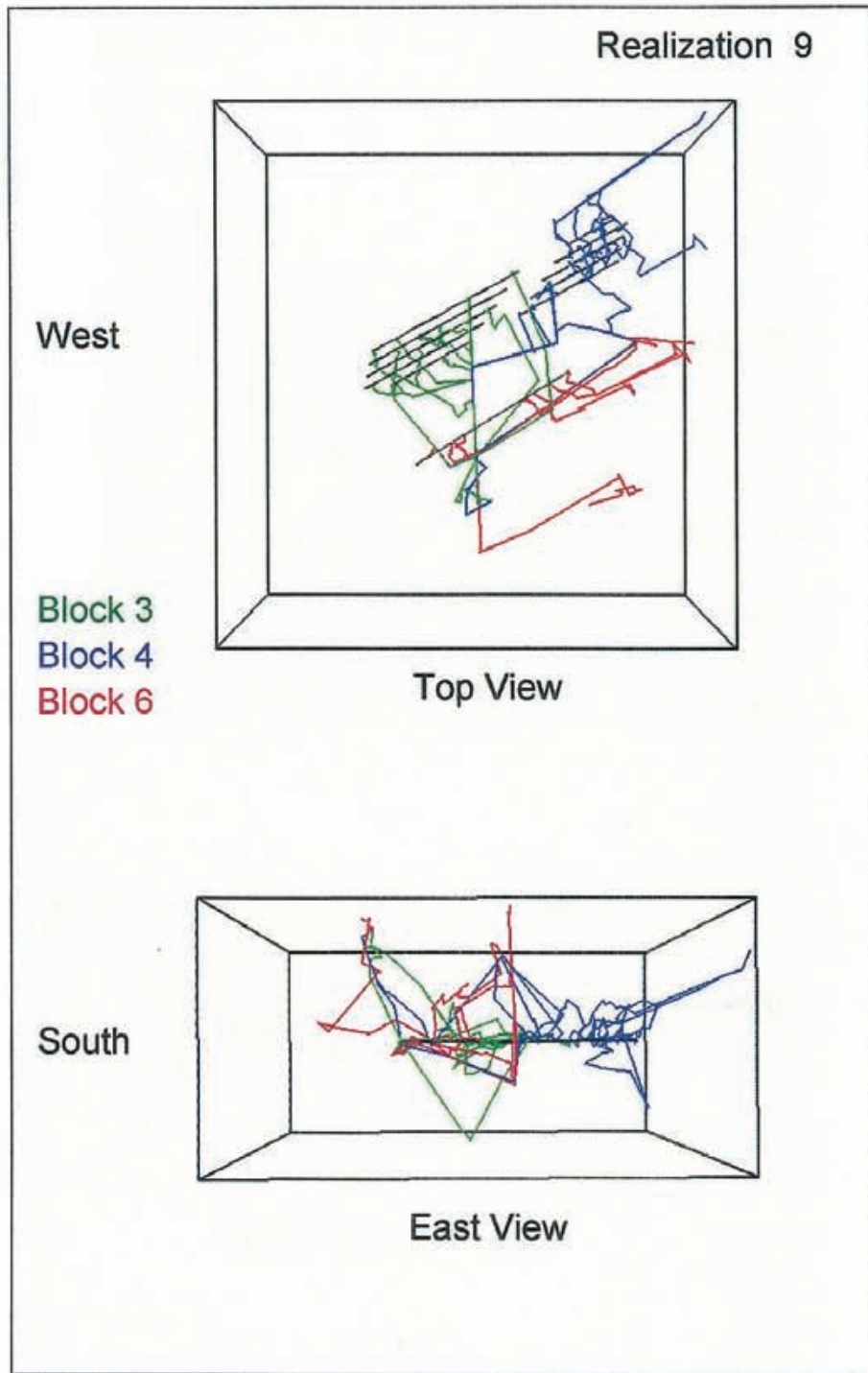


Figure D-12 Particle pathways for realization 9 between the modeled canisters of Sectors 3, 4 and 6 and the external boundaries of the model domain. Section view from east.

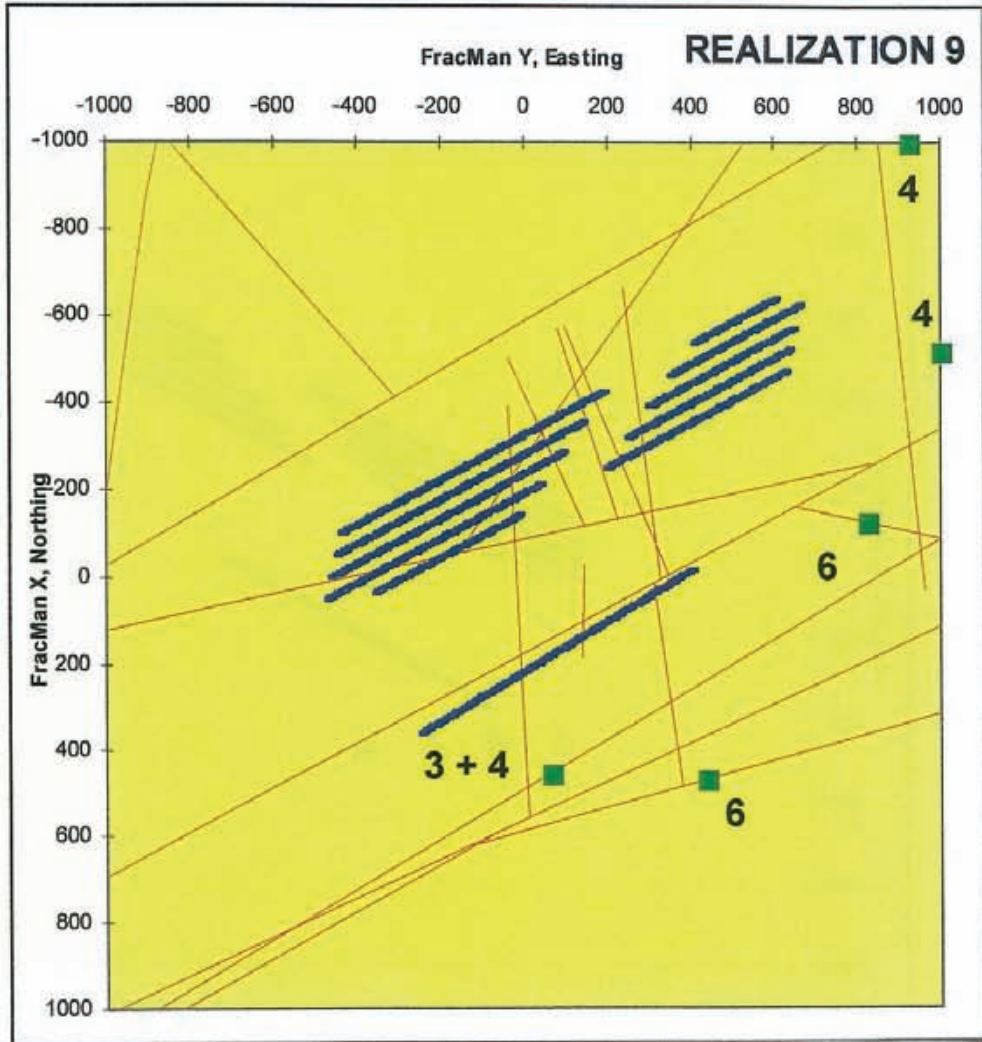


Figure D-13 Plane view of the pathway discharge points of realization 9.

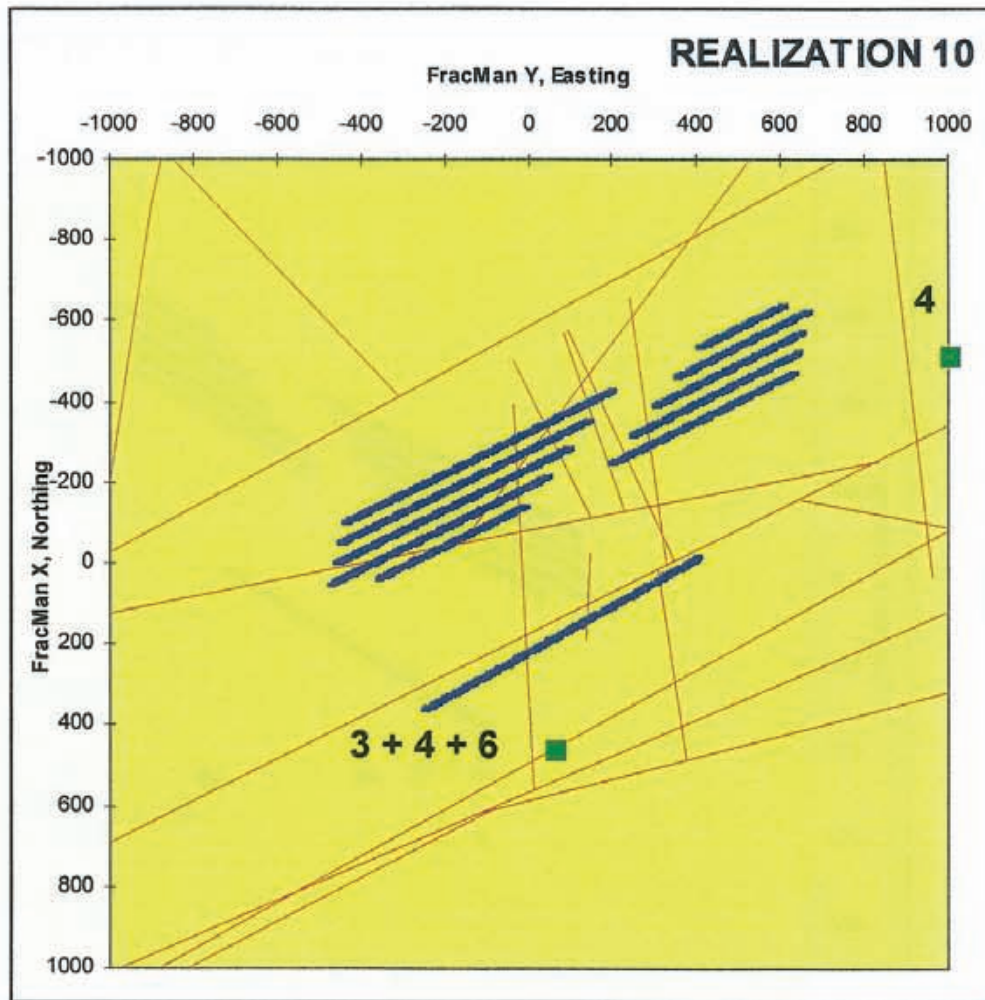


Figure D-14 Plane view of the pathway discharge points of realization 10.